ELSEVIER

Physics Reports 366 (2002) 1–101

PHYSICS REPORTS

www.elsevier.com/locate/physrep

The synchronization of chaotic systems

S. Boccaletti[a,b,*], J. Kurths[c], G. Osipov[d], D.L. Valladares[b,e], C.S. Zhou[c]

[a] *Istituto Nazionale di Ottica Applicata, Largo E. Fermi, 6, I50135 Florence, Italy*
[b] *Department of Physics and Applied Mathematics, Institute of Physics, Universidad de Navarra, Irunlarrea s/n, 31080 Pamplona, Spain*
[c] *Institut für Physik, Universität Potsdam, 14415 Potsdam, Germany*
[d] *Department of Radiophysics, Nizhny Novgorod University, Nizhny Novgorod 603600, Russia*
[e] *Department of Physics, Univ. Nac. de San Luis, Argentina*

Received 2 January 2002
editor: I. Procaccia

Abstract

Synchronization of chaos refers to a process wherein two (or many) chaotic systems (either equivalent or nonequivalent) adjust a given property of their motion to a common behavior due to a coupling or to a forcing (periodical or noisy). We review major ideas involved in the field of synchronization of chaotic systems, and present in detail several types of synchronization features: complete synchronization, lag synchronization, generalized synchronization, phase and imperfect phase synchronization. We also discuss problems connected with characterizing synchronized states in extended pattern forming systems. Finally, we point out the relevance of chaos synchronization, especially in physiology, nonlinear optics and fluid dynamics, and give a review of relevant experimental applications of these ideas and techniques. © 2002 Published by Elsevier Science B.V.

PACS: 05.45.−a

Contents

* Corresponding author. Istituto Nazionale di Ottica Applicata, Largo E. Fermi 6, 50125 Florence, Italy. http://www.ino.it/∼stefano.
E-mail address: stefano@ino.it (S. Boccaletti).

0370-1573/02/$ - see front matter © 2002 Published by Elsevier Science B.V.
PII: S0370-1573(02)00137-0

1. Introduction

1.1. The concept of chaos synchronization

The origin of the word synchronization is a greek root (*σὺγ χρόνος* which means "to share the common time"). The original meaning of *synchronization* has been maintained up to now in the colloquial use of this word, as agreement or correlation in time of different processes [1].

Historically, the analysis of synchronization phenomena in the evolution of dynamical systems has been a subject of active investigation since the earlier days of physics. It started in the 17th century

with the finding of Huygens that two very weakly coupled pendulum clocks (hanging at the same beam) become synchronized in phase [2]. Other early found examples are the synchronized lightning of fireflies, or the peculiarities of adjacent organ pipes which can almost reduce one another to silence or speak in absolute unison. For an exhaustive overview of the classic examples of synchronization of periodic systems we address the reader to Ref. [3].

Recently, the search for synchronization has moved to chaotic systems. In this latter framework, the appearance of collective (synchronized) dynamics is, in general, not trivial. Indeed, a dynamical system is called *chaotic* whenever its evolution sensitively depends on the initial conditions. The above said implies that two trajectories emerging from two different closeby initial conditions separate exponentially in the course of the time. As a result, chaotic systems intrinsically defy synchronization, because even two identical systems starting from slightly different initial conditions would evolve in time in an unsynchronized manner (the differences in the systems' states would grow exponentially). This is a relevant practical problem, insofar as experimental initial conditions are never known perfectly. The setting of some collective (synchronized) behavior in coupled chaotic systems has therefore a great importance and interest.

The subject of the present report is to summarize the recent discoveries involving the study of synchronization in coupled chaotic systems. As we will see, not always the word *synchronization* will be taken as having the same colloquial meaning, and we will need to specify what synchrony means in all particular contexts in which we will describe its emergence.

As a preliminary definition, we will refer to *synchronization* of chaos as a process wherein two (or many) chaotic systems (either equivalent or nonequivalent) adjust a given property of their motion to a common behavior, due to coupling or forcing. This ranges from complete agreement of trajectories to locking of phases.

The first thing to be highlighted is that there is a great difference in the process leading to synchronized states, depending upon the particular coupling configuration. Namely, one should distinguish two main cases: unidirectional coupling and bidirectional coupling. In the former case, a global system is formed by two subsystems, that realize a drive–response (or master–slave) configuration. This implies that one subsystem evolves freely and drives the evolution of the other. As a result, the response system is slaved to follow the dynamics (or a proper function of the dynamics) of the drive system, which, instead, purely acts as an external but chaotic forcing for the response system. In such a case external synchronization is produced. Typical examples are communication with chaos. A very different situation is the one described by a bidirectional coupling. Here both subsystems are coupled with each other, and the coupling factor induces an adjustment of the rhythms onto a common synchronized manifold, thus inducing a mutual synchronization behavior. This situation typically occurs in physiology, e.g. between cardiac and respiratory systems or between interacting neurons or in nonlinear optics, e.g. coupled laser systems with feedback. These two processes are very different not only from a philosophical point of view: up to now no way has been discovered to reduce one process to another, or to link formally the two cases. Therefore, along this report, we will summarize the major results in both situations, trying to emphasize the different dynamical mechanisms which rule the emergence of synchronized features.

In the context of coupled chaotic elements, many different synchronization states have been studied in the past 10 years, namely complete or identical synchronization (CS) [4–6], phase (PS) [7,8] and lag (LS) synchronization [9], generalized synchronization (GS) [10,11], intermittent lag synchronization (ILS) [9,12], imperfect phase synchronization (IPS) [13], and almost synchronization (AS)

[14]. All these phenomena will be referred to in this report, along with the most relevant examples in which their occurrence was found.

CS was the first discovered and is the simplest form of synchronization in chaotic systems. It consists in a perfect hooking of the chaotic trajectories of two systems which is achieved by means of a coupling signal, in such a way that they remain in step with each other in the course of the time. This mechanism was first shown to occur when two identical chaotic systems are coupled unidirectionally, provided that the conditional Lyapunov exponents of the subsystem to be synchronized are all negative [6].

GS goes further in using completely different systems and associating the output of one system to a given function of the output of the other system [10,11].

Coupled nonidentical oscillatory or rotatory systems can reach an intermediate regime (PS), wherein a locking of the phases is produced, while correlation in the amplitudes remain weak [7]. The transition to PS for two coupled oscillators has been firstly characterized with reference to the Rössler system [7].

LS is a step between PS and CS. It implies the asymptotic boundedness of the difference between the output of one system at time t and the output of the other shifted in time of a lag time τ_{lag} [9]. This implies that the two outputs lock their phases and amplitudes, but with the presence of a time lag [9].

ILS implies that the two systems are most of the time verifying LS, but intermittent bursts of local nonsynchronous behavior may occur [9,12] in correspondence with the passage of the system trajectory in particular attractor regions wherein the local Lyapunov exponent along a globally contracting direction is positive [9,12].

Analogously, IPS is a situation where phase slips occur within a PS regime [13].

Finally, AS results in the asymptotic boundedness of the difference between a subset of the variables of one system and the corresponding subset of variables of the other system [14].

The first scenario of transition among different types of synchronization was described for symmetrically coupled nonidentical systems and consisted in successive transitions between PS, LS and a regime similar to CS when increasing the strength of the coupling [9].

The natural continuation of these pioneering works was to investigate synchronization phenomena in spatially extended or infinite dimensional systems [15–20], to test synchronization in experiments or natural systems [21–32], and to study the mechanisms leading to desynchronization [33,34]. These topics will be treated specifically in different sections of this report.

1.2. Outline of the report

The present report is organized as follows.

In Section 2 we describe the complete synchronization phenomenon, both for low and for high-dimensional situations, and illustrate possible applications of the introduced techniques in the field of communicating with chaos.

In Section 3 we move from identical to nonidentical systems, and summarize the concepts of phase synchronization, lag synchronization, imperfect phase synchronization, and generalized synchronization. We also describe a general transition scenario between a hierarchy of different types of synchronization for chaotic oscillators.

In Section 4 we further extend to the case of structurally different systems. Here, collective dynamics may emerge in the case of a coupling between systems which are confined onto chaotic attractors with different structural properties. Analogies and differences with structurally equivalent systems are pointed out.

In Section 5 we discuss the situation of uncoupled systems subjected to a common external source, and we summarize the main results related to noise-induced synchronization. Furthermore, we analyze the case of weakly coupled systems, where synchronization is enhanced by the action of external noise.

Section 6 is devoted to the discussion of synchronization between space-extended systems. We first describe the situation of a large ensemble of coupled chaotic elements, and then move to the case of continuous space-extended systems, i.e. systems extended in space whose evolution is ruled by partial differential equations.

Finally, in Section 7 we summarize the main synchronization features observed so far in laboratory experiments and in natural phenomena, with a particular attention to the data analysis tools which are nowadays used to detect epochs of synchronization in practical situations.

2. Synchronization of identical systems

2.1. Complete synchronization

As said in the Section 1, chaotic systems are dynamical systems that defy synchronization, due to their essential feature of displaying high sensitivity to initial conditions. As a result, two identical chaotic systems starting at nearly the same initial points in phase space develop onto trajectories which become uncorrelated in the course of the time. Nevertheless, it has been shown that it is possible to synchronize these kinds of systems, to make them evolving on the same chaotic trajectory [4–6,35,36].

When one deals with coupled identical systems, synchronization appears as the equality of the state variables while evolving in time. We refer to this type of synchronization as *complete synchronization* (CS). Other names were given in the literature, such as *conventional synchronization* [37] or *identical synchronization*.

In this section, we will discuss main properties of this kind of synchronization. While our discussion will focus on continuous systems, most of the exposed ideas can be easily extended to discrete systems, such as chaotic mappings.

As for the coupling, one has to distinguish between two different situations. When the evolution of one of the coupled systems is unaltered by the coupling, the resulting configuration is called *unidirectional coupling* or *drive–response coupling*. On the contrary we will refer to *bidirectional coupling* when both systems are connected in such a way that they mutually influence each other's behavior. Inside this classification, the appearance and robustness of synchronization states have been established by means of several different coupling schemes, such as the Pecora and Carroll method [6,36,38], the negative feedback [39], the sporadic driving [40], the active–passive decomposition [41,42], the diffusive coupling and some other hybrid methods [43]. A description and analysis of some different coupling schemes is given in Ref. [44] in a single mathematical framework.

In the following we will concentrate our attention to explain the essential points of two particular coupling schemes, namely the Pecora and Caroll ($\mathscr{PC}$) method and the active–passive decomposition ($\mathscr{APD}$) method. Furthermore, we will discuss the very relevant issue of the stability of the synchronized motion.

2.2. The $\mathscr{PC}$ configuration

Let us begin by considering a chaotic system whose temporal evolution is ruled by the following equation:

$$\dot{\mathbf{z}} = \mathbf{F}(\mathbf{z}) \,. \tag{2.1}$$

Here $\mathbf{z} \equiv \{z_1, z_2, \ldots, z_n\}$ is a n-dimensional state vector, with $\mathbf{F}$ defining a vector field $\mathbf{F}: R^n \to R^n$.

The $\mathscr{PC}$ scheme consists in supposing the dynamical system of Eq. (2.1) to be *drive decomposable*, i.e. to be divisible into three subsystems

$$\left.\begin{aligned} \dot{\mathbf{u}} &= \mathbf{f}(\mathbf{u}, \mathbf{v}) \\ \dot{\mathbf{v}} &= \mathbf{g}(\mathbf{u}, \mathbf{v}) \end{aligned}\right\} \text{driver} \,,$$

$$\left.\begin{aligned} \dot{\mathbf{w}} &= \mathbf{h}(\mathbf{u}, \mathbf{w}) \end{aligned}\right\} \text{response} \,, \tag{2.2}$$

where $\mathbf{u} \equiv \{u_1, u_2, \ldots, u_m\}$, $\mathbf{v} \equiv \{v_1, v_2, \ldots, v_k\}$, $\mathbf{w} \equiv \{w_1, w_2, \ldots, w_l\}$ and $n = m + k + l$. The first subsystem of Eqs. (2.2) defines the *driver* system, whereas the second subsystem of Eqs. (2.2) represents the *response* system, whose evolution is guided by the driver trajectory by means of the driving signal $\mathbf{u}$.

In this framework, complete synchronization is defined as the identity between the trajectories of the response system $\mathbf{w}$ and of one replica $\mathbf{w}'$ of it $\dot{\mathbf{w}}' = \mathbf{h}(\mathbf{u}, \mathbf{w}')$ for the same chaotic driving signal ($\mathbf{u}(t)$). The existence of CS implies that the response system is asymptotically stable ($\lim_{t\to\infty} \mathbf{e}(t) = 0$, $\mathbf{e}(t)$ being the *synchronization error* defined by $\mathbf{e}(t) \equiv \|\mathbf{w} - \mathbf{w}'\|$). In other words, the response system *forgets* its initial conditions, though evolving on a chaotic attractor.

Refs. [6,36] establish that this kind of synchronization can be achieved provided that all the Lyapunov exponents of the response system under the action of the driver (the *conditional Lyapunov exponents*) are negative (see Section 2.5). Such a condition can be met if $\mathbf{u}$ is a *synchronizing signal*. However, given a chaotic system, not all possible selections of the driving signal lead to a synchronized state, as we will show momentarily.

Let us build a $\mathscr{PC}$ drive–response configuration with a drive system given by the Lorenz system and with a response system given by the subspace containing the (x, z) variables [45]

$$\left.\begin{aligned} \dot{x} &= \sigma(y - x) \\ \dot{y} &= -xz + rx - y \\ \dot{z} &= xy - bz \end{aligned}\right\} \text{driver} \,,$$

$$\left.\begin{aligned} \dot{y}' &= -xz' + rx - y' \\ \dot{z}' &= xy' - bz' \end{aligned}\right\} \text{response} \,. \tag{2.3}$$

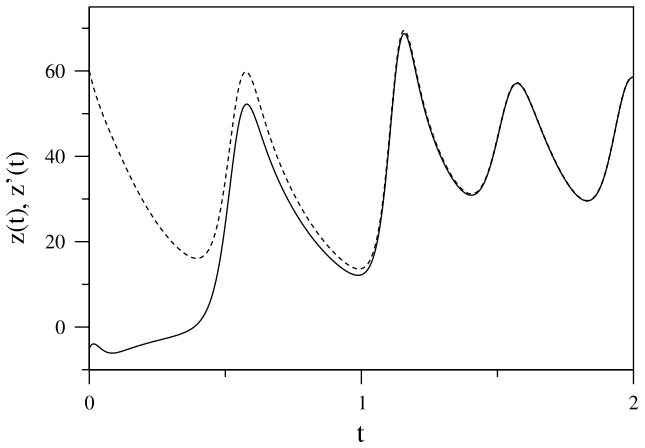

Fig. 2.1. Complete synchronization of system given by Eq. (2.3), dashed line (solid line) represents z (z') in function of time.

Table 2.1
Conditional Lyapunov exponents for different drive–response configurations of the Lorenz system [27]

System	Drive	Response	Lyapunov exponents
Lorenz	x	(y,z)	$(-2.5,-2.5)$
$\sigma=16,\ b=4,\ r=45.92$	y	(x,z)	$(-3.95,-16.0)$
	z	(x,y)	$(+7.89\times10^{-3},-17.0)$

Here $\sigma=16$, $r=45.92$ and $b=4$, so as Eqs. (2.3) give rise to a chaotic dynamics. With this particular choice of the driving, CS sets in rather soon as shown in the Fig. 2.1. It is important to remark that the configuration of Eqs. (2.3) is called a *homogeneous driving* configuration, insofar as $\mathbf{h}\equiv\mathbf{g}$.

By splitting the main system of Eq. (2.3) in a different way, CS could not exist. In Table 2.1 we report the conditional Lyapunov exponents for all possible drive–response subsystems into which one can divide the Lorenz system. Only two choices induce the appearance of CS, namely (x,z) driven by y and (y,z) driven by x. For the other possible choice ((x,y) driven by z), CS comes out to be unstable. A detailed discussion over the CS features of the Lorenz system can be found in Ref. [46].

While the $\mathscr{PC}$ configuration is not the most general way to couple dynamical systems, this scheme and the one considered in Ref. [5] were proposed with the idea of considering *explicitly* chaotic synchronization as a new and important concept. Other previous and contemporary studies had surfaced this idea in the analysis of arrays of coupled systems [4,47]. For a detailed discussion on this latter situation we address the reader to Section 6 of the present report.

In the following section, before discussing the stability of the complete synchronized state, we will describe an alternative coupling configuration for a drive–response scheme.

2.3. The $\mathscr{APD}$ configuration

Ref. [41] introduced a very general driver–response scheme in order to construct identical chaotic synchronized systems, called *the active–passive decomposition method* ($\mathscr{APD}$). This method explicitly treats a chaotic autonomous system and rewrites it as a nonautonomous system

$$\dot{\mathbf{x}} = \mathbf{f}(\mathbf{x}, \mathbf{s}(t)) \,, \tag{2.4}$$

where $s(t)$ is some driving signal $\mathbf{s} = \mathbf{h}(\mathbf{x})$ or $\dot{\mathbf{s}} = \mathbf{h}(\mathbf{x})$, and $\mathbf{f} : R^n \to R^n$. Again, the complete synchronized state refers to the identity between the system of Eq. (2.4) and one replica (the response system) that is driven by the same signal $s(t)$. Note that this latter statement does not exclude a chaotic behavior of $\mathbf{x}(t)$, since it is driven by a chaotic signal $s(t)$.

In order to illustrate this configuration, Ref. [41] analyzed the following scheme for a Lorenz system

$$\begin{aligned} \dot{x} &= -10x + s(t) \,, \\ \dot{y} &= 28x - y - xz \,, \\ \dot{z} &= xy - 2.666z \end{aligned} \tag{2.5}$$

driven by $s(t) = h(\mathbf{x}) = 10y$, and by the use of a Lyapunov function showed that the response system synchronizes with its copy for all considered types of driving signal $\mathbf{s}(t)$.

While the $\mathscr{PC}$ scheme (previous section) allows for a given chaotic system only a finite number of possible decompositions to produce synchronization, here the freedom to choose the driving signal $\mathbf{s}(t)$ (or alternatively the function $\mathbf{h}(\mathbf{x})$) makes the $\mathscr{APD}$ scheme very powerful and general, due to its extreme flexibility in applications.

The two synchronization schemes described here and several other drive–response configurations have been used into the design of communication devices, which is perhaps the most promising application of synchronized chaotic behavior [42,43,48–50]. For example, one can have two remote systems behaving chaotically, but synchronized with each other through only one driving signal. A sender can add a given message to the drive, thus masking the information from any third party who wants to intercepts it. The receiver can extract the message by using the synchronization error between the drive and the regenerated signal, where the message appears as desynchronization episodes (see Section 7).

2.4. Complete synchronization for bidirectional coupling

A bidirectional coupling scheme between identical chaotic systems is tantamount to introducing additional dissipation in the dynamics:

$$\begin{aligned} \dot{\mathbf{x}} &= \mathbf{f}(\mathbf{x}) + \hat{\mathbf{C}} \cdot (\mathbf{y} - \mathbf{x})^{\mathrm{T}} \,, \\ \dot{\mathbf{y}} &= \mathbf{f}(\mathbf{y}) + \hat{\mathbf{C}} \cdot (\mathbf{x} - \mathbf{y})^{\mathrm{T}} \,. \end{aligned} \tag{2.6}$$

Here $\mathbf{x}$ and $\mathbf{y}$ represent the N-dimensional state vectors of the chaotic systems, while $\mathbf{f}$ is a vector field $\mathbf{f} : R^n \to R^n$. Finally, $\hat{\mathbf{C}}$ is a $n \times n$ matrix whose coefficients rule the dissipative coupling. T represent matrix transposition.

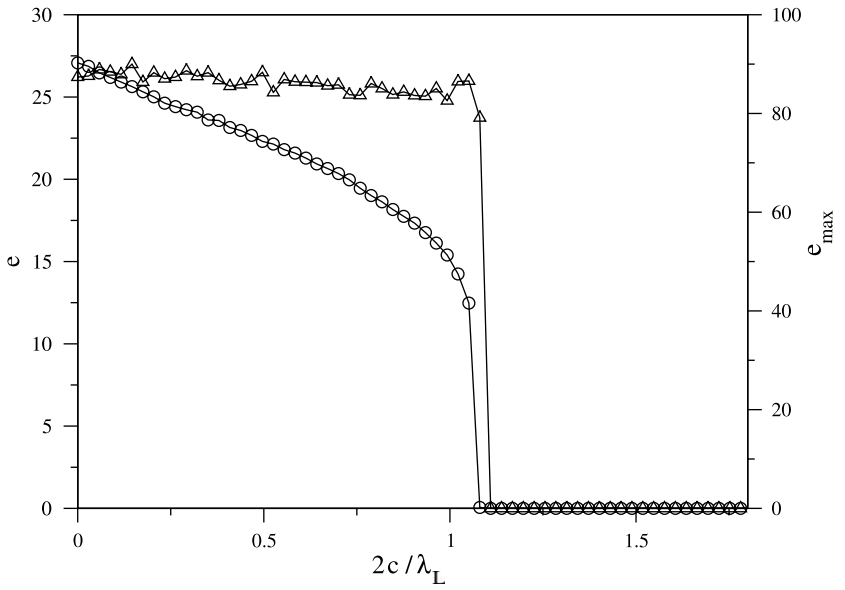

Fig. 2.2. The mean synchronization error $\langle e\rangle \equiv \langle\sqrt{(x_2-x_1)^2+(y_2-y_1)^2+(z_2-z_1)^2}\rangle$ (o) and $e_{\max} \equiv \mathrm{Max}\,(e)$ ($\triangle$) vs. the coupling strength c for the system given by Eq. (2.7).

When increasing the coupling strength (the coefficients of $\hat{\mathbf{C}}$), system (2.6) displays a transition to a complete synchronized state at a critical value of the coupling that depends on the particular structure of the coupling matrix. In particular, when $\hat{\mathbf{C}} = c\hat{\mathbf{I}}$, both systems synchronize completely for $c > \frac{1}{2}\lambda_L$ (λ_L being the largest Lyapunov exponent of the uncoupled chaotic systems [4]). The reason for this transition is that the long-term behavior of the coupled systems is determined by two counterbalancing strengths, namely the action of the instability of the synchronization manifold and that of the diffusion. As a result, when the diffusion overcomes the instability, the systems synchronize.

This coupling scheme can be illustrated by referring to a pair of bidirectionally coupled Lorenz systems [45]

$$\begin{aligned}
\dot{x}_{1,2} &= \sigma(y_{1,2} - x_{1,2}) + c(x_{2,1} - x_{1,2})\,,\\
\dot{y}_{1,2} &= (r - z_{1,2})x_{1,2} - y_{1,2} + c(y_{2,1} - y_{1,2})\,,\\
\dot{z}_{1,2} &= x_{1,2} - bz_{1,2} + c(z_{2,1} - z_{1,2})\,.
\end{aligned} \tag{2.7}$$

Parameters are chosen to be $\sigma = 16.0$, $b = 4.0$, $r = 40.0$ in order to produce a chaotic dynamics in the uncoupled systems. For this choice, the Lyapunov exponents of each uncoupled Lorenz system are $\lambda_1 = 1.37$, $\lambda_2 = 0.0$ and $\lambda_3 = -22.37$. Fig. 2.2 shows the mean synchronization error e defined as the averaged distance to the synchronization manifold, i.e. the identity hyperplane ($\mathbf{x} = \mathbf{y}$), and the maximum distance $e_{\max}$ to this manifold as a function of the coupling strength c.

This coupling scheme (Eq. (2.6)) is effective in completely synchronizing the dynamical variables of the chaotic systems, due to the additional dissipation introduced whenever they are not

following the same trajectory $\mathbf{x}_1(t) \neq \mathbf{x}_2(t)$, $\mathbf{x}_1$ and $\mathbf{x}_2$ being the state vectors of the coupled systems of Eq. (2.7).

2.5. The stability of the synchronized motion

Stability of the synchronized motion is a very relevant issue, and many criteria have been established in the literature to cope with it. One of the most popular and widely used criterion is the use of the Lyapunov exponents as average measurements of expansion or shrinkage of small displacements along the synchronized trajectory. Along the present section, we will summarize this and other criteria designed to characterize the stability of the complete synchronized state of identical coupled chaotic systems and we will describe the transition between the nonsynchronized state and the synchronized one.

The stability problem of identical coupled systems can be formulated in a very general way by addressing the question of the stability of the CS synchronization manifold $\mathbf{x} \equiv \mathbf{y}$, or equivalently by studying the temporal evolution of the synchronization error $\mathbf{e} \equiv \mathbf{y} - \mathbf{x}$ ($\mathbf{x}$ and $\mathbf{y}$ being the state vectors of the coupled systems). The evolution of $\mathbf{e}$ is given by

$$\dot{\mathbf{e}} = \mathbf{f}(\mathbf{x}, \mathbf{s}(t)) - \mathbf{f}(\mathbf{y}, \mathbf{s}(t)) \,, \tag{2.8}$$

where $\mathbf{x}$ and $\mathbf{y}$ represent the state vectors of the response system and its replica. Eq. (2.8) can be written in both $\mathscr{PC}$ and $\mathscr{APD}$ schemes, since it explicitly includes the driving signal $\mathbf{s}(t)$.

A CS regime exists when the synchronization manifold is asymptotically stable for all possible trajectories $\mathbf{s}(t)$ of the driving system within the chaotic attractor. This property can be proved by using stability analysis of the linearized system for small $\mathbf{e}$

$$\dot{\mathbf{e}} = \mathbf{D}_{\mathbf{x}}(\mathbf{s}(t))\mathbf{e} \,, \tag{2.9}$$

where $\mathbf{D}_{\mathbf{x}}$ is the Jacobian of the vector field $\mathbf{f}$ evaluated onto the driving trajectory $\mathbf{s}(t)$. Normally, when the driving trajectory $\mathbf{s}(t)$ is constant (fixed point) or periodic (limit cycle), the study of the stability problem can be made by means of evaluating the eigenvalues of $\mathbf{D}_{\mathbf{x}}$ or the Floquet multipliers [51,52]. However, if the response system is driven by a chaotic signal, this method will not work.

A possible solution is calculating the Lyapunov exponents of system equation (2.9). In the context of driver–response coupling schemes, these exponents are usually called *conditional Lyapunov exponents* because they are the Lyapunov exponents of the response system under the explicit constrain that they must be calculated on the trajectory $\mathbf{s}(t)$ [36,41]. Alternatively, they are called *transversal Lyapunov exponents* because they correspond to directions which are transverse to the synchronization manifold $\mathbf{x} \equiv \mathbf{y}$ [43,53]. These exponents could be defined, for an initial condition of the driver signal $\mathbf{s}_0$ and initial orientation of the infinitesimal displacement $\mathbf{u}_0 = \mathbf{e}(0)/|\mathbf{e}(0)|$ as

$$\begin{aligned} h(\mathbf{s}_0, \mathbf{u}_0) &\equiv \lim_{t\to\infty} \frac{1}{t} \ln\left(\frac{|\mathbf{e}(t)|}{|\mathbf{e}_0|}\right) \\ &= \lim_{t\to\infty} \frac{1}{t} \ln |\mathbf{Z}(\mathbf{s}_0, t) \cdot \mathbf{u}_0| \,, \end{aligned} \tag{2.10}$$

where $\mathbf{Z}(\mathbf{s}_0, t)$ is the matrix solution of the linearized equation

$$\mathrm{d}\mathbf{Z}/\mathrm{d}t = \mathbf{D}_{\mathbf{x}}(\mathbf{s}(t))\mathbf{Z} \tag{2.11}$$

subject to the initial condition $\mathbf{Z}(\mathbf{0}) = \mathbf{I}$. The synchronization error $\mathbf{e}$ evolves according to $\mathbf{e}(t) = \mathbf{Z}(\mathbf{s}_0, t)\mathbf{e}_0$ and then the matrix $\mathbf{Z}$ determines whether this error shrinks or grows in a particular direction. In most cases, however, the calculation cannot be made analytically, and therefore numerical algorithms should be used [54–56].

It is very important to emphasize that the negativity of the conditional Lyapunov exponents is only a necessary condition for the stability of the synchronized state. The conditional Lyapunov exponents are obtained from a temporal average, and therefore they characterize the global stability over the whole chaotic attractor. Relevant cases exist where these exponents are negative and nevertheless the system is not perfectly synchronized, thus indicating that additional conditions should be fulfilled to warrant synchronization in a necessary and sufficient way [57].

While this criterion has been successfully used in order to predict and study the stability of the synchronized motion [6,36,42,43], it is in general hard to get accurate approximations of Lyapunov exponents, so that the application of alternative criteria may be in order in practical cases.

The stability of a CS manifold can also be studied by the use of the Lyapunov function [41,48,58], a method giving necessary and sufficient conditions for stability. With reference to the study of temporal evolution of the synchronization error $\mathbf{e}$ (Eq. (2.8)), the Lyapunov Function $\mathscr{L}(\mathbf{e})$ can be defined as a continuously differentiable real valued function with the following properties:

(a) $\mathscr{L}(\mathbf{e}) > 0$ for all $\mathbf{e} \neq \mathbf{0}$ and $\mathscr{L}(\mathbf{e}) = 0$ for $\mathbf{e} = \mathbf{0}$.
(b) $\mathrm{d}\mathscr{L}/\mathrm{d}t < 0$ for all $\mathbf{e} \neq \mathbf{0}$.

If for a given coupled system one can find a Lyapunov function, then the CS manifold is globally stable.

To give an example of the use of this function, we follow Ref. [41] and consider the drive–response system given by Eq. (2.5). Here, the vector (x, y, z) refers to the response and the vector (x', y', z') to its replica. One should note first that the component of the synchronization error $e_1 \equiv x' - x$ converge to zero because $\dot{e}_1 = -10e_1$. Therefore, the evolution of the remaining two components for the limit $t \to \infty$, is given by

$$\dot{e}_2 = -e_2 - xe_3 \ ,$$

$$\dot{e}_3 = xe_2 - 2.666e_3 \ . \tag{2.12}$$

One can show that the complete synchronization manifold is globally stable for any choice of the driving signal $s(t)$ considering $\mathscr{L}(\mathbf{e}) \equiv e_2^2 + e_3^2$ and showing that $\mathrm{d}\mathscr{L}/\mathrm{d}t = -2(e_2^2 + 2.666e_3^2)$, which fulfills both conditions defining a Lyapunov function.

Unfortunately, whether such functions exist and how one should construct them is known only in a very limited number of cases, whereas a general procedure to obtain these functions is not yet available.

A further criterion for the stability of synchronized states is given in Refs. [59,60]. The equation of the linearized system for the synchronization error $\mathbf{e}$ (Eq. (2.8)) is divided into a time independent part $\mathbf{A}$ and an explicitly time dependent part $\mathbf{B}(\mathbf{x}, t)$

$$\mathbf{e} = \mathbf{A} + \mathbf{B}(\mathbf{x}, t) \ . \tag{2.13}$$

Assuming that **A** can be diagonalized and transformed into the coordinate system defined by the eigenvectors of **A**, the following sufficient condition for the stability of the synchronization manifold is obtained

$$-\mathrm{Re}[\lambda_m] > \langle \|\mathbf{P}^{-1}\mathbf{B}\mathbf{P}\| \rangle \ . \tag{2.14}$$

Here, $\mathrm{Re}[\lambda_m]$ is the real part of the largest eigenvalue of **A** and $\mathbf{P} \equiv [v_1, v_2, \ldots, v_d]$ where v_j are the eigenvectors of **A**. $\langle \bullet \rangle$ denotes a time average along the driving trajectory. The reason why this condition is only sufficient relies in the fact that it is based in matrix norms. As a result, a driving configuration may fail the above condition and still produce stable synchronized motion.

We have addressed the stability problem of synchronized motion by referring to the stability of the CS synchronization manifold, i.e. $\mathbf{x} = \mathbf{y}$. When we deal with nonidentical coupled systems, similar stability criteria can be formulated, but additional problem will appear due to the more complicate structure of the synchronization manifold. We will outline this problem in the next section.

At this stage, let us summarize the validity of the stability criteria discussed above. Only Lyapunov functions give a necessary and sufficient condition for the stability of the synchronization manifold, whereas the negativity of the conditional Lyapunov exponents provides a necessary condition, and the criteria of Eq. (2.14) gives a sufficient one. While the Lyapunov function criterion gives a local condition for stability, the other two involve temporal averages over chaotic trajectories of the driving signal, and therefore they establish conditions for global stability. As a consequence, none of these latter criteria prevents from local desynchronization events that could occur within the CS manifold.

This point is discussed in Ref. [53], where the synchronized behavior of two chaotic circuits coupled in a drive–response configuration is studied. It is shown there that long CS intervals are interrupted by brief and persistent desynchronization events. To demonstrate that the Lyapunov exponents do not prevent from local desynchronization events, the average distance from the CS manifold $|X_\perp|_{\mathrm{rms}}$ and its maximal observed value $|X_\perp|_{\max}$ are measured. $|X_\perp|_{\mathrm{rms}}$ is sensitive to global stability, while $|X_\perp|_{\max}$ is sensitive to local stability of the CS state. Fig. 2.3 reports these quantities as well as the largest conditional exponent $\lambda_\perp^1$ against the coupling strength c. In order to predict this intermittent loss of synchronization, the authors of Ref. [53] propose two different parameters whose negativity would determine the local stability of the synchronization manifold. One of them is the maximal transverse Lyapunov exponent of the most unstable invariant set $\eta_\perp$, whose dependence on c is also shown in Fig. 2.3. Although this criterion rigorously and clearly predicts the synchronized state, its application may be difficult in practice, due to the infinite number of invariant sets where stability should be determined.

The appearance of these local desynchronized states, despite Lyapunov exponents are negative, is also related with a small parameter mismatch between the coupled systems and low levels of noise, which are unavoidable effects in experimental devices and in numerical integration. Now, we will address this problem describing the type of bifurcation appearing at the transition point between the nonsynchronized state and the synchronized one. We refer to this problem as the *desynchronization problem*.

As we have outlined in previous paragraphs, the phenomenon of chaotic synchronization is sometimes described in terms of invariant sets or invariant manifolds, in particular when we deal with the stability of the synchronization state. In order to explain the meaning of the invariant sets in this

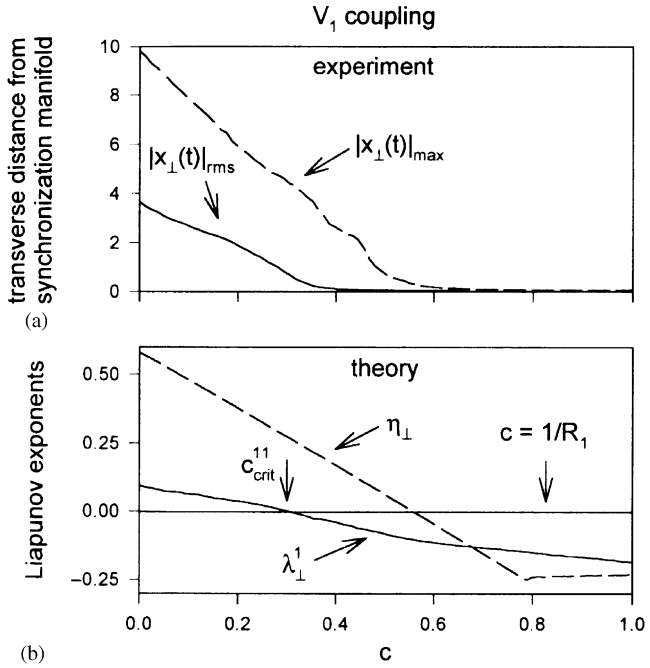

Fig. 2.3. (a) Degree of synchronization experimentally observed in coupled chaotic circuit. (b) Theoretically predicted stability of the synchronized state (see the text for a definition of different variables) [53].

context, let us refer to the coupling configuration given by Eq. (2.6). In this case, if the oscillators are synchronized at some instant of time, the coupling term is zero because both oscillators are identical and the coupling is given by the difference between the states of two oscillators. Then, the future evolution from any initial synchronized state is restricted to a set embedded in the entire phase space: the synchronized state set. This set is an invariant manifold $\mathscr{M}$ for any value of the coupling. Furthermore, in any synchronized state, the dynamics of the coupled systems are the same as that of a single free-running chaotic oscillator. Therefore, there is a chaotic attractor embedded in the synchronization manifold, where the systems would evolve if the dynamic could be restricted to this manifold.

This kind of problem, i.e. the existence of a chaotic attractor (A) embedded in an invariant manifold ($\mathscr{M}$) of the entire phase space, has attracted considerable attention in the past years beyond the desynchronization problem, especially about the conditions under which the attractor A is also an attractor of the entire phase space.

Ashwin et al. describe a possible mechanism for the loss of stability of the attractor A, which is called the *bubbling bifurcation* and it is entirely applicable to the desynchronization problem [61]. Let us describe the bubbling bifurcation in a general context. We consider the following situation. The transverse dynamics of the synchronization manifold is ruled by a parameter ε, but this parameter does not affect the dynamics on the invariant manifold, i.e. ε is the coupling parameter. There exists a critical value ε_c, such that for $\varepsilon > \varepsilon_c$ all invariant sets in the attractor A are stable with respect to perturbations transverse to the invariant manifold. As ε is decreased below ε_c an invariant set in A first

becomes unstable to perturbations transverse to the invariant manifold. For $\varepsilon > \varepsilon_c$ all the trajectories close to A asymptotically approaches A, i.e. the chaotic oscillators will eventually synchronize. When $\varepsilon < \varepsilon_c$, most initial conditions close to A remain close to A, but as a consequence of the existence of an unstable invariant set embedded in A, some initial conditions move far away from the invariant manifold containing A, evolving in a repelled orbit. This kind of transition at $\varepsilon = \varepsilon_c$ is the *bubbling transition* or the *bubbling bifurcation* [61,62].

At this point, we should consider two possible situations. If the dynamic system is such that the repelled orbits are attracted to a set off the invariant manifold, then it is said that the basin of attraction of A is *riddled* and it is referred as *riddling transition* [63–65]. After a riddling transition, the basin of attractor A appears as filled of "holes" which belongs to the basin of the other attractor. On the other hand, if the dynamical system is such that all possible trajectories are bounded and A is the only attractor of the entire phase space, then a trajectory repelled from A eventually returns to the vicinity of A after a transient, in which the orbit makes several excursions away from the invariant manifold. This transient phase appears as bursts that suddenly interrupts the typical behavior of any state variable at the synchronization state.

As the coupling parameter is further reduced away of ε_c, new sets in A lose their transverse stability. By means of this process, the invariant manifold $\mathscr{M}$ itself becomes transversely unstable at ε_b, leading to a new bifurcation, which is called the *blowout bifurcation* [66]. For $\varepsilon < \varepsilon_b$ all orbits are repelled from A.

In the case of coupled chaotic oscillators which are identical, the system exits from the synchronization state because A becomes unstable in the normal direction to $\mathscr{M}$. But, the bubbling and the riddling transitions can be triggered by very low levels of noise or by a small parameter mismatch between the coupled systems, then both can be observed as intermediate stages. Let us recall that this process can occur no matter how small is the mismatch or how low is the noise. As the coupling decreases from a fully synchronized state, the bubbling bifurcation happens when a periodic orbit embedded in the chaotic attractor A loses its stability in a direction transverse to $\mathscr{M}$. This kind of periodic orbits, which loses stability in a transverse direction, are called *saddle periodic orbits*. A saddle periodic orbit usually becomes unstable via a pitchfork (period-doubling) bifurcation which creates new unstable orbits outside of $\mathscr{M}$. As the coupling parameter is further reduced, new orbits in A lose their transverse stability leading to the creation of new unstable orbits outside $\mathscr{M}$. By means of this process the invariant manifold $\mathscr{M}$ itself becomes transversely unstable, leading to the blowout bifurcation.

This scenario for the desynchronization process has been described and analyzed in the case of coupled identical chaotic electronic circuits [61], and for coupled chaotic maps [33,67,68].

The dynamic of two coupled identical logistic maps is analyzed in the Ref. [67]. In this case, it is shown that the loss of synchronization via a sequence of bifurcations of saddle periodic orbits induces bubbling and riddling transition in the system. The bubbling bifurcation is determined by the bifurcation of a saddle periodic orbit embbeded in the attractor A, while the phenomenon of riddled basins occurs through a bifurcation of a periodic orbit outside $\mathscr{M}$.

In Ref. [68], the effects of noise and asymmetry on the bubbling transition are studied. It is shown that, in the presence of noise or asymmetry, the attractor A is replaced either by a chaotic transient or by an intermittently bursting time evolution. Scaling relations are derived for the average chaotic transient lifetime and for the average interburst time interval as a function of the strength of the asymmetry and the amplitude of the noise.

Different kinds of bubbling transition have been identified in Ref. [69]. In this work, it is shown that, as a parameter is varied through a critical value, the transition to bubbling can be "hard" (the bursts appear abruptly with large amplitude) or "soft" (the maximum burst amplitude increases continuously from zero). This parameter is associated with the asymmetry of the coupling between the systems.

When the coupled chaotic oscillators are nonidentical, the chaotic synchronization could occur in a more complicated synchronization manifold $\mathbf{x} = \phi(\mathbf{y})$ (see Section 3.6). The study of the desynchronization problem in this case has great relevance. In spite of the fact that a similar process of desynchronization can occur, the complicated topology of $\mathscr{M}$ can render a very problematic task to cope with the identification of bubbling-type or blowout-type bifurcations. This situation has been addressed in Ref. [33]. This work analyzed the desynchronization problem in the case of a driver–response configuration of coupled maps, where a continuous differentiation between the driver and the response takes place decreasing the coupling parameter. It proposed a method that allows to describe the desynchronization problem by using a subsystem decomposition based on the identification of unstable periodic orbits of the driver. By means of this formalism, the creation and evolution of the complicated set of orbits that develops outside of the synchronization manifold is described. This set is called the emergent set. A critical transition point of this process is also identified. In addition, it is shown that the desynchronization process takes place first by means of the migration of the set of unstable periodic orbits embedded in the attractor A. This migration appears to occur before any orbit loses its transverse stability. As the coupling parameter is decreased the orbits' stability properties evolve in its migration, until a bubbling-type bifurcation occurs.

Before describing the chaotic synchronization of nonidentical systems, we mention an interesting subject appeared recently, the so called "anticipating synchronization" [70]. It shows that some kinds of coupled chaotic systems might synchronize so as their response "anticipates" the drivers, by synchronizing with their future states. In Ref. [70] different unidirectional coupling schemes of identical systems are considered, such as a nonlinear time-delayed feedback either in the driver or in both coupled systems. The results elucidate that the *anticipating synchronization manifold* (where the response anticipates the driver) can be globally stable due to the interplay between delayed feedback and dissipation, for any relatively small value of the lag time between response and driver. Furthermore, two coupled Rössler systems are considered where the nonlinear time-delayed term is introduced in the dissipative coupling. In this latter case, the anticipating synchronization manifold is stable only for small delays. In addition, it has been shown that it is possible to achieve anticipation times larger than characteristic time scales of the system's dynamics, thus introducing a novel way of reducing the unpredictability of chaotic dynamics [71].

3. Synchronization in nonidentical low-dimensional systems

In the last section, it has been shown that when identical chaotic systems are coupled properly with strong-enough coupling strength, they can achieve complete synchronization by following the same chaotic trajectory. Synchronization in this case is associated with the transition of the largest transverse Lyapunov exponents of the synchronization manifold from positive to negative values.

However, experimental and even more real systems are often not fully identical, especially there are mismatches in parameters of the systems. It is thus important and also interesting to investigate

synchronization behavior between nonidentical systems. In general, completely identical synchronization may not be expected in nonidentical systems because there does not exist such an invariant manifold $\mathbf{x} = \mathbf{y}$. In this section, we describe different types of synchronization behavior in coupled nonidentical low-dimensional chaotic systems. For chaotic oscillators, starting from uncoupled non-synchronized oscillatory systems, with the increase of coupling strength, firstly a rather weak degree of synchronization, the *phase synchronization* (PS) [7], may occur where the suitably defined phases of the chaotic oscillators become locked, while the amplitudes remain highly uncorrelated. If the chaotic oscillations cover a broad range of time scales (periods of unstable orbits), the phases will not fully synchronize, but synchronization epochs are interrupted by intermittent phase slips. This phenomenon is called *imperfect phase synchronization* [13]. Further increase of the coupling strength moves the system into a regime of a stronger degree of synchronization, where also the amplitudes become strongly correlated. There the states of the two chaotic oscillators become effectively identical with a proper shifting of time, known as *lag synchronization* (LS) [9]. At stronger coupling strengths, the time lag almost approaches zero, and two nonidentical systems become almost completely synchronized.

When different chaotic systems $\dot{\mathbf{x}} = \mathbf{f}_1(\mathbf{x})$ and $\dot{\mathbf{y}} = \mathbf{f}_2(\mathbf{y})$ are coupled with a strong enough coupling strength, the dynamics is constrained to a subspace in the whole phase space of the system $(\mathbf{x}, \mathbf{y})$. Due to the nonidentity, this subspace is not $\mathbf{x} = \mathbf{y}$, but a more complicated functional relationship, e.g. $\mathbf{y} = \mathbf{h}(\mathbf{x})$ may be established between both subsystems. Known as *generalized synchronization* (GS) [10,41], this hidden synchronization behavior can be regarded as a generalization of complete synchronization where the function takes the special form of identity function.

In phase synchronization of coupled chaotic oscillators, only phases of the subsystems are locked, while the dynamics is hyper-chaotic; in generalized synchronization, the dynamics of the coupled systems is restricted to a manifold which is often very complicated. In both cases, synchronization is hidden and special tools are required for detecting it, especially in experimental and natural systems where most likely the only accessible information is a recorded nonlinear time series of the subsystems.

3.1. Phase synchronization of chaotic systems

3.1.1. Synchronization of periodic oscillators

We start with the classical notion of synchronization of two coupled periodic oscillators, usually defined as locking of the phases $\phi_{1,2}$ with a ratio $n:m$ (n and m are integers), i.e. $|n\phi_1 - m\phi_2| < \text{const}$. As a result of phase synchronization, the frequencies $\omega_i = \dot{\phi}_i$ are also locked, i.e. $n\omega_1 - m\omega_2 = 0$, while the amplitudes can be quite different, so that nonidentical periodic oscillators can be phase synchronized with each other by a rather weak coupling. Hence, PS of weakly coupled periodic oscillators can be described by the dynamics of the phase difference $\theta = n\phi_1 - m\phi_2$, i.e.

$$\dot{\theta} = \Delta\omega - C\sin\theta\ , \tag{3.1}$$

where $\Delta\omega = n\omega_1^0 - m\omega_2^0$ is the difference between the natural frequencies $\omega_{1,2}^0$ of the oscillators, and C is the coupling strength. Synchronization is achieved when the parameters satisfy

$$\left|\frac{\Delta\omega}{C}\right| \leqslant 1\ , \tag{3.2}$$

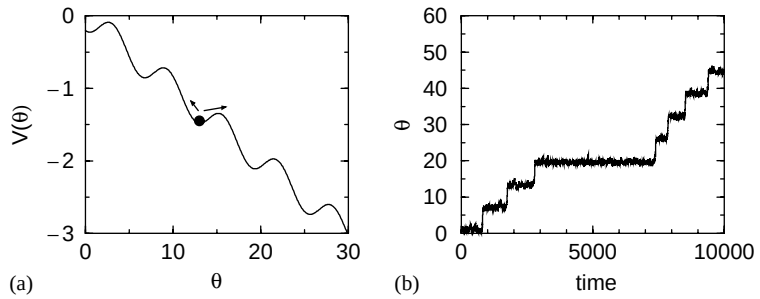

Fig. 3.1. (a) Systematic plot of the washboard potential $V(\theta) = -\theta\Delta\omega - C\cos\theta$ for the system equation (3.1). (b) Noise makes the phase difference θ fluctuate and induces phase slips.

which forms the synchronization region known as the Arnold tongue [72]. In the synchronization region, the system is stable at the fixed point $\theta_0 = \arcsin(\Delta\omega/C)$ which corresponds to a minimum of the washboard potential $V(\theta) = -\theta\Delta\omega - C\cos\theta$. In general, perfect phase synchronization and frequency locking are destroyed when the oscillators are in the presence of noise $\xi(t)$ which is unavoidable in experimental or real systems. The dynamics of the phase difference is now described by

$$\dot{\theta} = \Delta\omega - C\sin\theta + \xi(t)\ . \tag{3.3}$$

A detailed analytical description of this system is possible using the Fokker–Planck equation [73] if we assume the noise $\xi(t)$ to be Gaussian delta-correlated [74]. In general, noise makes the phase difference fluctuate around the minimum of the washboard potential $V(\theta)$, and climb over the energy barrier occasionally to move into the neighboring minima, as illustrated in Fig. 3.1(a). As a result, we can observe noise-induced 2π phase slips (Fig. 3.1(b)). PS in the presence of noise will be discussed in more detail in Sections 4 and 7 in the context of noise-induced PS and PS in experimental and natural systems.

Here we take the periodically driven Rössler oscillator [75] as an illustrative example:

$$\begin{aligned} \dot{x} &= -\omega y - z + E\sin(\Omega_e t)\ , \\ \dot{y} &= \omega x + a y\ , \\ \dot{z} &= f + z(x - c) \end{aligned} \tag{3.4}$$

with parameters $\omega = 0.97$, $f = 0.2$ and $c = 10$. When setting $a = 0.04$, the free Rössler oscillator exhibits a periodic motion with a frequency $\Omega = 0.981$. Fig. 3.2(a) shows that this periodic motion is locked with the ratio $n:m = 1:1$ to the weak external periodic signal with amplitude $E = 0.4$ and $\Omega_e = 1.0$. The whole Arnold tongue for $1:1$ synchronization is shown in Fig. 3.2(b).

3.1.2. Phase of chaotic signals

This classical notion of synchronization has recently been extended to chaotic oscillators [7]. Fig. 3.3(a) shows a time series $x(t)$ of autonomous chaotic oscillations in the Rössler oscillator of Eq. (3.4) for $a = 0.165$. To study phase synchronization of chaotic systems, the first important problem is to determine the time-dependent amplitude $A(t)$ and phase $\phi(t)$ of a chaotic signal. A

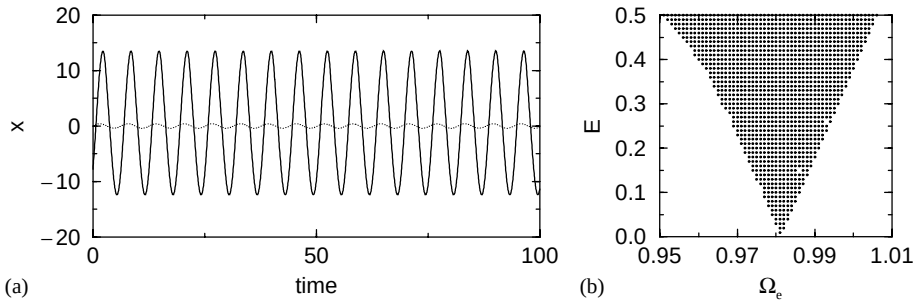

Fig. 3.2. (a) Synchronization of periodic oscillation (solid line) to a weak periodic driving signal (dotted line). (b) Arnold tongue of the 1 : 1 synchronization.

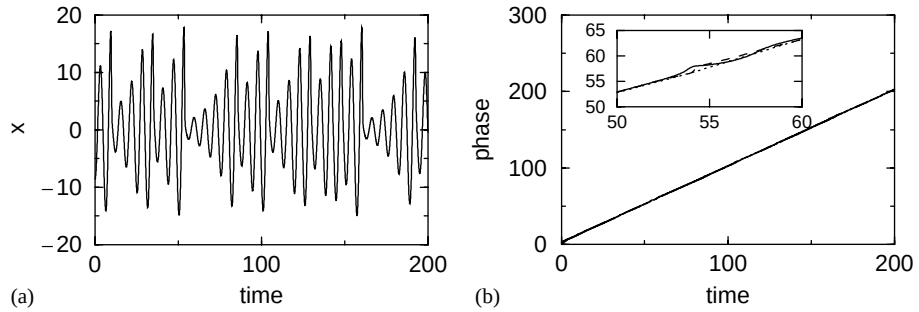

Fig. 3.3. (a) Chaotic signal $x(t)$ of the chaotic Rössler oscillator. (b) Phase of the chaotic signal. Solid line: phase of Eq. (3.5); dashed line: phase of Eq. (3.7); and dotted line: phase of Eq. (3.8).

few approaches have been proposed [7] to calculate phases of chaotic oscillators. Most generally, one can apply the analytic signal approach introduced by Gabor [76]. The analytic signal $\psi(t)$ is a complex function defined as

$$\psi(t) = s(t) + \mathrm{j}\tilde{s}(t) = A(t)\mathrm{e}^{\mathrm{j}\phi(t)} , \tag{3.5}$$

where the function $\tilde{s}(t)$ is the Hilbert transform of the observed scalar time series $s(t)$

$$\tilde{s}(t) = \frac{1}{\pi}\,\mathrm{P.V.}\int_{-\infty}^{\infty}\frac{s(\tau)}{t-\tau}\,\mathrm{d}\tau , \tag{3.6}$$

where P.V. stands for the Cauchy principal value for the integral.

If the flow of the chaotic oscillators has a proper rotation around a certain reference point, the phase can be defined in a more intuitive and straightforward way. For example, in the Rössler chaotic oscillators at $a=0.165$, the projection of the chaotic attractor into the x–y plane looks like a smeared limit cycle (see Fig. 3.4(a)), and the phase can be simply defined by the angle

$$\phi(t) = \arctan\left(y(t)/x(t)\right) . \tag{3.7}$$

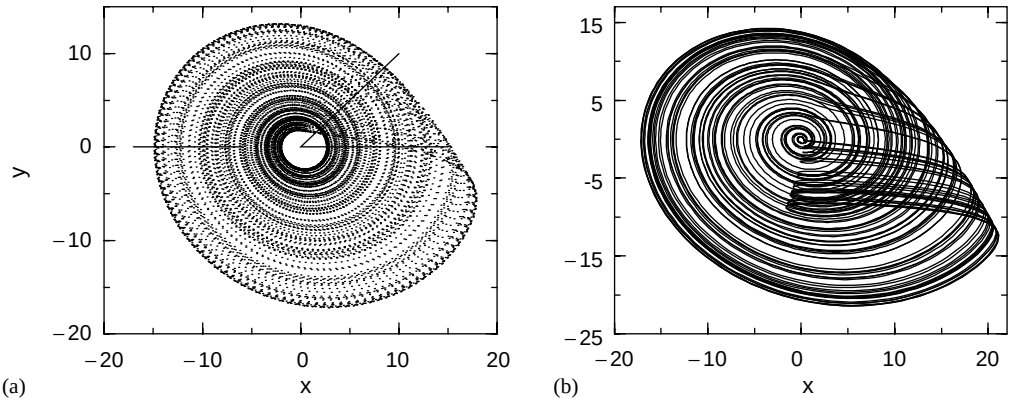

Fig. 3.4. Projection of the chaotic Rössler attractor on the x–y plane. (a) Phase coherent attractor. Phases of this attractor can be calculated with the analytic signal method, the Poincare' section (e.g. the heavy dashed line in the figure) or simply the rotation angle. Phase dynamics in this system is very coherent: the return time $\tau_k - \tau_{k-1}$ has only a rather narrow distribution. (b) Funnel chaotic Rössler attractor. Now it is difficult to define a phase variable for the system.

Phases of a chaotic flow can also be defined based on an appropriate Poincare' section with which the chaotic orbit crosses once for each rotation (Fig. 3.4(a)). Successive crossing with the Poincare' section can be associated with a phase increase of 2π and the phases in between can be computed with a linear interpolation, i.e.

$$\phi(t) = 2\pi k + 2\pi \frac{t - \tau_k}{\tau_{k+1} - \tau_k} \qquad (\tau_k < t < \tau_{k+1}), \tag{3.8}$$

where τ_k is the time of the kth crossing of the flow with the Poincare' section. As seen in Fig. 3.4(a), the successive maxima or minima of the chaotic time series correspond to a particular Poincare' section. This means that phase can be defined equivalently by examining the maxima or minima of the scalar chaotic time series without reconstruction of the dynamics in a higher dimensional phase space and finding a Poincare' section.

Fig. 3.3(b) shows phases calculated in these different ways for the chaotic signal in Fig. 3.3(a), and they are in very good agreement. But we have to emphasize that, there is so far no unique definition of a phase in chaotic oscillators. In spite of different definitions, phase is a monotonously increasing function of time. However, both Eqs. (3.5) and (3.7) reveal that phases are not increasing uniformly due to pronounced fluctuations in the amplitude of the signal (see inset in the Fig. 3.3(b) for $t \sim 55$). These fluctuations around the average linear increase can be characterized by the phase diffusion D_ϕ defined as

$$\langle (\phi(t) - \langle \phi(t) \rangle)^2 \rangle = 2D_\phi t \ , \tag{3.9}$$

where $\langle \cdot \rangle$ denotes ensemble average. D_ϕ measures the degree of phase coherence of the chaotic signal. As seen in Fig. 3.3(b), the fluctuation of the phase around the linear increase is almost invisible, and correspondingly a very small D_ϕ indicates that phase is very coherent in this case.

It is important to point out that the phase of a chaotic flow is closely related to the zero Lyapunov exponent in the autonomous chaotic systems [7]. The zero Lyapunov exponent corresponds

to the translation $d\mathbf{x}(t)$ along the chaotic trajectory. In a system where the chaotic flow has a proper rotation around a certain reference point, $d\mathbf{x}(\mathbf{t})$ can be uniquely mapped to a shift of the phases $d\phi(t)$ of the oscillator. Due to this connection, phase synchronization of chaotic oscillators can be manifested by a transition in the zero Lyapunov exponent, as will be shown later in this section.

However, a suitable phase variable may not be defined for a chaotic oscillator which is far from being phase coherent. An example is shown by the funnel chaotic attractor of the Rössler oscillator at $a = 0.25$ in Fig. 3.4(b). It is seen that the chaotic trajectory does not cycle the unstable fixed point in all rotations. If we define the phase with Eq. (3.7), it does not increase monotonously with time, and a proper Poincare' section crossing once with the chaotic trajectory in each rotation is not available now. Readers can find more detailed discussion on the definition of phase of chaotic oscillations in Refs. [74,77].

It is very helpful to put the definition of phase of chaotic oscillation on a more rigorous mathematical base, as performed in [72,77,78]. As shown above, for a chaotic oscillatory system $\dot{\mathbf{x}} = \mathbf{F}(\mathbf{x})$ it is frequently possible to define a phase $\phi(t)$ which increases almost linearly with a natural period T such that

$$|\phi(T + t) - \phi(t)|_{\mathrm{mod}\, 2\pi} < \eta \ll 1 \ , \tag{3.10}$$

which is equivalent to a small phase diffusion D_ϕ. Ref. [78] has proved that if in addition $\phi(t)$ is strictly increasing with time, then there *exists* a change of coordinates of radial distance $\mathbf{R}$ and phase Φ, $(\mathbf{R}, \Phi)$, in the neighborhood of the chaotic attractor of the system, such that

$$\begin{aligned} \dot{\mathbf{R}} &= \mathbf{F}(\mathbf{R}, \Phi) \ , \\ \dot{\Phi} &= 1 + \delta(\mathbf{R}, \Phi) \ , \end{aligned} \tag{3.11}$$

where Φ is T-periodic. With this coordinate transformation, the phase dynamics is similar to that of a periodic orbit, except that there is a term $\delta(\mathbf{R}, \Phi)$ showing a sensitivity to the $\mathbf{R}$ variables, which is required to be small, e.g. $\int_0^T \delta(\mathbf{R}, \phi)\, d\phi = O(\eta)$ with $\eta \ll 1$. Ref. [78] has developed an analytical tool for a quantitative description of the phase-locked states with such coordinates, and provides sufficient conditions for phase-locking to occur. This technique has been applied in [78] to a phase-coherent chaotic electric circuit model which can be viewed as a piece-wise linear simplification of the chaotic Rössler oscillator. The point we want to emphasize here is that, in the phase coherent chaotic oscillators, the phases defined in different ways are equivalent up to discrepancies of size at most η, according to rigorous mathematical consideration in Ref. [78], and they will lead to practically the same results in studying phase synchronization.

3.1.3. Phase synchronization of chaotic oscillators by external driving

Now we turn to demonstrate phase synchronization of chaotic oscillators by periodic driving. Here we illustrate the synchronization behavior with the system equation (3.4) in a chaotic regime with $a = 0.165$. As shown in Fig. 3.5, when the system is phase locked to the driving signal, the stroboscope of the system state (x, y) at each period of the driving signal is restricted to an arc area of the chaotic attractor, while it is distributed relatively uniformly over the whole attractor when the system is out of the phase-locking region. The whole synchronization region shown in Fig. 3.6 is

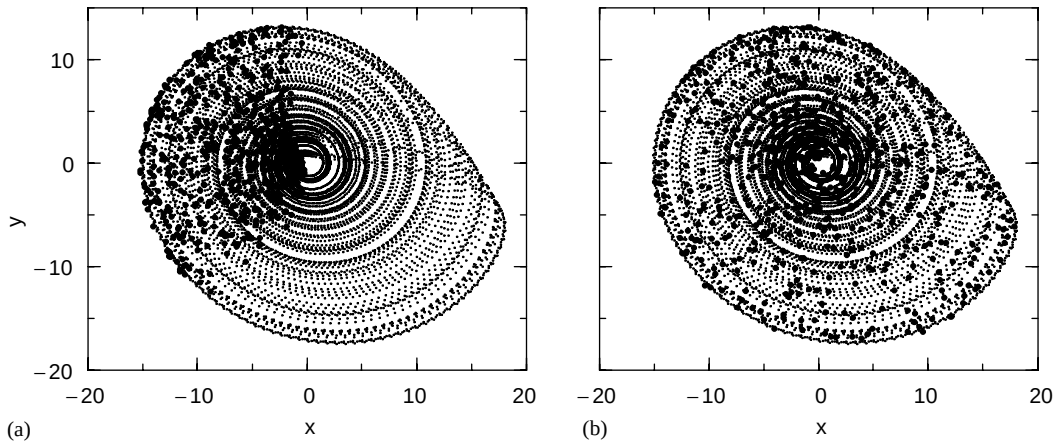

Fig. 3.5. Stroboscopic plot of the Rössler system state (x, y) (filled cycles) at each period of the driving signal (Eq. (3.4)). The dotted background is the unforced chaotic attractor. (a) $E = 0.15$, $\Omega_e = 1.0$, phase is synchronized. (b) $E = 0.15$, $\Omega_e = 1.02$, phase is not synchronized.

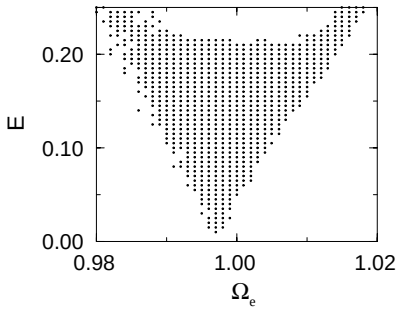

Fig. 3.6. Synchronization region of the chaotic Rössler oscillator by an external periodic force (Eq. (3.4)).

very similar to the Arnold tongue of the periodic oscillators in Fig. 3.2(b). These properties were firstly reported in Ref. [79] and studied more intensively in Ref. [74].

Intuitively, we can expect this similarity because we have noticed that the phases of phase-coherent chaotic oscillations increase almost linearly as in periodic oscillations. To obtain a deeper insight into this similarity and to reveal new features, we study phase synchronization of chaotic oscillators in terms of unstable periodic orbits [80,81]. A stroboscopic recording of the amplitude (denoted by x now) and phase ϕ of the chaotic signal at each period of the external force gives [80]

$$x(n+1) = f(x(n), \phi(n)),$$
$$\phi(n+1) = \phi(n) + \Omega + \varepsilon \cos[2\pi\phi(n)] + g(x(n)) \tag{3.12}$$

which is essentially the circle map coupled to a chaotic map f. In this presentation, Ω denotes the difference between the natural frequency of the chaotic oscillator and the frequency of the

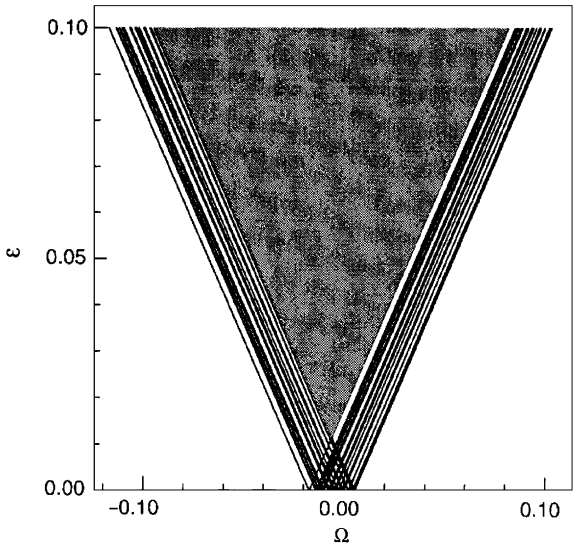

Fig. 3.7. From Ref. [80]. Phase-locking regions for periodic orbits with periods 1–5 in the system equation (3.12). The region of full phase synchronization, where all the phase-locking regions overlap, is delineated with black.

driving force. ε represents the coupling strength which is proportional to the amplitude of the driving force, and $g(x(n))$ corresponds to the nonuniformity of the phase rotations in the chaotic oscillators as a result of chaotic fluctuations of the amplitude x. The average growth rate of the phase, i.e. $\Delta\Omega = \lim_{n\to\infty}[\phi(n) - \phi(0)]/n$, corresponds to the phase rotation number, and $\Delta\Omega = 0$ indicates synchronization of the chaotic oscillator to the external force. Without loss of generality, the chaotic tent map $f(x,\phi) = 1 - 1.9|x| + 0.05\varepsilon\sin[2\pi\phi(n)]$ and $g(x) = 0.05x$ are studied in Ref. [80].

The analysis of Eq. (3.12) is based on the presentation of a chaotic attractor through its unstable periodic orbits embedded in it [3]. A periodic orbit of period N has its real period $T \approx T_0 N$, where T_0 is the average return time of the period one periodic orbit. For different periodic orbits, T_0 shows fluctuations around the average return time of the chaotic oscillations, as is modeled in the map system by the term $g(x)$. Due to these fluctuations, each periodic orbit has its individual phase-locking region under the periodic external forcing, as seen in Fig. 3.7. In this illustrative mapping model, the region of full phase synchronization is given by the overlapping region of the Arnold tongues of all the unstable periodic orbits. Calculating the phase locking regions of the unstable periodic orbits embedded in the continuous-time Rössler attractor, it has been found that the results quantitatively agree with the above consideration [81]. Additionally under the influence of the force, some unstable periodic orbits of the autonomous oscillator leave the bulk of the attractor and may be visited extremely rarely.

Investigation of phase synchronization of chaos in terms of unstable periodic orbits is very useful to understand special features not observed in synchronization of periodic oscillations. More details will be discussed in later sections in the context of phase synchronization transition and imperfect phase synchronization.

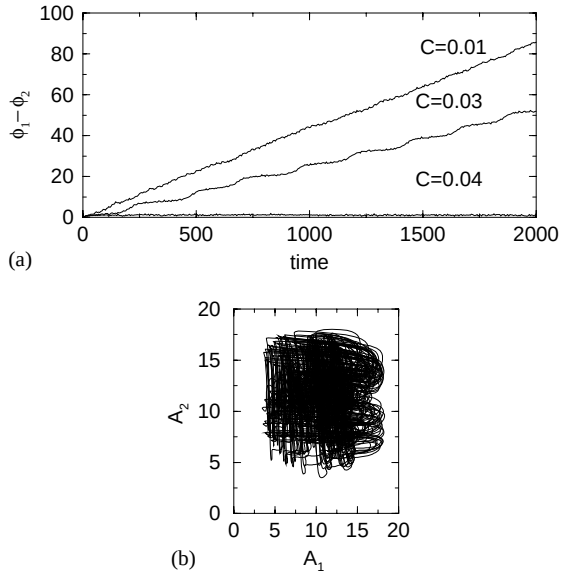

Fig. 3.8. Illustration of phase synchronization of two coupled nonidentical Rössler chaotic oscillators (3.13). (a) Time series of phase difference for different coupling strengths C. When $C > 0.036$, phases are nearly perfectly synchronized. (b) Amplitude A_1 vs. A_2 for the phase synchronized case at $C = 0.04$. Although the phases are locked, the amplitudes remain chaotic and nearly uncorrelated.

3.1.4. Phase synchronization of coupled chaotic oscillators

Next it is demonstrated that also two nonidentical chaotic oscillators are able to synchronize their phases due to coupling. This is shown for two coupled chaotic Rössler oscillators [7]

$$\begin{aligned} \dot{x}_{1,2} &= -\omega_{1,2} y_{1,2} - z_{1,2} + C(x_{2,1} - x_{1,2}) \,, \\ \dot{y}_{1,2} &= \omega_{1,2} x_{1,2} + a y_{1,2} \,, \\ \dot{z}_{1,2} &= f + z_{1,2}(x_{1,2} - c) \,, \end{aligned} \tag{3.13}$$

with a small parameter mismatch $\omega_{1,2} = 0.97 \pm \Delta\omega$. The other parameters, $a = 0.165$, $f = 0.2$ and $c = 10$, are the same for the two oscillators. Both oscillators have very coherent phase dynamics due to the proper rotation with a small variation in the return time, but they have different average frequencies as a result of the mismatch $\Delta\omega$.

As is illustrated in Fig. 3.8(a), for a fixed $\Delta\omega = 0.02$, there is a transition from the nonsynchronous regime, where the phase difference increases almost linearly with time, $\phi_1 - \phi_2 \sim \Delta\Omega t$, to a synchronous state, where the phase difference does not grow with time, i.e. $|\phi_1 - \phi_2| < \text{const}$ and the difference $\Delta\Omega = \Omega_1 - \Omega_2$ between both mean frequencies $\Omega_i = \langle \dot{\phi}_i \rangle$ vanishes, i.e. $\Delta\Omega = 0$. It is important to emphasize that although the phases of the two oscillators are locked, the amplitudes are nearly uncorrelated, as seen in Fig. 3.8(b), which corresponds to a very small value of the normalized cross correlation $C(A_1, A_2) \approx 0.008$. Thus PS stands for a weaker degree of synchronization in chaotic systems in contrast to CS discussed in Section 2. It occurs already for extremely weak couplings, as can be seen by the synchronization region in the parameter space C vs. $\Delta\omega$ in Fig. 3.9,

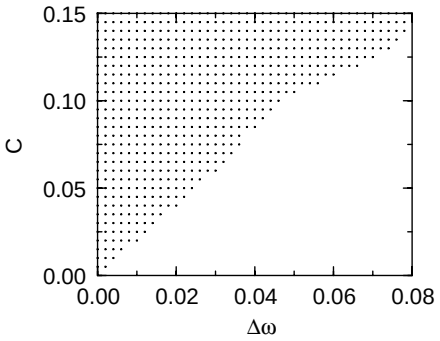

Fig. 3.9. Synchronization region (dotted points) of two coupled Rössler chaotic oscillators in the parameter space of C vs. $\Delta\omega$.

which is very similar to the "Arnold tongue" structure of coupled periodic oscillators. PS is also visible in the occurrence of peaks in the power spectra [82]; however this is only a necessary but not sufficient condition for PS.

PS of chaotic Rössler oscillators can be better understood by converting the original system into the dynamics of amplitude and phase. By introducing

$$\phi = \arctan(y/x), \quad A = (x^2 + y^2)^{1/2} , \tag{3.14}$$

we get

$$\begin{aligned}
\dot{A}_{1,2} &= aA_{1,2}\sin^2\phi_{1,2} - z_{1,2}\cos\phi_{1,2} + C(A_{2,1}\cos\phi_{2,1}\cos\phi_{1,2} - A_{1,2}\cos^2\phi_{1,2}) , \\
\dot{\phi}_{1,2} &= \omega_{1,2} + a\sin\phi_{1,2}\cos\phi_{1,2} + z_{1,2}/A_{1,2}\sin\phi_{1,2} \\
&\quad - C(A_{2,1}/A_{1,2}\cos\phi_{2,1}\sin\phi_{1,2} - \cos\phi_{1,2}\sin\phi_{1,2}) , \\
\dot{z}_{1,2} &= f - cz_{1,2} + A_{1,2}z_{1,2}\cos\phi_{1,2} .
\end{aligned} \tag{3.15}$$

As carried out in Ref. [9], the main idea in studying the phase dynamics is to use averaging over rotations of the phases $\phi_{1,2}$, assuming that the amplitudes vary slowly. Introducing the "slow" phases $\theta_{1,2}$ according to $\phi_{1,2} = \omega_0 t + \theta_{1,2}$, and averaging the equations for them, one gets

$$\frac{\mathrm{d}}{\mathrm{d}t}(\theta_1 - \theta_2) = 2\Delta\omega - \frac{C}{2}\left(\frac{A_2}{A_1} + \frac{A_1}{A_2}\right)\sin(\theta_1 - \theta_2) . \tag{3.16}$$

When we neglect the fluctuations of the amplitudes, Eq. (3.16) has a fixed point

$$\theta_1 - \theta_2 = \arcsin\frac{4\Delta\omega A_1 A_2}{C(A_1^2 + A_2^2)} \tag{3.17}$$

when the coupling strength C is larger than the critical value $C_{\mathrm{PS}} = 4\Delta\omega A_1 A_2/(A_1^2 + A_2^2)$. C_{PS} is then the onset of PS. This makes clear that PS of coupled chaotic oscillators is very similar to the classical case of phase synchronization of coupled periodic oscillators in Eq. (3.1), except that the phase difference now is not a constant value, but fluctuates due to chaotic fluctuations of the amplitudes.

Phase synchronization in chaotic oscillators is significant because it reveals a weaker degree of collective behavior and a new type of interdependence among coupled oscillators displaying complicated dynamics: the oscillators only adjust their time scales by weak coupling, while the amplitudes can be only weakly correlated. The synchronized time scales and the chaotic states provide both coherence (order) and feasibility (complexity) in the system. This twofold feature has already found several applications in experimental as well as in natural systems. Details will be discussed in Section 7.

3.1.5. Phase synchronization of two coupled circle maps

So far we have presented continuous in time systems, to demonstrate chaotic PS. In this section conditions for an onset of chaotic PS in a system of two coupled discrete in time models, namely, nonidentical circle maps (CMs) [83], are studied. Chains of coupled CMs will be considered in Section 6.2. The simplest CM yielding chaotic behaviour is

$$\phi^{k+1} = b + \phi^k - F(\phi^k) \,. \tag{3.18}$$

This map relates the phase variable ϕ^k at adjacent times $k=1,2,\ldots$; $b \in [0; 2\pi]$ is a positive parameter which can be interpreted as frequency; $F(\phi)$ is a piece-wise linear 2π-periodic function of the form $F(\phi) = c\phi/\pi$ defined in the interval $[-\pi, \pi]$, and c is the control parameter. System (3.18) is one of the basic models in nonlinear dynamics, and it has been studied in many mathematical (cf. [84]), physical (cf. [85]) and technical (in particular, in the theory of digital phase-locked loops (DPLL) [86–88]) issues. This map with nonuniformity of the phase rotation is considered in Section 3.1.3.

The dynamics of an individual CM can be determined by the rotation number ρ, which is defined as the average growth rate of the phase:

$$\rho = \frac{1}{2\pi} \lim_{M\to\infty} \frac{\phi^M - \phi^1}{M} \,, \tag{3.19}$$

where M is the number of iterations.

For uncoupled CM there are three different types of behavior [88]:

(i) for $c>0$ for every value of b, the map (3.18) has only one attractive set Ω. For a rational rotation number $\rho = p/q$ this Ω coincides only with attracting periodic trajectories of period q; for an irrational rotation number the set Ω is a Cantor attractive set on which the map (3.18) acts like a rotation;
(ii) if $c = 0$, then (3.18) becomes a continuous map of a circle rotated through the angle b;
(iii) for $c<0$ the map (3.18) demonstrates a chaotic dynamics. Only the case of chaotic behavior, i.e. $c<0$ is studied below.

We now consider a pair of symmetrically coupled maps (3.18), i.e. we get the two-dimensional system:

$$\begin{aligned} \phi_1^{k+1} &= b_1 + \phi_1^k - F(\phi_1^k) + d\sin(\phi_2^k - \phi_1^k) \,, \\ \phi_2^{k+1} &= b_2 + \phi_2^k - F(\phi_2^k) + d\sin(\phi_1^k - \phi_2^k) \,. \end{aligned} \tag{3.20}$$

System (3.20) can be regarded as a model of coupled partial DPLL connected in parallel by phase-mismatching signals. Some similar one- and two-dimensional in space models of coupled identical CMs have been studied in [89]. This type of nonlinear coupling between partial elements in the form of *sinus* of phase differences naturally arises in models of ensembles of weakly coupled time continuous oscillators. Respectively, pattern formation and synchronization in networks of phase oscillators with such kind of coupling between nearest neighbors have been investigated in [90].

As in the case of continuous in time systems, one can use two criteria to test for $m_1 : m_2$ synchronization, where $m_{1,2}$ are integers. $m_1 : m_2$ PS of chaotic rotations between two CMs is defined as phase entrainment or locking

$$|m_1\phi_1^k - m_2\phi_2^k| < \text{Const} \tag{3.21}$$

for all $k = 1, 2, \ldots$. Synchronization of rotations is analogous defined as the coincidence of their rotation numbers:

$$m_1\rho_1 = m_2\rho_2. \tag{3.22}$$

For different values of the frequency mismatch $\Delta b = b_2 - b_1$, the existence of synchronization regions has been found (Fig. 3.10) [83]. The geometrical structure and the size of such regions strongly depend on the rotation number difference $\Delta\rho = \rho_2 - \rho_1$ and the coherence properties of rotations. These properties are defined by the parameter c of the function $F(\phi)$. For $c = 0$, the rotations are completely coherent, i.e. it is a rotation with constant angle frequency. If $|c|$ grows, the noncoherence of the rotation increases. At relatively small $|c|$ values, the difference of the rotation numbers $\Delta\rho$ plays the crucial role in the synchronization. At larger $\Delta\rho$ values, a larger value of coupling is needed to achieve synchronization. The sizes of the synchronization regions become smaller with increasing $|c|$. This happens due to an increase of noncoherent properties of the rotation. At large $|c|$ values, the noncoherence of rotations is very large. Due to that, even at a very small frequency mismatch and as a consequence of that at very small rotation number difference, synchronization cannot be achieved. The existence of time intervals with a strongly different phase growth rate makes locking of rotations impossible.

In contrast to PS of chaotic oscillators, synchronization of chaotic rotators is not necessarily accompanied by bifurcations of the chaotic set and can occur via a crisis transition to a *band-structured attractor*. For system (3.20) the Lyapunov exponents are given by

$$\lambda_1 = \ln\left|1 - \frac{c}{\pi}\right|,$$

$$\lambda_2 = \lim_{M\to\infty}\frac{1}{M}\sum_{k=1}^{M}\ln\left|1 - \frac{c}{\pi} - 2d\cos(\phi_2^k - \phi_1^k)\right|. \tag{3.23}$$

Since the first Lyapunov exponent λ_1 is constant and positive for all values of d, we expect that only the sign of the second Lyapunov exponent λ_2 is important for the occurrence of chaotic PS. If both Lyapunov exponents are positive, there is *a hyper-chaotic regime* that determines usually a nonsynchronized regime. If, with increase of coupling, the second Lyapunov exponent becomes negative, there is a strong indication for the occurrence of PS. This situation takes place at the transitions to $1 : 1$ synchronization in all simulations presented in Figs. 3.11 and 3.12. Such a bifurcation is observed in chaotic PS of continuous in time systems (e.g. see [7]).

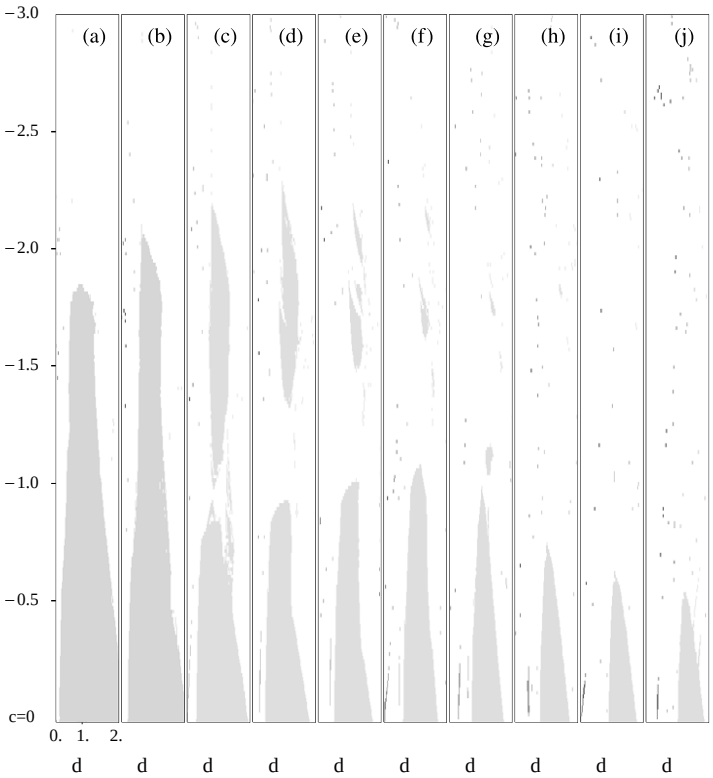

Fig. 3.10. Regions of chaotic phase synchronization for $b_1 = 0.6$ and different values of b_2 : 0.8 (a), 1.0 (b), 1.2 (c), 1.4 (d), 1.6 (e), 1.8 (f), 2.0 (g), 2.2 (h), 2.4 (i), 2.6 (j). The main gray regions correspond to 1 : 1 synchronization. In columns (c–j) for relatively small $-c$ small regions of 2 : 1 (c–g), 3 : 1 (f–h) and 4 : 1 (i, j) synchronization are presented. They are visible as small stripes in the left bottom areas.

But this is not the only scenario for the transition from nonsynchronous to synchronous behavior for which criteria (3.21) and (3.22) are satisfied. This is illustrated with plots of dependencies of the winding number $w = \rho_2/\rho_1$ and the second Lyapunov exponent λ_2 on the coupling coefficient d (Fig. 3.11) and phase diagrams for nonsynchronous (Fig. 3.12(a,b)), and synchronous (Fig. 3.12(c)), regimes. In the interval $d \in [0.285, 0.32]$ the winding number is equal $w = 3/1$ that corresponds to a 3 : 1 synchronization, but the second Lyapunov exponent remains positive $\lambda_2 \approx 0.05$, i.e. synchronized hyper-chaos exists. Also there are intervals of d in which 2 : 1 and 1 : 1 hyper-chaos synchronizations are observed. The transition to (or from) synchronized hyper-chaos are accomplished with a drastic change in the structure of the chaotic set (Fig. 3.12). In the case of nonsynchronous hyper-chaos (Fig. 3.12(a)(b)), the chaotic trajectory covers practically the whole phase space; i.e. the square $[-\pi : \pi; -\pi : \pi]$ with different densities. When the value of coupling is close to the critical value corresponding to the transition to the synchronized hyper-chaos, we observe a localization of areas visited by the chaotic trajectory. The appearance of more dense bands of motions can be clearly seen (Fig. 3.12(b)(c)). From the synchronization point of view the attendances of gaps between these bands are corresponding to slips in the phase difference $\theta^k = \phi_2 - 3\phi_1$, i.e. jumps of 2π [80]

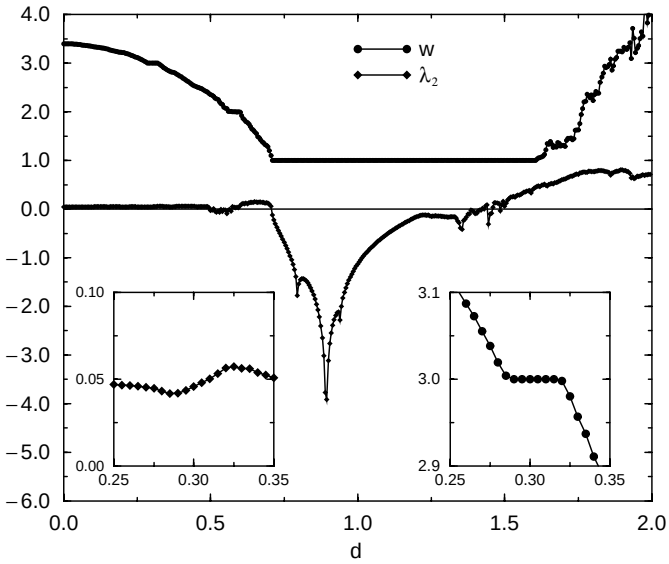

Fig. 3.11. The winding number $w=\rho_2/\rho_1$ and the second Lyapunov exponent λ_2 vs. the coupling coefficient d for $b_1=0.6$, $b_2=2.0$ and $c=-0.15$. Regions of $3:1$, $2:1$ and $1:1$ synchronization are existing. Enlargements of the interval $[0.25; 0.35]$ are presented in the insets (left: λ_2, right: w).

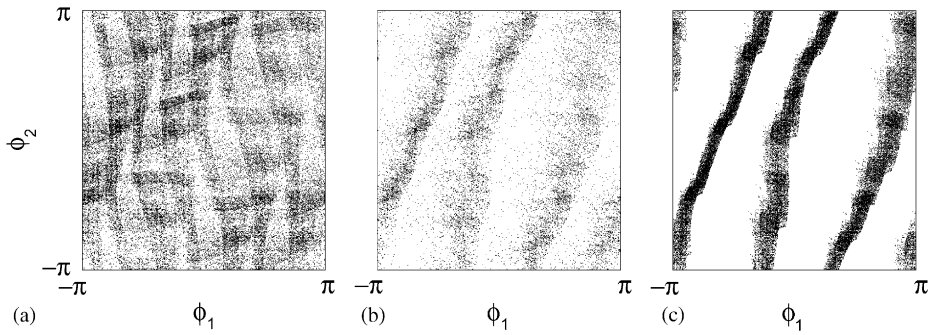

Fig. 3.12. Phase portraits of system (3.20) for $b_1 = 0.6$, $b_2 = 2.0$, $c = -0.15$ and different d within (c) ($d = 0.3$) and outside (a) ($d = 0.25$) and (b) ($d = 0.275$) of the $3:1$ synchronization region. In all three cases a hyper-chaotic regime ($\lambda_1, \lambda_2 > 0$) exists.

(see Fig. 3.13). A decrease of the number of slips exhibits the tendency of the system to perfect PS where no slips exist. At synchronized hyper-chaos, the chaotic trajectory is placed only in relatively narrow bands in the phase space (Fig. 3.12(c)). This transition to synchronous motions corresponds to the transition of the phase difference $\theta^k = \phi_2^k - 3\phi_1^k$ from rotation to oscillation. Thus the transition from nonsynchronous to synchronous behavior in a two-element CMs system occurs through *interior crisis* [3] of the hyper-chaotic set, i.e. in both regimes both Lyapunov exponents are positive.

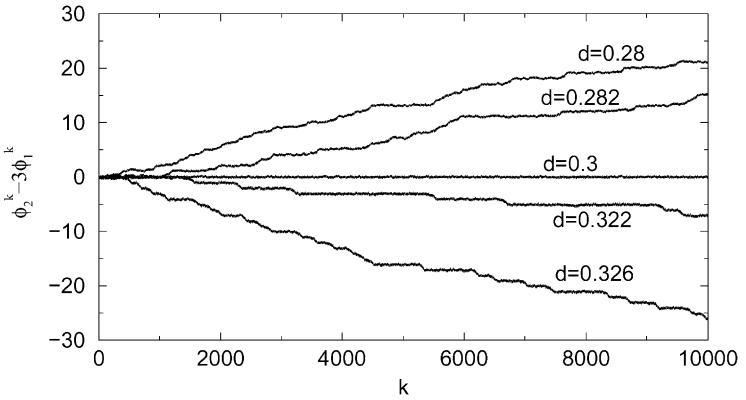

Fig. 3.13. Evolution of phase difference $\theta^k = \phi_2^k - 3\phi_1^k$ for synchronous ($d = 0.30$) and nonsynchronous ($d = 0.28; 0.282; 0.322; 0.326$) cases of system (3.20). Parameters: $b_1 = 0.6$, $b_2 = 2.0$ and $c = -0.15$.

3.2. Transition to phase synchronization of chaos

In this section, we discuss in more detail the transition to phase synchronization, or in other words, how desynchronization occurs when a parameter moves out the phase-locking region.

As it has been seen in Fig. 3.8, when the coupling strength is well outside the synchronization region, the phase difference increases almost linearly. When it approaches the border of phase synchronization, many phase-synchronized epochs characterized by plateaus of the phase difference are observed. The average duration of the synchronization epochs becomes longer and longer, and phase synchronization is only interrupted intermittently by 2π phase slips when the coupling strength is getting more and more closer to the border till the system achieves perfect phase-locking inside the synchronization region.

In the classical case of coupled periodic oscillators where the phase dynamics can be described by Eq. (3.1), the transition to phase synchronization corresponds to a saddle-node bifurcation, and the intermittency of the phase dynamics just outside the synchronization region is characterized by a type-I intermittency [91]. The average duration τ_1 between phase slips scales as

$$\tau_1 \sim |C - C_{\mathrm{PS}}|^{-1/2} \tag{3.24}$$

with C_{PS} being the transition point of phase synchronization. Here the parameter C can be either the coupling strength or the frequency of the driving signal.

As has been discussed in Section 3.1.3, the synchronization region of the chaotic oscillators corresponds to overlapping of phase-locking regions of the unstable periodic orbits embedded in the chaotic attractor. In the PS region, and for a particular unstable periodic orbit, Eq. (3.1) has a stable fixed point ϕ_s and an unstable fixed point ϕ_u, and accordingly, each of the unstable periodic orbit is associated with an attractor and a repeller in the direction of ϕ. In the generalized phase space (x, ϕ), the attractor (x, ϕ_s) and the repeller (x, ϕ_u) are well separated, as shown in Fig. 3.14(a) for the mapping system of Eq. (3.12). In this generalized phase space with unwrapped phase variable (the phase variable is considered on the real line rather than on the circle, and phase points separated

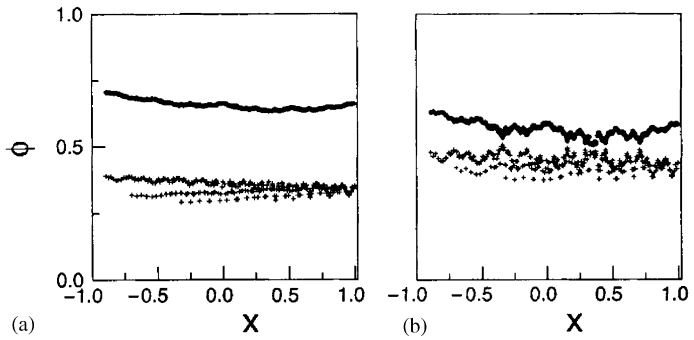

Fig. 3.14. From Ref. [80]. Stable (in the ϕ direction) (pluses) and unstable (filled circles) periodic orbits with periods 1–8 forming the skeletons of the attractor and repeller, respectively (Eq. (3.12)). (a) Inside the full phase-locking region, where the attractor and the repeller are distinct. (b) Just beyond the border of the phase-locking region at which the attractor and repeller collide, the chaotic attractor as a whole is no longer attractive in the ϕ direction.

by 2π are not considered as the same), the repellers are periodic orbits on the basin boundary of the attractors [8]. When the parameter moves close and crosses the phase-locking boundary, the attractor and the repeller of a few unstable periodic orbits approach to each other, coalesce and annihilate as a result of the saddle-node bifurcation, as illustrated in Fig. 3.14(b). Hence, these unstable periodic orbits are not locked by the external force and phase slips may occur. The dynamics in the weakly unstable direction ϕ is the same as in the usual saddle-node bifurcation with a characteristic time between phase slips given by Eq. (3.24). However, just beyond the transition point, most of the unstable periodic orbits are still attractive in the ϕ direction, and phase slips can only develop when the chaotic trajectory comes close to an unlocked periodic orbit. To allow at least one slip to occur, the chaotic trajectory should stay for a time period τ_1 in a close vicinity of the unlocked periodic orbit. Because of ergodicity, the probability for a trajectory to stay close to a particular unstable periodic orbit for a duration τ_1 is proportional to $\exp(-\lambda\tau_1)$, where λ is the largest Lyapunov exponent of the chaotic system [3]. The average time between successive phase slips is the inverse of this probability, which reads,

$$\tau \sim \exp(k\,|\,C - C_{\mathrm{PS}}|^{-1/2})\ . \tag{3.25}$$

This relation indicates that PS epochs are extremely long for C close to C_{PS}. It follows immediately that close to the transition point, the average frequency difference, which is proportional to the inverse of τ, scales as

$$\ln|\,\Delta\Omega\,| \sim -\,|C - C_{\mathrm{PS}}\,|^{-1/2}\ . \tag{3.26}$$

The above consideration applies to both transitions where the system leaves the phase-locking region when varying the external frequency.

Such super-long laminar periods between phase slips have been verified in numerical simulation of mapping Eq. (3.12) [80], as well as in direct simulation of the chaotic Rössler oscillator driven by external forcing [8,81]. The results are shown in Fig. 3.15.

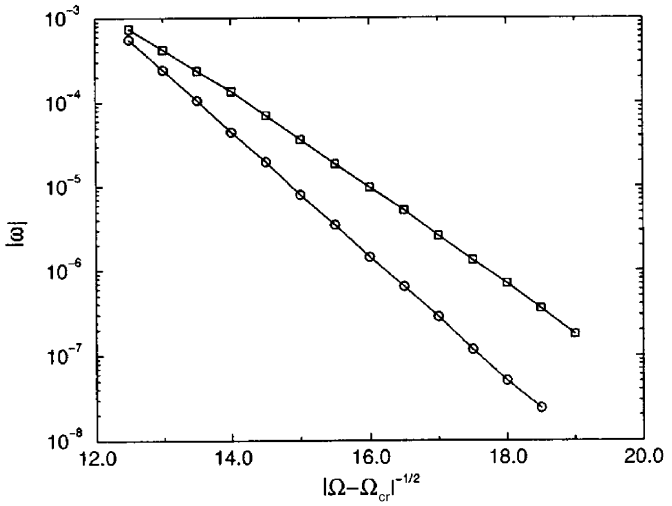

Fig. 3.15. From Ref. [80]. Frequency difference at the two borders of the phase locking region for the mapping system in Eq. (3.12).

Similar arguments may be applied to coupled chaotic oscillators. However, the organization of the phase-locking region of unstable periodic orbits may be much more complicated and has not yet been calculated directly. Nevertheless, these super-long laminar periods of PS have been observed for C rather close to C_{PS} [92]. When C is getting further away from the critical point C_{PS}, many unstable periodic orbits are outside the phase-locking region. The probability to encounter an unlocked periodic orbit becomes effectively unity and phase slips occur much more frequently. The intermittency shifts then from the super-long type to the usual type-I intermittency characterized by a power law in Eq. (3.24) [92,93].

It has been also shown that in the PS region, additive noise has similar effects to destabilize some of the unstable periodic orbits in the direction of ϕ and the noise-induced intermittent loss of PS has the same scaling law as in Eq. (3.25) [22,94], which has been verified experimentally in Ref. [95] with coupled Chua's circuits, as an example of superpersistent chaotic transients. However, if the noises in both oscillators are strongly correlated, they tend to enhance phase synchronization when C is outside the phase synchronization region, as will be discussed in Section 5.

As it is pointed out, desynchronization of phase-locking occurs when a certain unstable periodic orbit becomes unstable in the direction of phase. This bears much similarity to the riddling bifurcation in coupled identical systems where a certain unstable periodic orbit becomes unstable in the transverse direction [96]. This similarity has been discussed in coupled periodically driven chaotic pendulums where the phase itself is chaotic [97].

It is also interesting to note that the Rössler system undergoes a periodic-doubling bifurcation when the parameter a is changed. When driven periodically by an external signal, there is a corresponding Arnold tongue for each periodic orbit. Ref. [98] studies the critical behavior of the limit of the periodic-doubling cascade at the edge of the Arnold tongue, showing that the transition behavior belongs to the cycle-type universal critical behavior [99] with scaling exponents distinct from those of the usual Feigenbaum cascade [100].

3.3. Imperfect phase synchronization

In PS of chaotic oscillators, the time scales of one oscillator is entrained with another chaotic or periodic oscillator. One would expect that the distribution of the time scales plays an important role in the synchronization behavior. For example, in the chaotic Rössler oscillators discussed above, the return time varies, but the relative variation is rather small so that phase increases almost linearly with time. As a result of this narrow distribution of time scales, the chaotic Rössler oscillators can be rather easily synchronized by weak forcing with a period close to the average return time [8,74,79,81]. Considered from the viewpoint of unstable periodic orbits, these orbits have narrowly distributed periods, and consequently, the phase-locking regimes are similar and all corresponding Arnold tongues have an overlapping to guarantee complete PS of the chaotic attractor. In general, a similar behavior can be observed in other systems with chaotic attractors originating from the periodic-doubling scenario. However, as pointed in Ref. [78], it may not be possible to synchronize some phase-coherent systems, even if they exhibit very small phase diffusion D_ϕ. This may occur when the phase has a sensitive dependence on the amplitudes in the presence of an external force.

However, the scenario changes if the system has a rather broad distribution of time scales of periodic orbits. An external signal with a given frequency then may not be able to entrain all the time scales in the system: phase slips occur when the chaotic flow comes to oscillate with time scales outside the synchronization region of the driving signal and *imperfect phase synchronization* is observed.

Refs. [13,101,102] have carried out a comparative study of perfect and imperfect PS with the example of a periodically driven Lorenz system,

$$\begin{aligned} \dot{x} &= 10(y - x) \,, \\ \dot{y} &= rx - y - xz \,, \\ \dot{z} &= xy - 2.667z + E\cos(\Omega t) \,. \end{aligned} \tag{3.27}$$

The unforced Lorenz system exhibits rich bifurcations when the parameter r is varied [45]. For $r = 210$, chaotic oscillations result from a periodic-doubling scenario, and the system can be synchronized perfectly by a periodic driving signal with a frequency close to the average frequency $\Omega = 24.92$ of the chaotic oscillations, as it can be seen by the plateau of the vanishing frequency difference $\omega - \Omega = 0$ in Fig. 3.16. The situation becomes different for $r = 28$ where a certain plateau of $\omega - \Omega = 0$ appears; however, this plateau is neither horizontal nor lies at zero. As a result, PS in this case is not perfect, as shown by 2π or 4π phase slips in Fig. 3.17

The reason for this imperfect phase synchronization lies in the broad distribution of the time scales of the chaotic oscillations at $r = 28$. For this parameter, there is a saddle point $(0, 0, 0)$ embedded in the chaotic attractor. The trajectory slows down considerably when passing near the saddle point, while the oscillation is much quicker when the trajectory rotates around one of the two unstable foci [45]. Thus the time scales have a relatively large variation around the average value, as can be seen in the distribution of the frequency of different unstable periodic orbits (Fig. 3.18). Due to this large variation of the frequencies, the phase-locking regions of the unstable periodic orbits do not overlap to produce a full synchronization region of the chaotic attractor. For a given frequency and

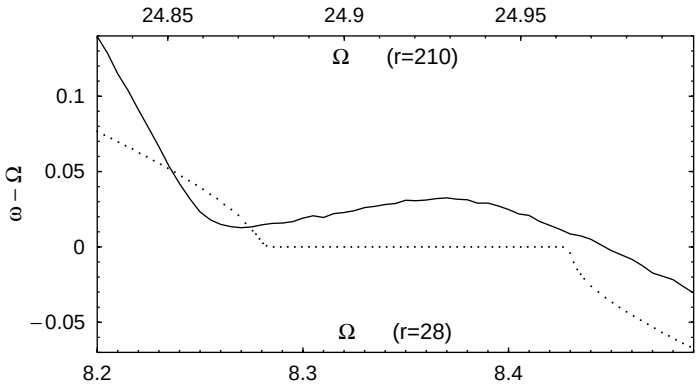

Fig. 3.16. From Ref. [13]. Perfect and imperfect phase synchronization for periodically forced Lorenz systems (Eq. (3.27)); solid line: $r = 28$, $E = 6$; dotted line: $r = 210$, $E = 3$.

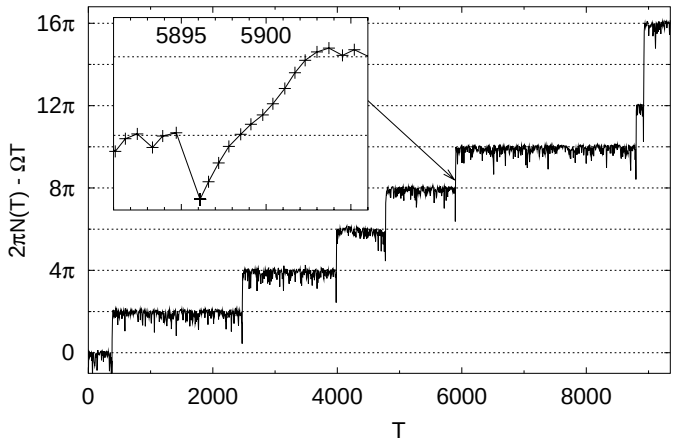

Fig. 3.17. From Ref. [13]. Phase slips of imperfect phase synchronization in periodically driven Lorenz system at $r = 28$ (Eq. (3.27)).

amplitude of the external driving signal, there exist certain unstable orbits which are not locked and imperfect phase synchronization characterizes this complicated locking behavior.

Using the approach of unstable periodic orbits, it is demonstrated in Refs. [13,101,102] that a phase slip develops when the system comes close to a certain unstable periodic orbit which is not in a $1:1$ phase-locking with the driving signal. More interestingly, a careful study reveals that during such a phase slip, the system is in fact phase-locked with the driving signal with another locking ratio, such as $(l-1):l$ or $(l-2):l$. The possible value of l for these cases are $l \geqslant l_0$ and $l \geqslant 2l_0$, respectively, where l_0 is determined by the largest and smallest frequencies of the unstable periodic orbits, i.e. $l_0 = \omega_{\max}/(\omega_{\max} - \omega_{\min})$ (smaller l becomes possible due to the broadening of the Arnold tongues). In such cases, the $1:1$ phase-locking regions of some periodic orbits overlap with the $(l-1):l$ or $(l-2):l$ phase-locking regions of some other periodic orbits, as explicitly illustrated in

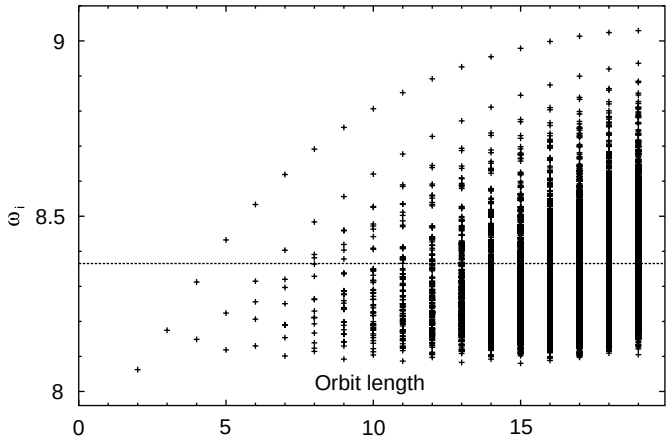

Fig. 3.18. From Ref. [13]. Individual frequencies of unstable periodic orbits embedded into the Lorenz attractor at $r = 28$; dashed line: mean frequency of the autonomous chaotic motion.

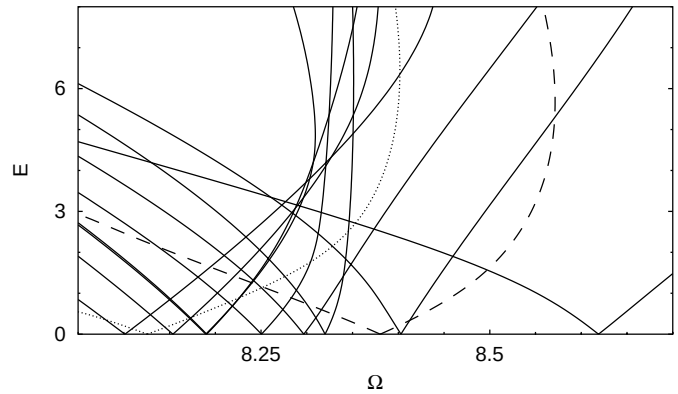

Fig. 3.19. From Ref. [13]. Overlapping of phase-locking regions of different locking ratios in the periodically driven Lorenz system at $r = 28$ (Eq. (3.27)). Solid line: $l = 7$ (1 : 1), dashed line: $l = 15$ (14 : 15); dotted line: $l = 20$ (18 : 20).

Fig. 3.19. As a result, the system actually establishes phase locking to the driving signal with another locking ratio rather than 1 : 1 phase-locking during the seeming phase slip. During the time course, the system alternates among different locking ratios when it visits periodic orbits with overlapping Arnold tongues of different locking ratios.

This study has made clear that PS is a matter of adjusting time scales by interaction. Synchronization with different locking ratios can be established when the system is shifting among different time scales. In the Lorenz system, the drifting of the time scales occurs when the chaotic trajectory accesses closely to different unstable periodic orbits. In other cases, the drifting can be induced by nonstationarity of the process, such as in the human cardiorespiratory system, where alternating locking ratio can be also observed [21,103], see Section 7.

3.4. Lag synchronization of chaotic oscillators

It has been shown that when nonidentical chaotic oscillators are weakly coupled, the phases can be locked while the amplitudes remain highly uncorrelated. What happens when the coupling strength becomes larger? One would expect that with stronger coupling, a relationship between amplitudes may be established. Indeed, it has been demonstrated that there exists a regime of *lag synchronization* [9] where the states of two oscillators are nearly identical, but one system lags in time to the other. To see how lag synchronization is established, we focus on the dynamics of the amplitudes (Eq. (3.15)). With similar averaging processing except for the terms containing both the fast phases $\phi_{1,2}$ and the variables $z_{1,2}$, one gets

$$\begin{aligned}\dot{A}_{1,2} &= \frac{a}{2}A_{1,2} - z_{1,2}\cos(\omega_0 t + \theta_{1,2}) + \frac{C}{2}(A_{2,1}\cos(\theta_1 - \theta_2) - A_{1,2}) \,, \\ \dot{z}_{1,2} &= f - cz_{1,2} + A_{1,2}z_{1,2}\cos(\omega_0 t + \theta_{1,2}) \,, \end{aligned} \tag{3.28}$$

which is a system of two coupled periodically driven oscillators. The driving signals $\cos(\omega_0 t + \theta_{1,2})$ in both systems, however, are not identical, but have a phase shift as in Eq. (3.17). If the two oscillators are identical, then $\theta_1 - \theta_2 = 0$ and complete synchronization will be observed when $C > C_{CS} = 0.095$. C_{CS} is the coupling threshold where one of the two positive Lyapunov exponent crosses zero and becomes negative. A small parameter mismatch $\Delta\omega = 0.02$ shifts this transition point to $C_{CS} = 0.11$, and more importantly, introduces a nonvanishing phase shift in Eq. (3.17). For $C > C_{CS}$, the system states may remain almost identical but with a time lag $\tau_0 = (\theta_1 - \theta_2)/\omega_0$, i.e.

$$x_2(t + \tau_0) \approx x_1(t), \quad y_2(t + \tau_0) \approx y_1(t), \quad z_2(t + \tau_0) \approx z_1(t) \,, \tag{3.29}$$

which is called lag synchronization.

To characterize lag synchronization quantitatively, a similarity function $S(\tau)$ has been introduced as the time averaged difference between the variable $x_1(t)$ and $x_2(t + \tau)$ (with mean values being dropped)

$$S^2(\tau) = \frac{\langle (x_2(t + \tau) - x_1(t))^2 \rangle}{\sqrt{\langle x_1^2(t) \rangle \langle x_2^2(t) \rangle}} \tag{3.30}$$

and searched for its minimum $\sigma = \min_\tau S(\tau) = S(\tau = \tau_0)$. This measure is similar to the cross correlation function $\langle (x_2(t+\tau)x_1(t))^2 \rangle$, but S is especially suitable for measuring lag synchronization from bivariate time series because $S(\tau_0) \approx 0$ at a certain nonzero τ_0 indicates lag synchronization.

A typical feature of S for the coupled Rössler oscillators are shown in Fig. 3.20 for different values of coupling C. When the system is in the PS regime, a minimum of S can already be seen clearly, but σ is well above zero, because even though the phases are locked, the phase differences fluctuate considerably around the average value $\omega_0\tau_0$. With increasing C both τ_0 and σ decrease. When C approaches $C_{lag} = 0.14$ where σ effectively reaches zero at a nonzero τ_0, the system undergoes a transition to lag synchronization. After identifying the time delay τ_0 by this similarity function S, lag synchronization can be graphically illustrated directly by plots of $x(t + \tau_0)$ vs. $x(t)$ which is restricted to an almost straight line, as seen in Fig. 3.21(b). Ref. [104] has shown experimentally that lag synchronization is robust to perturbations to some extent.

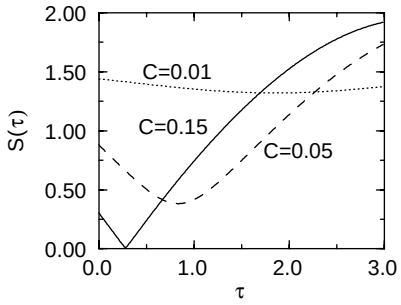

Fig. 3.20. Similarity function $S(\tau)$ (Eq. (3.30)) obtained for two coupled Rössler oscillators (Eq. (3.13)) for different values of the coupling strength C. In the phase synchronization regime (e.g. $C = 0.05$), the curve has a clear minimum $\sigma \neq 0$. Lag synchronization occurs when σ becomes effectively zero (e.g. $C = 0.15$).

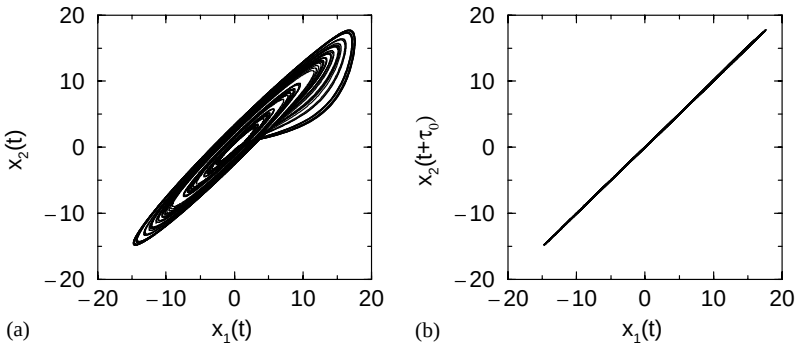

Fig. 3.21. Same system as in Fig. 3.20. Illustration of lag synchronization at $C = 0.20$. (a) Plot of $x_1(t)$ vs. $x_2(t)$ shows that the system are not completely synchronized; (b) Plot of $x_1(t)$ vs. $x_2(t + \tau_0)$ with $\tau_0 = 0.21$, the straight line exhibits lag synchronization.

One should note that with the increase of the coupling strength C, the phase shift in Eq. (3.17) approaches to zero. With vanishing τ_0, the two nonidentical oscillators tend to be synchronized almost completely, i.e. $\mathbf{x}_1(t) \approx \mathbf{x}_2(t)$.

It is also important to point out that the transition to lag synchronization at $C_{\text{lag}} = 0.14$ is well beyond the transition where one of the positive Lyapunov exponent becomes negative at $C_{\text{CS}} = 0.11$. The difference in between will be discussed in the next section.

3.5. From phase to lag to complete synchronization

We have shown that two coupled nonidentical chaotic oscillators undergo transitions from phase to lag and then to almost complete synchronization with increasing coupling strengths. As has been pointed out in Section 3.1.2, in a deterministic time-continuous autonomous chaotic flow there is a zero Lyapunov exponent corresponding to the translation $\mathrm{d}\mathbf{x}(t)$ along the chaotic trajectory. In a phase coherent chaotic oscillator, $\mathrm{d}\mathbf{x}(t)$ can be uniquely mapped to a shift of the phases $\mathrm{d}\phi(t)$ of

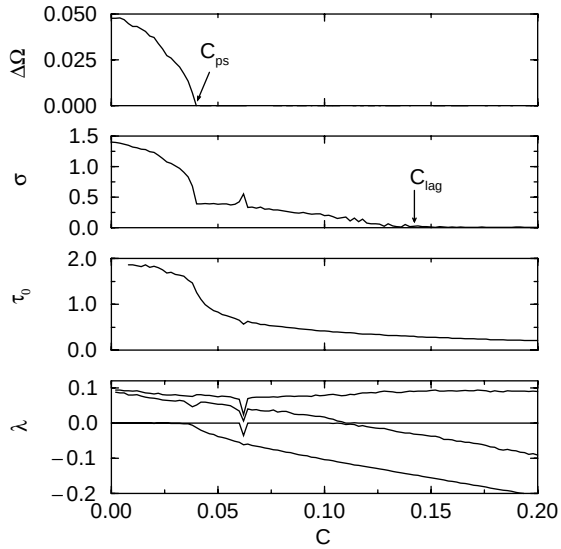

Fig. 3.22. The frequency difference $\Delta\Omega$, the minimum σ of the similarity function, the time delay τ_0 and the four largest Lyapunov exponents λ of two coupled Rössler oscillators vs. the coupling strength C. The parameter mismatch $\Delta\omega$ is 0.02.

the oscillator. If both oscillators are not phase synchronized, there are two zero-Lyapunov exponents linked to individual phases. When the two coupled chaotic oscillators achieve PS, the initial phase difference converges to that in Eq. (3.17), and in accordance with this stability of phases, one of the two zero Lyapunov exponents undergoes a transition to negative values. With further increase of the coupling strength, another Lyapunov exponent undergoes a transition from positive to negative values, and we get a strong correlations of the amplitudes too. When the parameter mismatch is small, this transition point is close to that of CS in coupled identical oscillators. As discussed in the last section, one would observe lag synchronization somewhere beyond this transition point in coupled nonidentical oscillators.

Ref. [9] has demonstrated this connection between the transitions of Lyapunov exponents and synchronization stages for the coupled Rössler systems. The results are summarized in Fig. 3.22. Shown along with the Lyapunov exponents are the average frequency difference $\Delta\Omega$, the minimum σ of $S(\tau)$ and the time lag τ_0. First, shortly before the transition to PS at $C_{\mathrm{PS}} = 0.036$, one of the zero Lyapunov exponents becomes negative, while the transition to lag synchronization at $C_{\mathrm{lag}} = 0.14$ happens significantly after the zero crossing of one of the positive Lyapunov exponents at $C_{\mathrm{CS}} = 0.11$.

Let us pay more attention to the regime in the region $0.11 < C < 0.14$ where σ has small values, but is not effectively zero. The typical behavior there is *intermittent lag synchronization* [9] where lag synchronization is interrupted by intermittent burst of large synchronization error $x_1(t) - x_2(t + \tau_0)$, as seen in Fig. 3.23(a) for $C = 0.13$, which is very similar to the intermittent loss of CS in coupled identical systems [61,105,106] when the coupling strength is just beyond the synchronization threshold and the system is subjected to small perturbations. To understand this bursting behavior of lag synchronization, we go back to Eq. (3.28). Introducing the lag variables for the second system $\tilde{A}_2 = A_2(t + \tau_0)$, $\tilde{z}_2 = z_2(t + \tau_0)$ where $\tau_0 = (\theta_1 - \theta_2)/\omega_0$, we can reduce system equation (3.28) to

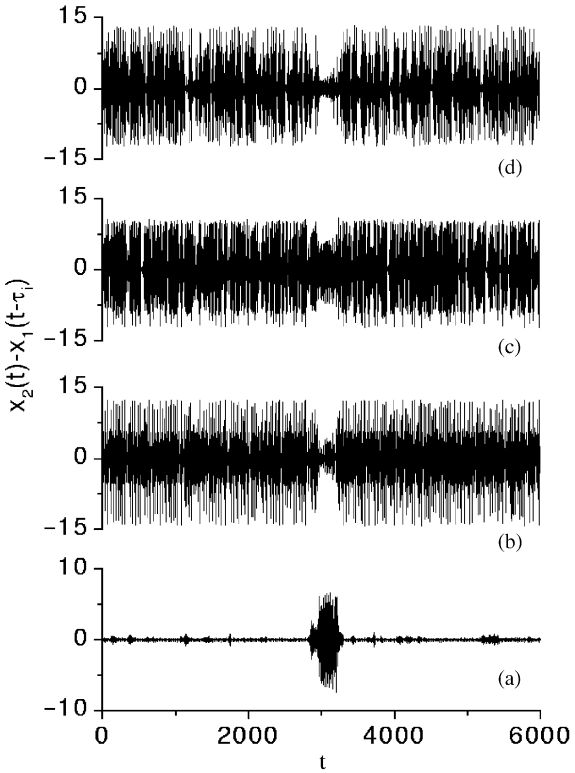

Fig. 3.23. Intermittent lag synchronization at $C = 0.13$. (a) $n = 0$, (b) $n = 1$, (c) $n = 2$, and (d) $n = 3$.

a system of two coupled identical systems under an identical driving signal and some additional perturbation terms η_1 and η_2,

$$\begin{aligned} \dot{A}_1 &= \frac{a}{2} A_1 - z_1 \cos(\omega_0 t + \theta_1) + \frac{C}{2}(\tilde{A}_2 - A_1) + \eta_1 \ , \\ \dot{z}_1 &= f - c z_1 + A_1 z_1 \cos(\omega_0 t + \theta_1) \end{aligned} \tag{3.31}$$

and

$$\begin{aligned} \dot{\tilde{A}}_2 &= \frac{a}{2} \tilde{A}_2 - z_2 \cos(\omega_0 t + \theta_1) + \frac{C}{2}(A_1 - \tilde{A}_2) + \eta_2 \ , \\ \dot{\tilde{z}}_2 &= f - c \tilde{z}_2 + \tilde{A}_2 \tilde{z}_2 \cos(\omega_0 t + \theta_1) \end{aligned} \tag{3.32}$$

with

$$\eta_1 = \frac{C}{2}(A_2 \cos(\theta_1 - \theta_2) - \tilde{A}_2)$$

and

$$\eta_2 = \frac{C}{2} A_1[\cos(\theta_1 - \theta_2) - 1] .$$

Now if we ignore the perturbation terms η_1 and η_2 for a moment, the two coupled identical oscillators will achieve CS, when one of the two positive Lyapunov exponents becomes negative at $C_{CS} = 0.11$, i.e. $A_1 = \tilde{A}_2$. Note that when the coupling strength is well beyond the synchronization threshold C_{CS}, CS is robust to perturbations, i.e. the synchronization error is limited to a level comparable to that of the perturbations. Furthermore, the perturbation terms in general decrease with decreasing τ_0 at stronger coupling strength. As a consequence, we observe lag synchronization with $A_1 \approx \tilde{A}_2$ after $C = 0.14$. Just beyond the transition point $C_{CS} = 0.11$, the CS of the system is sensitive to perturbations of η_1 and η_2, and the synchronization error $A_1 - \tilde{A}_2$ may have an excursion to large values comparable to the order of A_1 or $\tilde{A}_2$ during the burst of desynchronization. Correspondingly, we observe intermittent lag synchronization, as shown in Fig. 3.23(a). The desynchronization bursting becomes more and more frequently when C is approaching C_{CS}, and a clear lag synchronization can no longer be observed.

A more detailed investigation in Ref. [12] has shown that bursting of lag synchronization between $A_1(t)$ and $A_2(t + \tau_0)$ could be lag synchronization between $A_1(t)$ and $A_2(t + \tau_n)$ with another time lag $\tau_n = \tau_0 + nT$, where T is the mean return time of the chaotic orbits of the Rössler system. As illustrated in Fig. 3.23, large synchronization error during the desynchronization bursting between $A_1(t)$ and $A_2(t + \tau_0)$ becomes relatively small between $A_1(t)$ and $A_2(t + \tau_n)$ for $n = 1, 2, 3$. This understanding comes from the observation that the similarity function in Eq. (3.30) actually has multiple minima at $\tau_n = \tau_0 + nT$.

The above described synchronization transitions and their connection with the changes of the Lyapunov exponents should be general for phase coherent chaotic oscillations where a phase variable can be defined properly as a monotonously increasing function of time. However, in many chaotic oscillators, the time translation along the chaotic trajectory may not be able to be mapped uniquely to a phase variable, and perfect phase locking may not be observable. In such a case, generally one may not observe a coincidence of the transition of PS and that of zero Lyapunov exponent. PS of this type has been discussed with funnel chaotic Rössler oscillators [74,107,108]. Indirect criteria, such as the amplitude of the ensemble average of the system, has been proposed to detect PS of chaotic oscillators without coherent phase dynamics.

3.6. The generalized synchronization

In the previous paragraphs of this section, we have reviewed synchronization phenomena in coupled nonidentical chaotic oscillators. In general, when there exists an essential difference between the coupled systems, there is no hope to have a trivial manifold in the phase space attracting the system trajectories, and therefore it is not clear at a first glance whether nonidentical chaotic systems can synchronize. Two central issues are the "milestones" of the subject. The first is that one should *generalize* the concept of synchronization to include nonidenticity between the coupled systems. The second is that one should design some tests to detect it. Many works have shown that this type of chaotic synchronization can exist [5,10], and have called this phenomenon *generalized synchronization*. In most cases, evidence of it has been provided for unidirectional coupling schemes.

In order to define *generalized synchronization* (GS) for an unidirectional coupling scheme, let us consider the following coupled system:

$$\dot{\mathbf{x}} = \mathbf{F}(\mathbf{x}) ,$$
$$\dot{\mathbf{y}} = \mathbf{G}(\mathbf{y}, \mathbf{h}_\mu(\mathbf{x})) , \tag{3.33}$$

where $\mathbf{x}$ is the n-dimensional state vector of the driver and $\mathbf{y}$ is the m-dimensional state vector of the response. $\mathbf{F}$ and $\mathbf{G}$ are vector fields, $\mathbf{F}: R^n \to R^n$, and $\mathbf{G}: R^m \to R^m$. The coupling between response and driver is ruled by the vector field $\mathbf{h}_\mu(\mathbf{x}): R^n \to R^m$, where the dependence of this function upon the parameters μ is explicitly considered. When $\mu = 0$, the response system evolves independently of the driver, and we assume that both systems are chaotic.

Some slight differences in the definition of GS exist in the literature. Here, we will focus on the more general definition given in Refs. [10,11,109]. When $\mu \neq 0$, the chaotic trajectories of the two systems are said to be synchronized in a generalized sense if there exists a transformation $\psi: \mathbf{x} \to \mathbf{y}$ which is able to map asymptotically the trajectories of the driver attractor into the ones of the response attractor $\mathbf{y}(t) = \psi(\mathbf{x}(t))$, regardless on the initial conditions in the basin of the synchronization manifold $M = \{(\mathbf{x}, \mathbf{y}) : \mathbf{y} = \psi(\mathbf{x})\}$.

Let us illustrate the concept of GS with an example, which is taken from Ref. [10]. We consider two coupled Rössler systems in a driver–response configuration

$$\left.\begin{aligned} \dot{x}_1 &= -(y_1 + z_1) \\ \dot{y}_1 &= x_1 + a y_1 \\ \dot{z}_1 &= f + z_1(x_1 - \mu) \end{aligned}\right\} \text{driver} ,$$
$$\left.\begin{aligned} \dot{x}_2 &= -(y_2 + z_2) + \cdots + c(x_1 - x_2) \\ \dot{y}_2 &= x_2 + a y_2 \\ \dot{z}_2 &= f + z_2(x_2 - \mu) \end{aligned}\right\} \text{response} , \tag{3.34}$$

where $a = 0.2$, $f = 0.2$ and $\mu = 5.7$. For $c = 0.1$ the coupled systems are in an unsynchronized state, while for $c = 0.2$ they are in a CS state. This is shown in Fig. 3.24(a) and (b), where we have plotted $y_2(t)$ vs. $y_1(t)$. Here, the behavior of a CS state appears as a sharp straight line $y_2 = y_1$ for $c = 0.2$.

It is possible to construct other response system which exhibits a generalized kind of synchronization motion with the driver, by making a simple nonlinear transformation among the response variables (x_2, y_2, z_2). The following transformation is used in order to create a new response system:

$$x_3(t) = x_2(t) ,$$
$$y_3(t) = y_2(t) + \beta z_3(t) + \gamma z_3(t)^2 ,$$
$$z_3(t) = z_2(t) \tag{3.35}$$

with $\beta = 0.4$ and $\gamma = -0.008$.

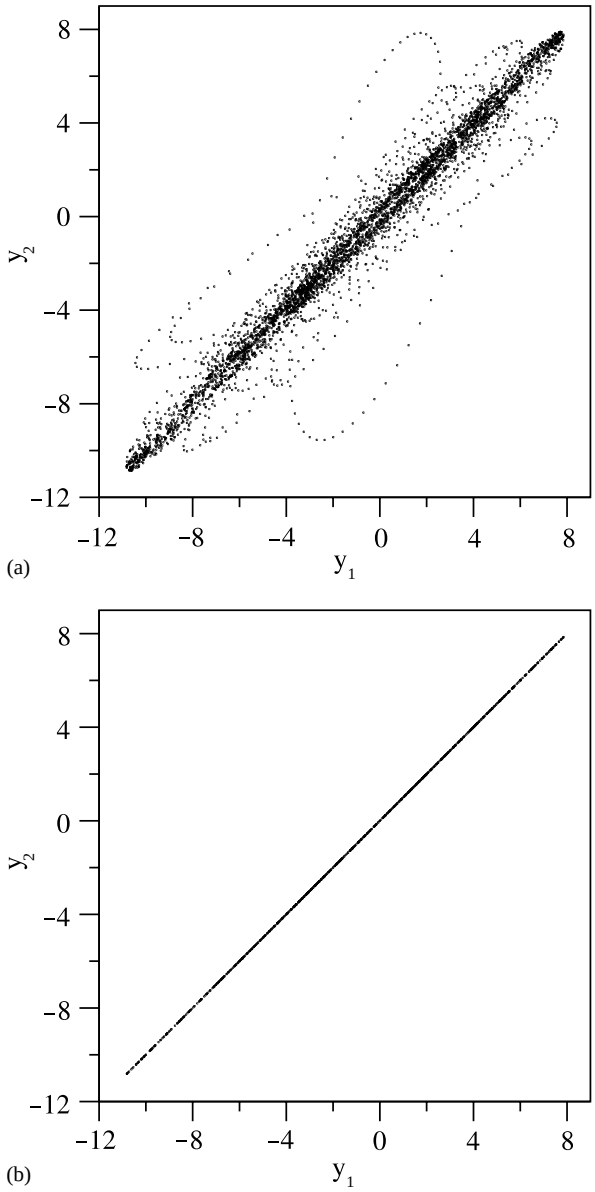

Fig. 3.24. The projection on the plane (y_2, y_1) of the chaotic attractor generated by Eq. (3.34) for a coupling strength of $c = 0.1$ (a) and $c = 0.2$ (b).

The new response system should be synchronized with the driver for $c = 0.2$, because it is obtained applying a smooth change of coordinates. However in this case, the motion does not occur in a single straight line as we can see in Fig. 3.25. There is a more complex object attracting the trajectories, which at glance could be taken as a sign of a nonsynchronized state. We can conclude from this simple example that GS can take place in an attractor with a complex structure. Then, to distinguish

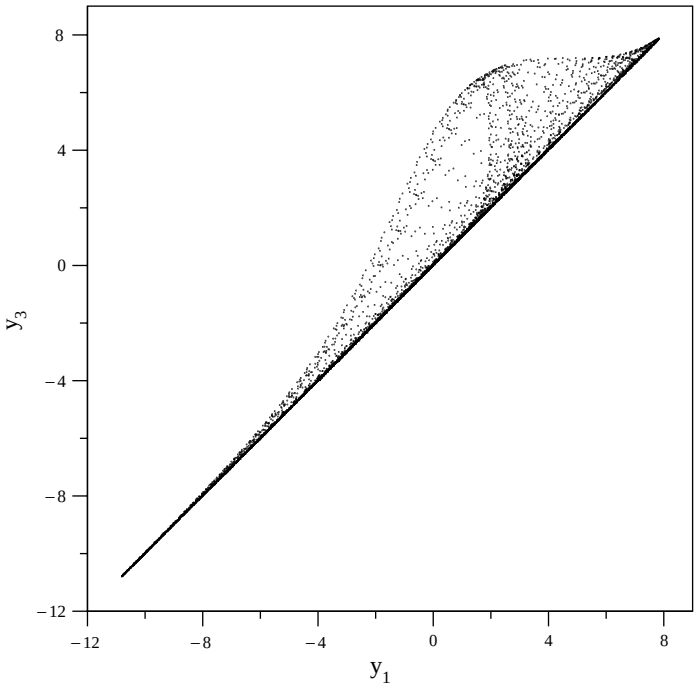

Fig. 3.25. The projection on the plane (y_3, y_1) of the chaotic attractor generated by Eq. (3.34) with the coordinate transformation given by (3.36), for a coupling strength of $c = 0.2$.

when two variables are synchronized in a generalized sense is a more complicated subject than detecting a CS state.

As said above, this is not the only definition of GS in the literature, the differences being based in the mathematical properties required for the map ψ. The notion of GS was introduced assuming essentially the existence of a homeomorphic map ψ [5], but later diffeomorphic properties have been required [110]. Furthermore, Ref. [37] distinguishes between two types of GS, namely the so-called *weak synchronization* ($\mathscr{WS}$) and the *strong synchronization* ($\mathscr{SS}$). $\mathscr{SS}(\mathscr{WS})$ corresponds to the case of a map ψ which is (which is not) smooth, in the sense of being (not being) differentiable. An even stronger version of $\mathscr{SS}$ is considered in Ref. [111], called *differentiable generalized synchronization*, requiring the continuous differentiability of ψ. All of these different approaches have relevant consequences when one looks for the existence of GS in experimental data, as we will outline later.

Kocarev and Parlitz [11] formulated the necessary and sufficient conditions for the occurrence of GS in the system (3.39). As in the case of CS, the notion of GS is equivalent to the asymptotic stability of the response system. Let us recall that the response system is said to be asymptotically stable if $\lim_{t\to\infty} \|\mathbf{y}(t, \mathbf{x}(\mathbf{0}), \mathbf{y}_1(\mathbf{0})) - \mathbf{y}(t, \mathbf{x}(\mathbf{0}), \mathbf{y}_2(\mathbf{0}))\| = 0$, where $(\mathbf{x}(\mathbf{0}), \mathbf{y}_1(\mathbf{0}))$ and $(\mathbf{x}(\mathbf{0}), \mathbf{y}_2(\mathbf{0}))$ are two generic initial conditions of system (3.33) in the basin of the synchronization attractor. In other words, a map $\mathbf{y} = \psi(\mathbf{x})$ (not necessarily smooth) exists whenever the action of the driver results in the response forgetting its initial condition. We will show later that this property allows one to introduce a useful criterion to detect GS [37,109].

The stability of the manifold M of GS can be determined as in the case of CS, i.e. by the negativity of conditional Lyapunov exponents [37], the use of Lyapunov functions [11] and the criterion given by Eq. (2.14) [112]. In addition to the problem of stability, other issues related with the existence of GS are crucial, especially when trying to detect it in experiments, where one is often interested in discerning whether some synchronization features appear. To this purpose, some useful statistical parameters have been introduced to test the existence of the map ψ and to determine its mathematical properties. One of these approaches is given in Ref. [10], which defines a mutual false neighbors' parameter r signaling the existence of a one to one smooth map between two dynamical variables. The definition of this parameter is based on the condition that the close points in the reconstructed space of the driver dynamics should have close images in the reconstructed space of the response dynamics, allowing to establish the continuity of ψ, and thus inferring the existence of a GS state. The definition and an application of r will be given in the next chapter.

Pecora et al. gave a complete discussion on how to characterize a functional relationship between two dynamical variables whose temporal behavior is obtained from time series in an experiment [110]. In this work, suitable statistical parameters are introduced and applied to test the mathematical properties of the map ψ, i.e. to test whether or not the mapping is continuous, injective, differentiable and with a continuous inverse. The implementation of these tests is discussed in a general context that includes the synchronization problem along with a test for determinism and the problem of filtering.

A further method to characterize dynamical interdependence among nonlinear systems based on mutual nonlinear prediction is given in Ref. [113]. This method provides information on the directionality of the coupling, and therefore it can be used to detect GS between dynamical variables. This technique was applied to detect GS in a neuronal ensemble.

Based on the equivalence between GS and the asymptotic stability of the response in system (3.33), a useful physical criterion have been suggested to detect GS in an experiment [37,109]. As said above, GS in the system (3.33) exists if the response system is asymptotically stable. Therefore, one can construct an auxiliary system (a system identical with the response), driven by the same driving system

$$\dot{\mathbf{y}}' = \mathbf{G}(\mathbf{y}', \mathbf{h}_\mu(\mathbf{x})) \,. \tag{3.36}$$

In this framework, $\mathbf{y}(t)$ is said to be synchronized with $\mathbf{x}(t)$ in a generalized sense if $\lim_{t\to\infty} \|\mathbf{y}'(t) - \mathbf{y}(t)\| = 0$. This is tantamount to state that GS between $\mathbf{x}(t)$ and $\mathbf{y}(t)$ occurs if CS takes place between $\mathbf{y}'(t)$ and $\mathbf{y}(t)$. The main advantage of this criterion is the easy detection of CS between $\mathbf{y}(t)$ and $\mathbf{y}'(t)$. On the other hand, the possibility of building an identical copy of an experimental device is often a very difficult task.

Let us now move to discuss an example of GS analyzed in Ref. [37], where it is shown how the properties of the map ψ change when the coupling is increased. Let us consider the following coupled systems

$$\left.\begin{aligned} \dot{x}_1 &= -\lambda(x_2 + x_3) \\ \dot{x}_2 &= \lambda(x_1 + 0.2x_2) \\ \dot{x}_3 &= \lambda(0.2 + x_3(x_1 - 5.7)) \end{aligned}\right\} \text{driver} \,,$$

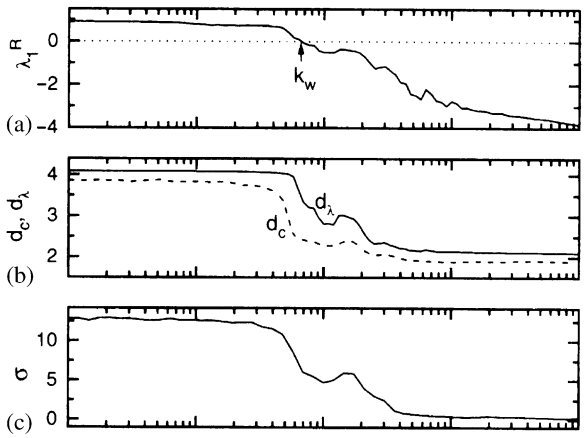

Fig. 3.26. From Ref. [37]. (a) Maximal conditional Lyapunov exponent; (b) correlation dimension d_c and Lyapunov dimension d_λ; (c) thickness parameter σ for the coupled system equation (3.37) as function of the coupling strength (see text).

$$\left.\begin{aligned} \dot{y}_1 &= 10(-y_1 + y_2) \\ \dot{y}_2 &= 28y_1 - y_2 - y_1 y_3 + kx_2 \\ \dot{y}_3 &= y_1 y_2 - \tfrac{8}{3} y_3 \end{aligned}\right\} \text{response} . \tag{3.37}$$

In the above equations, the driver is a Rössler system, whereas the response is a Lorenz system. The parameter λ sets the characteristic time scale of the driving. In addition, let us consider an auxiliary system $\mathbf{y}'(t)$. The coupling affects only the evolution of y_2 (via the term kx_2), and the coupling strength is ruled by k.

The behavior of the above system has been studied in Ref. [37], where a transition between $\mathscr{WS}$ and $\mathscr{SS}$ is shown as k increases. The threshold for this transition is found with the help of the auxiliary system $\mathbf{y}'(t)$ or by determining the value of k where the real part of the largest conditional Lyapunov exponent crosses zero ($\lambda_1^R = 0$). In Fig. 3 of Ref. [37], whose figures a, b and c are reproduced in the Fig. 3.26 of this report, it is shown that the threshold of $\mathscr{WS}$ is equal to $k_w \approx 6.66$ (Fig. 3.26(a)). The onset of $\mathscr{WS}$ is characterized by a noticeable decrease of the correlation dimension d_c [114] and the Lyapunov dimension d_λ [115] (Fig. 3.26(b)). In order to determinate how the smoothness of ψ changes when the coupling is increased, the thickness parameter σ is measured for each value of the coupling. σ is defined as the root of the local mean square deviation of a local linear interpolation map of points of the whole chaotic attractor. For $k > 40$, the value of d_c and d_λ saturates to the one corresponding to the attractor of the driving system, and σ saturates to zero. These features indicate that the map ψ is smooth, and then $\mathscr{SS}$ sets on.

The fact that a map $\mathbf{y} = \psi(\mathbf{x})$ exists suggests that the state of the response system could be predicted by knowledge of the state of the driver whenever they are in a GS state.

If the functions **F**, **G** and **h** in Eq. (3.33) are known, which is not the typical case in an experiment, the analytical technique for approximating ψ is based on the methods used on approximate center manifolds. An exhaustive discussion on center manifold theory can be found in Ref. [116] and the

application of this theory to the mapping between systems exhibiting GS can be found in Ref. [112]. In the following, we will briefly outline this technique.

If the drive and the response systems are given by (3.33), the following partial differential equation can be derived [116]:

$$\mathbf{G}(\boldsymbol{\psi}(\mathbf{x}), \mathbf{h}(\mathbf{x})) - \mathbf{D}_{\mathbf{x}}\boldsymbol{\psi}(\mathbf{x})\mathbf{F}(\mathbf{x}) = \mathbf{0} \tag{3.38}$$

which is valid on the synchronization manifold $\mathbf{y} = \boldsymbol{\psi}(\mathbf{x})$. Here again D_x represents the Jacobian matrix. While in most cases Eq. (3.38) cannot be solved exactly, an arbitrarily close solution can be approximated by a Taylor series

$$\boldsymbol{\psi}(\mathbf{x}) = \mathbf{A} + \mathbf{B} \cdot x + x \cdot \mathbf{L} \cdot x + \cdots . \tag{3.39}$$

Plugging (3.39) into (3.38), a solution can be written as a polynomial in powers of $\mathbf{x}$, when the coefficients of each power of $\mathbf{x}$ vanishes. By equating each coefficient to zero, one obtains a set of algebraic equations involving the parameters of the functions $\mathbf{F}(.)$, $\mathbf{G}(.)$, $\mathbf{h}(.)$ and the elements of $\mathbf{A}, \mathbf{B}, \mathbf{L}$. Finally, by solving the equations for the coefficients of $\mathbf{A}, \mathbf{B}, \mathbf{L}$, in terms of the parameters of the functions $\mathbf{F}(.)$, $\mathbf{G}(.)$ and $\mathbf{h}(.)$, one can obtain a proper approximation for $\boldsymbol{\psi}$.

However, the most general case corresponds to unknown functions in system (3.33). In this situation and when GS is stable, one can approximate $\boldsymbol{\psi}$ only by means of numerical methods. One of these methods uses local polynomial mapping in the reconstructed spaces of the driving and response systems [10,109]. The nonlinear function $\mathbf{G}(.)$ is represented as a collection of local polynomial mappings, which are different for different neighborhoods in the phase space. The parameters of each map are determined by least-squared fittings using simultaneous measurements of the driver and the response. An alternative numerical procedure for approximating $\boldsymbol{\psi}$ is based in the expansion of this map in a set of basis functions [112].

3.7. A mathematical definition of synchronization

In the previous sections, we have discussed different types of synchronized motions. The above plethora of theoretical studies as well as the large number of experimental verifications call for a unifying framework for synchronization of coupled dynamical systems. In the course of the last decades, several attempts have been put forward in that direction, and we will refer here to the most recent ones.

After a first attempt to define synchronized motion [117], recently Brown and Kocarev [118] provided a mathematical definition, assuming to have a system divisible into two subsystems in which functions (or properties) can be defined, consisting in mappings from the space of trajectories and time to some Cartesian space. Formally, this implies that the total system is seen as $w = [x, y]$, $w \in R^{m_1+m_2}$, $x \in R^{m_1}$, $y \in R^{m_2}$, with each subsystem forming a trajectory $\phi_x(w_0)$ and $\phi_y(w_0)$ (w_0 being a given initial condition). The two trajectories are then mapped by the properties g_x and g_y to a new space R^d. Finally, in order to define a synchronized state, Ref. [118] requires a function $h(g_x, g_y)$ with either $\|h\| = 0$ or $\|h\| \to 0$ asymptotically, with the choices of g_x, g_y and h determining the type of synchronization. This approach leads to the idea that there are different kinds of synchronization which might be captured in a single formalism.

The definition of Ref. [118] makes use of trajectory spaces, that are needed because several definitions of synchronization are based on averages or integrals over (infinitely) long time segments of system trajectories.

In fact, the formalism may be simplified and generalized, in such a way that it captures all the cases that the above approach does along with an entire class that were missed. This extension has been recently proposed [119], and will be summarized here.

To begin, assume that a system $\mathbf{Z} \in R^{m_1+m_2}$ can be divided into two subsystems, $\mathbf{X} \in R^{m_1}$ and $\mathbf{Y} \in R^{m_2}$. Typically, when one thinks of synchronized states, one means that an event in one subsystem (say y) corresponds *always* to a particular event in the other subsystem (say x). In a more mathematical language, these events can be identified with points in the phase or state space and one can capture the notion of predictability by saying that there exists a function from $\mathbf{X}$ to $\mathbf{Y}$ such that a particular point in $\mathbf{X}$ is mapped, uniquely, to one point in $\mathbf{Y}$.

More realistically, when one looks for evidence of synchronization in experiments or in numerics, one never has data falling right on a given $\tilde{x}$ or on a given $\tilde{y}$. Rather, the normal situation is that the closer $x(t)$ is to $\tilde{x}$ the closer $y(t)$ should be to $\tilde{y}$. This latter statement is rigorously attained with a *continuous* function, that is a mapping of the trajectories of $x(t)$ close to $\tilde{x}$ near to $\tilde{y}$ by a function that is continuous at the point $(\tilde{x}, \tilde{y})$.

However, a more stage is necessary. Suppose to consider a curved one-dimensional manifold in a two-dimensional phase space ($m_1 = m_2 = 1$), and assume that the dynamics hold on that manifold. The general case does not allow to construct a continuous function from x to y. However, suppose to consider a transformation $\mathscr{F} : \mathbf{Z} \to \mathbf{W}$ ($w = \mathscr{F}(z)$) that "straightens out" the manifold, and transforms it into a straight line. Now, the two projections of the transformed system $u = \mathscr{P}_1(w) \in \mathbf{U}$, $v = \mathscr{P}_2(w) \in \mathbf{V}$ form a synchronization manifold and one can define a synchronous state at any pair of points $(\tilde{u}, \tilde{v})$. From the above example we learn that, in order to investigate synchronization states, the separation of the global system into subspaces is a very delicate and crucial operation, and should be performed only after a proper transformation of the global phase space is selected to disentangle "hidden" or latent synchronization features. Furthermore, any types of property functions g_u and g_v used in Ref. [118] may be captured using a flow and then a general transformation $g = (g_u, g_v)$ which splits into the two properties.

Another important point to remark is that, for some applications, the dimensions of the final space may differ from the ones of the original phase space. Therefore, for the sake of generality, in the following we will refer to a function $\mathscr{F} : R^{m_1+m_2} \to R^{d_1+d_2}$, where $d_1 + d_2$ do not necessarily add to $m_1 + m_2 = m$.

At this point, we have all the main ingredients that are needed to build up a general definition of synchronization: (1) a function from the original phase space z to a new phase space (u, v), (2) the projections $\mathscr{P}_1$ and $\mathscr{P}_2$ onto the components of the new space, (3) the synchronization relation, a continuous function.

A first step is refining the definition of continuous function to include consistency with the dynamics.

Definition. A function f is a *synchronization function* at $(\tilde{u}, \tilde{v})$ if (a) $\tilde{v} = f(\tilde{u})$; (b) it is continuous at $\tilde{u}$ and (c) it is consistent with the dynamics $(u(t), v(t))$ locally, that is, if δ and ε are a valid pair for the continuity property ($|u - \tilde{u}| < \delta$ implies $|f(u) - \tilde{v}| < \varepsilon$), then the dynamics is such that if $|u(t) - \tilde{u}| < \delta$ we have $|v(t) - \tilde{v}| < \varepsilon$.

The above said means that, near $(\tilde{u},\tilde{v})$ the function f well describes the predictability of subsystem **V** from subsystem **U**.

Let us now pay attention to initial conditions and time. Let $\mathscr{B}$ be the basin of attraction of an attractor $\mathscr{A}$ for a dynamical system $\mathbf{Z}\subset R^m$, and let $\mathscr{P}_1$ and $\mathscr{P}_2$ be projectors from $R^{d_1+d_2}$ to R^{d_1} and to R^{d_2}, respectively.

Definition. For a given function $\mathscr{F}:R^m\to R^{d_1+d_2}$, a dynamical system $\mathbf{Z}\subset R^m$ contains *locally synchronous subsystems* in $\tilde{z}\in\mathscr{A}$ if $\forall z_0\in\mathscr{B}$ there is a time T such that for $t\geqslant T$ a synchronization function exists at $(\tilde{u}=\mathscr{P}_1(\mathscr{F}(\tilde{z})),\tilde{v}=\mathscr{P}_2(\mathscr{F}(\tilde{z})))$.

We first remark that the above definition is local, i.e. one can think of the subsystems as having properties u and v which are synchronous only near part of the trajectory (close to $\tilde{z}$), but cannot say what the relationship is between $u(t)$ and $v(t)$ anywhere else in the attractor. The particular type of synchronization is determined by the nature of the functions f and $\mathscr{F}$.

Of course, one is interested in extending the definition to the entire trajectory so as to have a single continuous function on the whole image of the attractor under $\mathscr{F}$. This extension, in spite of being just a matter of having enough points of local synchronization, is a very delicate process. Indeed, one wants every point on the trajectory be mapped by a unique continuous function between the two subsystems u and v, while the above definition warrants that a given function is associated with each synchronization pair $(\tilde{u},\tilde{v})$, and the functions may be different in their local continuity, that is the valid δ and ε pairs do not need to have any particular relationship between different synchronization functions. In order to cope with this situation, and to provide a rigorous extension in a theorematic way, one needs to add a further feature, namely a "covering" property.

Definition. If $\{u_i\}$ is a set of points on **U** and $\{f_i\}$ is a set of continuous functions, one associated with each u_i, from **U** to **V**, then the functions provide a *continuity covering* of **U** if $\forall\epsilon>0$ the set of all valid δ_i's associated with ϵ (one for each (u_i,f_i) pair) covers the set **U**.

Now we are ready for demonstrating the following theorem:

Theorem. *If the subsystem* **U** *contains a set of synchronization points* $\{u_i\}$ *and the associated functions* $\{f_i\}$ *provide a continuity covering of* **U**, *then there exists a unique*, *global*, *continuous synchronization function* $f:\mathbf{U}\to\mathbf{V}$.

Proof. Let us first demonstrate that the function f is uniquely defined. To this purpose, we proceed by absurdity, and suppose there exist two different realizations of the dynamics $z_1\in\mathscr{A}$ and $z_2\in\mathscr{A}$ such that $\mathscr{P}_1(\mathscr{F}(z_1))=\mathscr{P}_1(\mathscr{F}(z_2))=u$, $\mathscr{P}_2(\mathscr{F}(z_1))=v_1$, $\mathscr{P}_2(\mathscr{F}(z_2))=v_2$. We call $\eta=|v_1-v_2|$ the distance between the two images of z_1 and z_2 in R^{d_2}, and we pick $\epsilon<\eta/2$. We call u_k the synchronization point whose neighborhood of radius $\delta_k(\epsilon)$ contains u (the above covering property warrants its existence). Furthermore, we call f_k the associated synchronization function. Now, f_k is (by definition) consistent with the dynamics. Therefore, $|f_k(u_k)-v_1|<\epsilon$ and $|f_k(u_k)-v_2|<\epsilon$. The latter two inequalities may be added, and, by use of the triangular inequality, one obtains $|v_1-v_2|<\eta$, which contradicts the hypothesis. As a consequence, a unique function f exists mapping all points

$u \in \mathbf{U}$ into the corresponding points $v = f(u) \in \mathbf{V}$. The second part of the proof is to show that f is continuous at all points $u \in \mathbf{U}$. By definition, $\forall \epsilon/2$ there is a δ_j associated with one of the synchronization points u_j such that $|u - u_j| < \delta_j$. We pick $\delta > 0$ so that the set $S_\delta = \{u' : |u' - u| < \delta\}$ is completely contained in the set of points within δ_j around u_j. Due again to consistency of f_j with the dynamics, $\forall u' \in S_\delta$ one must have $|f(u') - f_j(u_j)| < \epsilon/2$. On the other side, one also has $|f_j(u_j) - f(u)| < \epsilon/2$. Therefore, by use again of the triangular inequality, it comes out that $|f(u') - f(u)| < \epsilon$ whenever $|u' - u| < \delta$. □

What is discussed above provides a definition of perfect synchronization. In many realistic applications (such as in experiments) noise or finite measurement resolutions are unavoidable. It is useful, therefore, to introduce a fuzziness parameter, setting up a minimal coarsening scale at which states in one projected set may be associated with states in the other.

Definition. For a given function $\mathscr{F} : R^m \to R^{d_1+d_2}$, a dynamical system $\mathbf{Z}$ contains *locally σ-synchronous subsystems* in $\tilde{z} \in \mathscr{A}$ if $\forall z_0 \in \mathscr{B}$ there is a time T such that $\forall \epsilon > \sigma$ $\exists \delta > 0$ such that $t \geqslant T$ and $|\mathscr{P}_1(\mathscr{F}(\Phi(t, z_0))) - \mathscr{P}_1(\mathscr{F}(\tilde{z}))| < \delta \Rightarrow |\mathscr{P}_2(\mathscr{F}(\Phi(t, z_0))) - \mathscr{P}_2(\mathscr{F}(\tilde{z}))| < \epsilon$.

It is evident that this last definition recovers the previous one for $\sigma \to 0$. $\sigma \neq 0$ is tantamount to saying that the consistency of the synchronization function with the dynamics holds only up to a minimum scale, which gives the minimal coarsening or precision scale that must be used in experiments to detect synchronization features.

An important remark is the following: even though the value of the fuzziness parameter is not constrained in the definition, if σ is larger than the diameter of $\mathscr{P}_2(\mathscr{F}(\mathscr{A}))$, then the above is trivially satisfied $\forall \delta > 0$ and $\forall z_0 \in \mathscr{B}$. The only relevant cases are the ones in which σ is considerably smaller than the diameter of $\mathscr{P}_2(\mathscr{F}(\mathscr{A}))$.

Finally, global σ-synchronization may be identified as the situation where local σ-synchronization is displayed regardless on the particular choice of $\tilde{z} \in \mathscr{A}$.

With the help of the above set of definitions, one can easily show that different synchronization phenomena can be encompassed within a single framework (for all details, we address the reader to Ref. [119]). Here we summarize the specifications for generalized, complete and lag synchronization.

GS and CS are characterized by the fact that the asymptotic evolution of the system occurs within a manifold defined by $y = K(x)$, K being a generic function (CS is the case for which $m_1 = m_2$ and K coincides with the identity). In our framework, GS can be considered as a particular case of global synchronization with $\sigma = 0$. Indeed, let $\mathscr{F}$ be the function with ith components given by $\mathscr{F}_i = K(x)_i$, $i = 1, \ldots, m_2$; $\mathscr{F}_i = y_i$, $i = m_2 + 1, \ldots, 2m_2$. Note that here $d_1 = d_2 = m_2$; therefore the dimensions of the final state equal m only when $m_1 = m_2$. Our definition of global synchronization (for $\sigma = 0$) is tantamount to saying that $\forall \epsilon > 0$ $\exists \delta > 0$ such that $|K(x) - K(\tilde{x})| < \delta \Rightarrow |y - \tilde{y}| < \epsilon$, $\forall \tilde{z} \equiv (\tilde{x}, \tilde{y})$. Now, if $\tilde{z}$ is on the synchronization manifold, GS implies that $|y - \tilde{y}|$ asymptotically equals $|K(x) - K(\tilde{x})|$, so that our definition is verified with $\delta = \epsilon$.

LS refers to a case in which asymptotically $|x(t) - y(t - \tau_{\text{lag}})| < R$, for a given lag time τ_{lag}. LS can be identified with a global σ-synchronization phenomenon. Consider $\mathscr{F}$ as having components given by $\mathscr{F}_i = z_i$, $i = 1, \ldots, m_1$; $\mathscr{F}_i = \Phi_i[-\tau, z(t)]$, $i = m_1 + 1, \ldots, m_1 + m_2$. Here, $\Phi[t, z_0]$ is the flow function giving $z(t)$ from the initial condition z_0, and we are explicitly

considering invertible flows. $\mathscr{F}$ is a point to point function in the space R^m. It is easy to show that $\sigma = 2R$ and $\delta(\epsilon) = \epsilon - 2R$ satisfy our definition of global σ synchronization in the transformed space.

Furthermore, practical analysis tools are nowadays available that allows to reconstruct dimensions of subspaces for coupled dynamical systems in order to validate the above formalism with multivariate data sets [120], or to detect dynamical interdependence [121] and synchronized motions [122]. These recent achievements have followed previous attempts of detecting synchronized motions and mutual dependence of variables in practical situations [113,123–129].

4. Synchronization in structurally nonequivalent systems

4.1. Synchronization of structurally nonequivalent systems

All what is said above describes the situation of coupled structurally equivalent systems, i.e. either equivalent systems or systems where the nonidentity resulted in a rather small parameter mismatch. Only recently the study of synchronization phenomena for large parameter mismatches has been addressed [130], by description of the appearance of synchronized collective motion in systems with more than 50% mismatch in parameters.

However, in nature one cannot expect to cope with coupled low-dimensional systems which are structurally equivalent. Therefore, it becomes important to extend the concept of synchronization to the case of structurally nonequivalent systems, i.e. systems generating chaotic attractors with high and different fractal dimensions. This process has been investigated in Ref. [20], and will be summarized along this section.

Let us begin with an example. Consider the symmetric coupling of two chaotic systems, the first giving rise to a solution x_1 with the fractal dimension D_1 and the second to a solution x_2 with the fractal dimension D_2 (with $D_1 \neq D_2$). Now, synchronization is associated with the emergence of some dynamical relations between the two outputs. Suppose the two systems reach a CS regime, which implies $x_1(t) = x_2(t) = x(t)$. Now, a natural question arises: which is the fractal dimension of the synchronization manifold $x(t)$? In other words, which is the dynamical process associated with the primer of synchronized states, bringing the two system to adjust themselves on the same structure (the synchronization manifold)? Ref. [20] has shown that synchronized states for structurally nonequivalent systems can be realized either in a chaotic manifold, with dimension lower with respect to both uncoupled systems, or even in a periodic manifold.

In what follows we will specialize the above example to the case of two coupled delayed dynamical systems (DDS). The general form for a DDS is $\dot{y} = \mathscr{F}(y, y_d)$, where y is a real variable and $y_d \equiv y(t - T)$, T being a delay time. The increasing interest of the physics community for DDS is due to the fact that they provide a natural link with space extended systems by means of the two variable representation of the time $t = \sigma + \theta T$ ($0 \leqslant \sigma \leqslant T$ being a continuous space-like variable, and θ being a discrete temporal variable). This representation, first introduced in Refs. [131,132], allows one to convert long-range interactions due to the delay into short-range interactions along the direction θ, since now $y_d \equiv y(\sigma, \theta - 1)$. Furthermore, in that framework, the formation and propagation of space–time structures, as defects and/or spatiotemporal intermittency has been identified [133] and controlled [134].

For the sake of exemplification, we now refer to a pair of symmetrically coupled Mackey–Glass systems:

$$\dot{x}_{1,2} = -0.1x_{1,2}(t) + 0.2\,\frac{x_{1,2}(t-T_{1,2})}{1+x_{1,2}(t-T_{1,2})^{10}} + \epsilon(x_{2,1}(t) - x_{1,2}(t))\,, \tag{4.1}$$

where $x_{1,2}$ are real variables, $T_{1,2}$ are delay times, and $0 \leqslant \epsilon < 1$ is a coupling strength. The case of identical DDS ($T_1 = T_2$) has been studied in Refs. [135,136], even in a high-dimensional chaotic case, while here we will focus explicitly on nonidentical DDS ($T_1 \neq T_2$). It is a well known property of DDS that their fractal dimensions depends linearly upon the delay time [137,138]. This means that, by selecting $T_1 \neq T_2$ and by choosing $T_{1,2}$ sufficiently large, for $\epsilon = 0$ the two systems (4.1) generate high-dimensional chaotic signals with quite different fractal dimensions, and therefore they come out to be confined within structurally different chaotic attractors.

Let us now move to investigate the effect of $\epsilon \neq 0$ in Eqs. (4.1). It is important to mention at this stage that the scenario we are going to describe is a general feature of system (4.1), regardless on the particular choice of the delay times. However, for the sake of exemplification, in the following we will select $T_1 = 100$ and $T_2 = 90$. The two signals $x_1(t)$ and $x_2(t)$ at $\epsilon = 0$ are shown in Fig. 4.1(a), and they appear to be uncorrelated (Fig. 4.1(b)).

A gradual increase in the coupling strength ϵ builds up correlations between x_1 and x_2, consistently with what was observed in Ref. [7] for a symmetric coupling between a chaotic and a hyper-chaotic Rössler system. (Fig. 4.1(c), $\epsilon = 0.3$), which is yet chaotic.

A final sharp transition is observed toward a periodic state, which is reached for large ϵ values (Fig. 4.1(e), $\epsilon = 0.65$), where the coupled system of Eqs. (4.1) collapsed onto a simple periodic attractor. As a result, a large structural change in system (4.1) is associated with the increasing of ϵ.

In order to more quantitatively characterize the appearance of synchronization in system (4.1), one can make use of the *mutual false nearest neighbors* (MFNN) parameter [10,139]. To this purpose, consider three embedding spaces, namely S_1, S_2 and S_3. S_1 is the embedding space of $x_1(t)$ at the fixed embedding dimension m_1, S_2 is the embedding space of $x_2(t)$ at variable embedding dimension m_2, and S_3 is the embedding space of $x_2(t)$ at the fixed embedding dimension m_1. One then chooses randomly n state vectors $\mathbf{x}_1^n$ in S_1 and considers the images $\mathbf{x}_2^n$ and $\mathbf{x}_3^n$ in S_2 and S_3. Furthermore, one calls $\mathbf{x}_{1,\mathrm{NN1}}^n$ ($\mathbf{x}_{3,\mathrm{NN3}}^n$) the nearest neighbor to $\mathbf{x}_1^n$ ($\mathbf{x}_3^n$) in S_1 (S_3). In the same way, the nearest neighbor $\mathbf{x}_{2,\mathrm{NN2}}^n$ to $\mathbf{x}_2^n$ in S_2 is considered, and one calls $\mathbf{x}_{1,\mathrm{NN2}}^n$ ($\mathbf{x}_{3,\mathrm{NN2}}^n$) the image of $\mathbf{x}_{2,\mathrm{NN2}}^n$ in S_1 (S_3). Finally, the MFNN parameter is defined as [10,139]

$$r = \left\langle \frac{|\mathbf{x}_1^n - \mathbf{x}_{1,\mathrm{NN2}}^n|^2}{|\mathbf{x}_1^n - \mathbf{x}_{1,\mathrm{NN1}}^n|^2} \frac{|\mathbf{x}_3^n - \mathbf{x}_{3,\mathrm{NN3}}^n|^2}{|\mathbf{x}_3^n - \mathbf{x}_{3,\mathrm{NN2}}^n|^2} \right\rangle_n , \tag{4.2}$$

where $\langle \cdots \rangle_n$ denotes the averaging process over n. In Refs. [10,139] it has been shown that $r \equiv 1$ for systems showing GS, whereas $r \neq 1$ for not synchronized systems.

In Fig. 4.2(a) we report the dependence of r upon m_2, at fixed $m_1 = 25$ for $\epsilon \leqslant 0.1$, as well as for $m_1 = 15$ at $\epsilon > 0.1$. On the other hand, Fig. 4.2(b) reports r as a function of ϵ for $m_2 = 35$, and $m_1 = 25$ ($\epsilon \leqslant 0.1$), $m_1 = 15$ ($\epsilon > 0.1$). The primer of a synchronized state is detected at $\epsilon \simeq 0.15$.

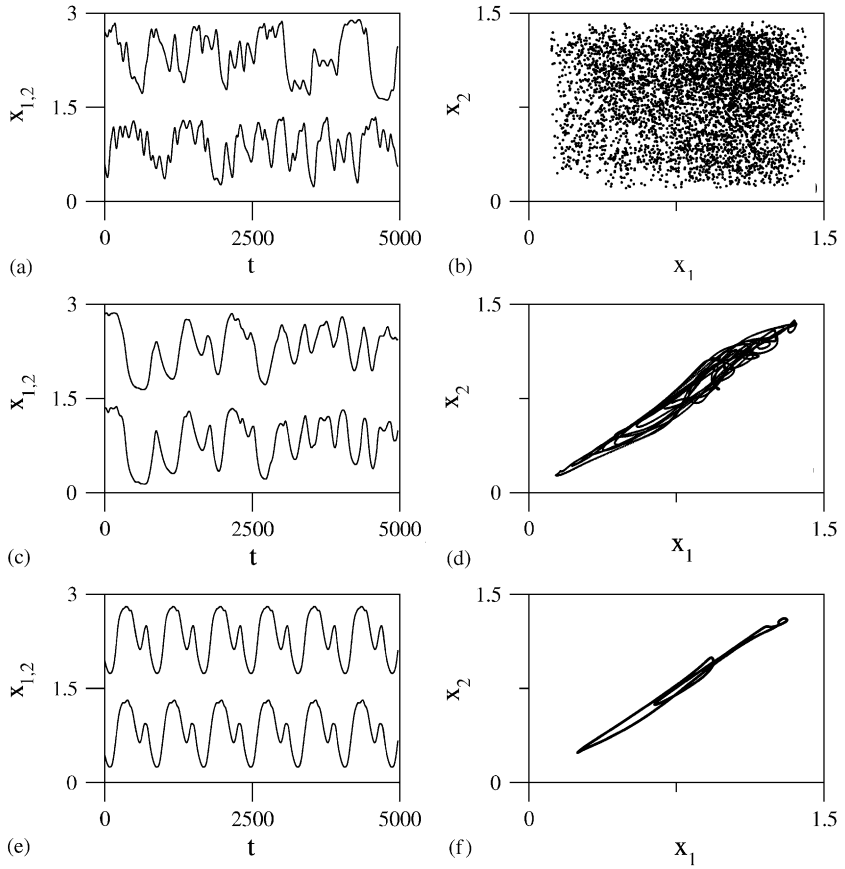

Fig. 4.1. (a, c, e) Time evolution of signals x_1 and x_2 of two coupled Mackey–Glass systems equation (4.1) for $\epsilon = 0$ (a, uncoupled case), $\epsilon = 0.3$ (c, synchronized chaotic state), and $\epsilon = 0.65$ (e, synchronized periodic state). (b, d, f) Projections of the attractor of system (4.1) on the plane (x_1, x_2) for $\epsilon = 0$ (b), $\epsilon = 0.3$ (d), and $\epsilon = 0.65$ (e). In (a, c, e) the signal x_2 is conveniently vertically shifted.

4.2. From chaotic to periodic synchronized states

When structurally equivalent systems are considered [7], in general the emergence of synchronization can be associated with a continuous slow variation in the Lyapunov spectrum, leading to sequential changes in the signs of the positive Lyapunov exponents. On the contrary, for structurally nonequivalent systems, the occurrence of a periodic synchronized state is associated with an abrupt transition in the Lyapunov spectrum. Here, many positive Lyapunov exponents passes to negative values at once.

What is said above is confirmed in Fig. 4.3, where the Kaplan–Yorke or Lyapunov dimension D_λ of Eq. (4.1) (Fig. 4.3(a)) as well as the number of positive Lyapunov exponents (Fig. 4.3(b)) are reported vs. the coupling strength. At small ϵ, a slow continuous decreasing process of the Lyapunov dimension is observed, in a consistent way with what happens for structurally equivalent systems.

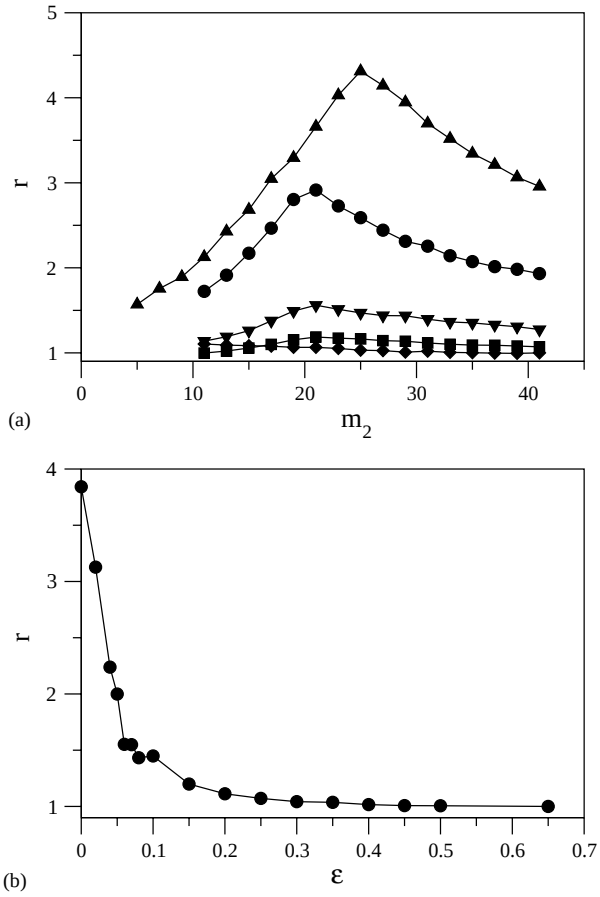

Fig. 4.2. (a) MFNN parameter r [10,139] (Eq. (4.2)) as a function of m_2 for $\epsilon = 0$ (upper triangles), $\epsilon = 0.05$ (circles), $\epsilon = 0.1$ (lower triangles), $\epsilon = 0.2$ (squares) and $\epsilon = 0.5$ (diamonds). The calculations have been done with 500,000 data points from the solution of system (4.1), and taking $n = 5000$ randomly selected state vectors for the averaging process of r. $m_1 = 25$ for $\epsilon \leqslant 0.1$. $m_1 = 15$ for $\epsilon > 0.1$. (b) MFNN parameter r as a function of ϵ for a fixed $m_2 = 35$, and the other parameters as above.

At larger couplings, however, two different dynamical regimes can be isolated. This first corresponds to the appearance of GS ($0.15 < \epsilon$), where a plateau in the Lyapunov dimension around $D \simeq 7.2$–7.5 sets in for $0.15 < \epsilon < 0.6$, thus indicating that GS is initially realized in a high-dimensional chaotic state. Correspondingly, the number of positive Lyapunov exponents does not change in the range $0.15 < \epsilon < 0.6$. A second regime is encountered for $0.6 < \epsilon$. Here, a sharp transition in the Lyapunov dimension is found, leading to the stabilization of a final periodic state. It is important to remark that such a transition corresponds to a sudden change in the Lyapunov spectrum, wherein all residual positive Lyapunov exponents suddenly jump to negative values at once (Fig. 4.3(b)). This phenomenon constitutes a remarkable difference with the synchronization features studied for structurally equivalent systems.

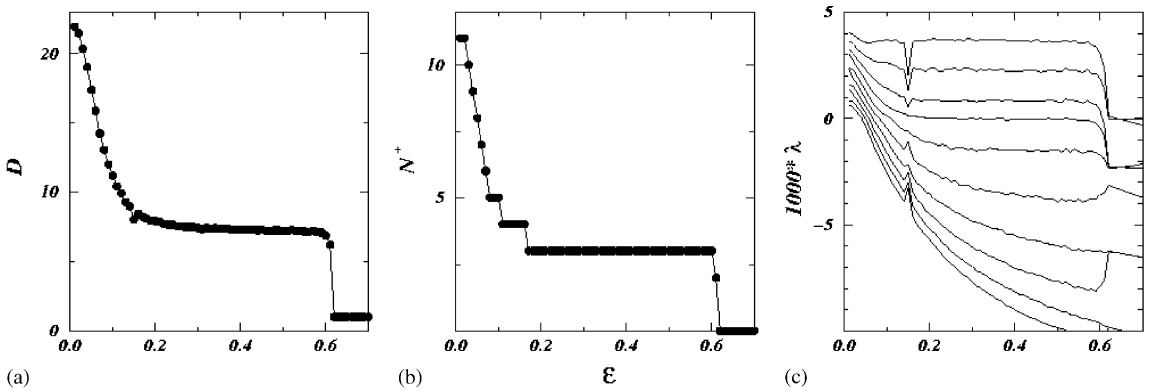

Fig. 4.3. From Ref. [20]. (a) Kaplan–Yorke dimension of Eq. (4.1) as a function of the coupling strength ϵ. (b) Number of positive exponents in the Lyapunov spectrum vs. ϵ. (c) Largest 10 exponents in the Lyapunov spectrum vs. ϵ. In all cases the calculations have been performed over a time $\bar{t} = 1,000,000$, corresponding to 10,000 delay units of the system with larger delay. The structural collapse at $\epsilon \simeq 0.6$ is marked by a sharp transition in the Kaplan–Yorke dimension (a) and by the fact that many positive Lyapunov exponents goes to negative value at once (c).

In order to further confirm these findings, one can calculate the 10 largest Lyapunov exponents in the spectrum of Eqs. (4.1) as functions of the coupling parameter ϵ (Fig. 4.3(c)). The calculations here reported have been performed over a time $\bar{t} = 1,000,000$, corresponding to 10,000 delay units of the system with larger delay.

If one focuses on the transition from a hyper-chaotic state to a periodic orbit near $\epsilon \approx 0.6$, an intermittent behavior is found, that is the system switches in time between two qualitative different types of dynamics: a motion close to a periodic orbit and a vastly irregular motion far away from it. A similar desynchronization scenario was characterized as on–off intermittency in the case of identical DDS [136].

We conclude this section by pointing out that this phenomenon is relevant insofar as the stabilization process of a periodic synchronized motion is here a consequence of a sufficiently large coupling strength between the two systems, but *it is not generated by external perturbations*, as in the case of the usual chaos control theory [140,141].

5. Noise-induced synchronization of chaotic systems

In the first four sections we have presented a review of synchronization behavior of two *coupled* chaotic systems. In this section, we consider the situation that two chaotic systems are not coupled directly or only weakly coupled, but subject to a common fluctuating driving signal which is assumed to be noise in many contexts.

Counterintuitive effects of noise in nonlinear systems have been a subject of great interest in the context of stochastic resonance [142–144], doubly stochastic resonance [145,146], and coherence resonance [147–150]. With stochastic resonance, noise can optimize a system's response to an external signal, while with coherence resonance, pure noise can generate the most coherent motion in the system.

The circumstance that different systems are not coupled or only weakly coupled but subjected to a common random forcing is of great relevance in biology, especially in neuroscience or ecology. In neural systems, different neurons commonly connected to another group of neurons, receive a common input signal which often approaches a Gaussian distribution as a result of integration of many independent synaptic currents [151]. We would emphasize the experimental observation of the spiking behavior of animal neocortical neurons in response to external stimulus. When the stimulus is a constant input current, the neurons generate different spike sequences in repeated experiments with the same driving signal. Remarkably, when an amount of Gaussian noise is added to the constant input to mimic the synaptic input in actual neural systems, the neurons produce repetitive spike sequences in repeated experiments with the same fluctuating driving signal. This reliability of spike timing is of significance for understanding signal encoding by spike timing of neurons. In ecology, food webs [152,153] and forest ecosystems [154] over a large geographical region are affected by similar environmental fluctuations. Actually, observations have shown synchronous oscillation of populations [152–154], and the common environmental fluctuations may play an important role in this collective behavior in ecology. It is important to emphasize that, in these systems, both the coupling and the common random forcing are often rather weak among the elements which are generically nonidentical.

However, investigation of noise-induced synchronization of chaotic systems has been a subject of long-standing debates. This section is devoted to review the previous debates and to clarify this controversy. We will also extend the study of noise-induced synchronization of identical chaotic systems to noise-induced PS in nonidentical systems. Finally, we discuss noise-enhanced PS in weakly coupled chaotic oscillators.

5.1. Noise-induced complete synchronization of identical chaotic oscillators

Synchronization of nonlinear systems coupled only by a common random force has drawn considerable attention. Firstly, it was shown that noise can induce synchronization in periodic oscillations [155–157]. More interesting, the phenomenon of noise-induced order was reported on the chaotic BZ map which is directly connected to the Belousov–Zhabotinsky chemical reaction [158]. There, a small amount of noise may change a chaotic trajectory of the system into a state similar to a periodic orbit smeared with noise [158], which makes the largest Lyapunov exponent (λ_1) negative, and leads to a slower decay of correlations and an improvement of the state predictability [159,160]. A negative largest Lyapunov exponent means that in an ensemble of systems with identical laws of motion and *common noise*, such as the motion of floating particles on a surface of incompressible fluid [52], the states in the phase space shrink into a single point [52,161], i.e. noise induces CS in chaotic systems. Near the transition point of the Lyapunov exponent, separation of trajectories exhibits very intermittent behavior [52], and the probability density of the separation satisfies a scaling law [161]. This intermittent behavior has been shown [106,162,163] to be on–off intermittency [164].

The effect of common noise on CS of identical chaotic systems was reconsidered [165]. In particular, Ref. [165] studied the logistic map

$$x_{n+1} = 4x_n(1 - x_n) + \eta \tag{5.1}$$

with the noise η uniformly distributed in $[-W, W]$. η is chosen such that $x_{n+1} \in (0,1)$, otherwise it is discarded and a new η is chosen. It was claimed in Ref. [165] that synchronization of logistic maps with common noise η occurs when $W > W_c = 0.5$. Ref. [165] also examined the Lorenz system

$$\begin{aligned} \dot{x} &= \sigma(y - x), \\ \dot{y} &= \rho x - y - xz, \\ \dot{z} &= -bz + xy \end{aligned} \tag{5.2}$$

with noise acting on the y variable which now iterates as

$$y(t + \Delta t) = y(t) + [\rho x(t) - y(t) - x(t)z(t)]\Delta t + W\eta\sqrt{\Delta t}\ .$$

The parameters are $\sigma = 10$, $\rho = 28$ and $b = 8/3$, and $\eta \in (0,1)$ is uniformly distributed biased noise. Synchronization was observed for $W > W_c \simeq 2/3$, while it does not occur for symmetric noise where η is replaced by $(\eta - 0.5)$ [165].

These results have spurred a long-standing dispute on the general conclusion of [165] that strong-enough noise is able to synchronize chaotic systems. Firstly, Pikovsky [166] pointed out that the largest Lyapunov exponent of the noisy logistic map is positive which is in contradiction to the criterion of negative largest Lyapunov exponent for synchronization [52,161]. The synchronization observed in [165] is actually an artifact of finite precision in numerical simulations [166,167]. Several other authors, on the other hand, restudied the problem by examining the properties of the noise applied to the systems. For the noisy logistic map, the noise is state-dependent and not symmetric [168], but has a negative mean value, i.e. it is biased [169], and it is this nonzero mean that plays an important role in synchronization and a zero-mean noise cannot lead to synchronization [169]. For the Lorenz system, synchronization was observed for uniform noise in $[0, W]$ with large enough W values, but not for unbiased one [165]. The largest Lyapunov exponent of the noisy Lorenz system is the same as that of the system driven constantly only by the mean value $W/2$ of the noise, indicating that the bias of the noise plays the crucial role in synchronization [168,170]. Recently, Sanchez et al. [171] analyzed synchronization of chaotic systems by noise in an experiment with Chua's circuit, drawing the general conclusion based on previous results [165–169] that synchronization might be achieved only by a biased noise, but not by an unbiased one, and synchronization is only a result of noise-induced order because the biased noise drives the system into a noise-smeared periodic orbit, similar as in [158].

However, this conclusion has stimulated further investigations. Ref. [172] showed that symmetric white noise can indeed induce synchronization in some chaotic maps, which are chaotic models of coupled neurons [173] and which have as an important ingredient significant contraction regions, i.e. regions where $|f'(x)| < 1$ (Fig. 5.1). Synchronization induced by unbiased noise has been also reported in other maps with similar exponential tails [172,174], as well as in the Lorenz system with a much larger intensity of unbiased noise [174]. In fact, the nonzero mean value of noise can be separated and viewed as an additional parameter which may move the system into another dynamical regime. When the dynamics is shifted to a periodic regime by this parameter, the symmetric noise component acts to smear out the periodic orbit, while it may leave the largest Lyapunov exponent negative. In this case, synchronization of two identical systems influenced by common

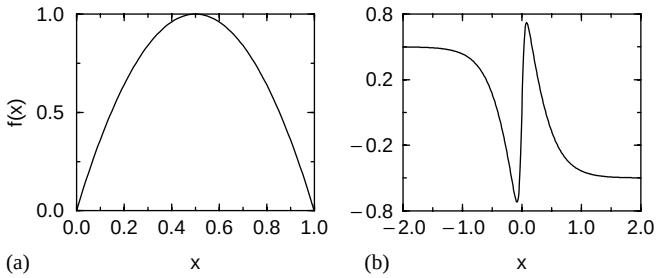

Fig. 5.1. (a) Logistic map $f(x) = 4x(1-x)$ where common noise does not induce synchronization. (b) A chaotic map $f(x) = \tanh(A_1 x) - B\tanh(A_2 x)$ with $A_1 = 20$, $A_2 = 2$ and $B = 1.5$. Noise can easily induce synchronization in this system due to large contraction regions where $|f'(x)| < 1$.

noise is a trivial result of noise-induced order. Considering the system with only a constant bias of noise as a new system which can still be chaotic, the controversy can be focused to the question whether unbiased noise can induce synchronization in originally chaotic systems. The reason has not been clearly addressed, although there are numerical and experimental examples of noise-induced synchronization.

To clarify the controversy, Ref. [175] have carried out a comparison study of noise-induced synchronization between the Rössler and the Lorenz systems.

An individual noisy Rössler system reads

$$\begin{aligned} \dot{x} &= -\omega y - z, \\ \dot{y} &= \omega x + 0.15y + D\xi(t), \\ \dot{z} &= 0.4 + z(x - 8.5) \end{aligned} \tag{5.3}$$

with $\omega = 0.97$. Again, the Lorenz system is the same as in Eq. (5.2), but with a noise term $D\xi(t)$ added to the y variable. The parameters $\sigma = 10$, $\rho = 28$ and $b = 8/3$ are the standard ones and are the same as in [165,174]. $\xi(t)$ is a Gaussian noise with $\langle \xi(t)\xi(t-\tau)\rangle = \delta(\tau)$.

To avoid numerical artifacts, the largest Lyapunov exponent λ_1 of the noisy system is calculated as a function of the noise intensity. Lyapunov exponents of noisy dynamical systems are well defined [176] similar to the deterministic case. Although Lyapunov exponents in stochastic systems generally no longer refer to the Kolmogorov–Sinai entropy, and thus are not a proper measure of the complexity of the systems [177,178], by definition, they naturally characterize synchronization between systems with *common* noise [161,172,174,176].

To measure synchronization directly, the average distance as a synchronization error $\langle |x_1 - x_2| \rangle$ between the two identical systems with common noise is also computed, with averaging over time and noise realizations. The results of λ_1 and $\langle |x_1 - x_2| \rangle$ for the Rössler system and the Lorenz system are shown in Fig. 5.2. In the Rössler system, λ_1 keeps positive till the systems become unstable for $D > 4$. Complete synchronization is never observed here. This behavior is similar if the noise is applied to the x variable, or to both x and y variables. Noise is not applied to the z variable, because rather small noise already makes the system then unstable. However, in the Lorenz system, λ_1 becomes negative for $D > 33.3$, and two identical Lorenz systems with common

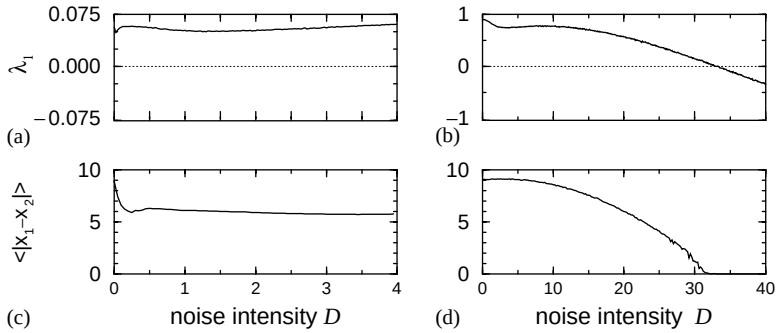

Fig. 5.2. Largest Lyapunov exponent λ_1 of the Rössler system (a) and the Lorenz system (b). Average synchronization error $\langle |x_1 - x_2| \rangle$ of the Rössler system (c) and the Lorenz system (d).

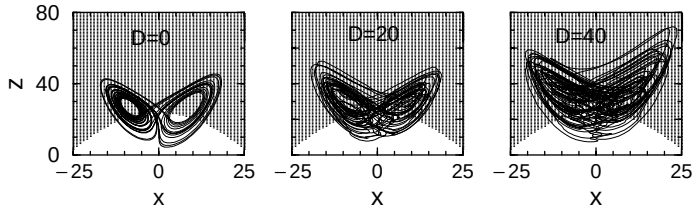

Fig. 5.3. Trajectories in the phase space of the Lorenz system at different noise intensities. The dotted background shows the contraction region in the plane $y = 0$.

noise achieve CS, as is further illustrated by a vanishing synchronization error after the transition point.

It is important to note that, in the Lorenz system, even for rather strong noise, the basic "butterfly" structure is preserved (Fig. 5.3). The systems explore a larger region of the phase space with increasing noise intensity D. In the CS regime $D > 33.3$, the trajectory is much more complex than a smeared periodic orbit and is quite different from the external noise. Since now Lyapunov exponents are no longer a proper measure of complexity of the systems [177,178], common noise-induced synchronization is not necessarily linked to noise-induced order, as claimed in Ref. [171].

Why is there a transition to CS in the Lorenz system but not in the Rössler system? In two systems $\dot{x} = f(x) + D\xi$ and $\dot{y} = f(y) + D\xi$ $(x, y \in R^n)$ with a common noise, small initial difference $\delta x = y - x$ evolves according to the linearized dynamics

$$\delta\dot{x} = Df(x)\delta x \ ,$$

where $Df(x)$ stands for the Jacobian matrix. This linearized equation is the same as in the noise-free case $(D = 0)$ where the system is chaotic, i.e. the maximal Lyapunov exponent

$$\lambda_1 = \lim_{T\to\infty} \frac{1}{T} \ln \frac{|\delta x|}{|\delta x_0|}$$

is positive. In the presence of noise, however, the trajectory x is different from that in the noise-free system, and may explore some regions in the phase space which are unreached by the original chaotic system. For CS to occur, λ_1 should become negative, which is possible only when there exists a *contraction region* where all the n eigenvalues of the Jacobian matrix $Df(x)$ have a negative real part, i.e. $\mathrm{Re}(\Lambda_i)<0$ $(i=1,\ldots,n)$ and nearby trajectories converge to each other.

In the Lorenz system with the parameters considered here, the origin $(0,0,0)$ is a saddle point embedded in the chaotic attractor. The chaotic trajectories leaving the neighborhood of this saddle point will come back to its neighborhood. Due to this homoclinic return of chaotic orbits, there exists a large contraction region in the z direction, close to the stable manifold of the saddle point (see Fig. 5.3). In the presence of noise, the system trajectories do not come very close to this saddle point, but explore deep into the contraction region, which changes the competition between contraction and expansion. When the contraction dominates over the expansion, the largest Lyapunov exponent becomes negative and CS occurs.

In the Rössler system, the trajectories spiral outwards following the guidance of the two-dimensional unstable manifold of the focus and are fold back by the nonlinearity. A contraction region with all three $\mathrm{Re}(\Lambda_i)<0$ does exist, but the contraction is very weak because the largest $\mathrm{Re}(\Lambda_i)$ is close to zero. In addition, in the presence of noise the system still spends only a small portion of time in the contraction region. The contraction is not sufficient to induce CS. There are also regions in the phase space where all $\mathrm{Re}(\Lambda_i)>0$, and strong enough noise $(D>4)$ makes the system access to such regions and breaks the system down easily.

This clarifies the controversy on the mechanism of noise-induced complete synchronization of chaotic systems. A significant contraction region plays a decisive role, as in one-dimensional chaotic maps [172]. Noise may change the balance between contraction or expansion, and synchronization occurs when contraction is dominating. Whether the noise is biased or unbiased is not the key point. If there does not exist a contraction region, CS cannot occur with any additive common driving signal. Noise-induced synchronization may be a result of noise-induced order, but they are not necessarily linked.

This understanding from the Lorenz system also guides us to observe the phenomenon in other systems. In general, it is expected that in a system possessing the structure of a saddle point embedded in a chaotic attractor and homoclinic return of orbits (homoclinic chaos), the generic existence of a large enough contraction region and sensitivity of the system to noisy perturbation near the saddle point will result in noise-induced synchronization. Note that such a structure is typical for the spiking behavior of many neural, chemical and laser systems, and noise-induced synchronization may play an important functional role there.

This rather general claim has also been verified by other systems. The first one is a Hodgkin–Huxley model [179] of thermally sensitive neurons, which mimics various types of spike train patterns in electroreceptors from dogfish and catfish, or from facial cold receptors and hypothalamic neurons of the rat [180]. The model equations read

$$C_M \frac{\mathrm{d}V}{\mathrm{d}t} = -I_l - I_d - I_r - I_{sd} - I_{sr} + D\xi(t) \,,$$

$$\frac{\mathrm{d}a_r}{\mathrm{d}t} = \frac{\phi(T)(a_{r\infty} - a_r)}{\tau_r} \,,$$

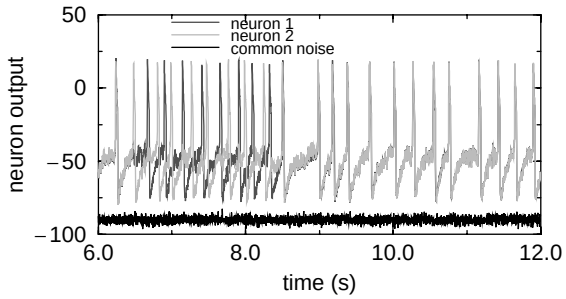

Fig. 5.4. Noise-induced complete synchronization of a Hodgkin–Huxley model (Eq. (5.4)) of thermally sensitive neurons.

$$\frac{\mathrm{d}a_{sd}}{\mathrm{d}t} = \frac{\phi(T)(a_{sd\infty} - a_{sd})}{\tau_{sd}} ,$$
$$\frac{\mathrm{d}a_{sr}}{\mathrm{d}t} = \frac{\phi(T)(-\eta I_{sd} - \theta a_{sr})}{\tau_{sr}} \tag{5.4}$$

with

$$I_d = \rho(T) g_d a_{d\infty}(V - V_d)$$

and

$$I_k = \rho(T) g_k a_k (V - V_k) \quad (k = r, sd) ,$$

where

$$a_{k\infty} = [1 + \exp(-s_k(V - V_{0k}))]^{-1}$$

and

$$\rho(T) = A_1^{(T-T_0)/10}, \quad \phi(T) = A_2^{(T-T_0)/10} .$$

Here V is the membrane potential, and I_l is the leakage current; I_d and I_r are fast currents representing Na and K channels. With this model, the classical Hodgkin–Huxley (HH) model [181], on the one hand, has been simplified, but on the other hand, has been extended by two additional slow currents I_{sd} and I_{sr} according to the experimental findings of spike-independent oscillations [182]. a_k is the activation variable, and $\rho(T)$ and $\phi(T)$ are temperature-dependent scaling factors. More detailed description of the model, its parameters, such as $C_M, g_k, \tau_k, \ldots$, and comparison with the experimentally observed temperature dependence of spike train patterns can be found in Ref. [180].

It has been shown that this system exhibits a homoclinic bifurcation, where the interspike interval becomes very long, when the control parameter temperature T is varied [183]. A saddle-focus is embedded in the chaotic attractor so that chaotic trajectory has very close recurrence to the neighborhood of the saddle point, similar to the situation in the Lorenz system. A large contraction region exists generically in the phase space due to this structure, and as expected, a common noise $\xi(t)$ can induce CS of spike trains of two identical neuron, as illustrated in Fig. 5.4. It is not necessary

that the neuron is close to the homoclinic bifurcation for synchronization to occur. Noise-induced synchronous spiking has been found in a large parameter space. The mechanism presented here for the realistic neuron model thus interprets the experimental observations of repetitive spiking in Ref. [151] and brings a new understanding on neuron encoding. Very similar noise-induced CS of spike trains has also been observed in homoclinic chaotic lasers [30], both numerically and experimentally.

5.2. Noise-induced phase synchronization of nonidentical chaotic systems

It is interesting to study whether noise can also induce weaker degrees of synchronization, especially phase synchronization, in particular in situations when it is not strong enough or not able to induce complete synchronization.

In Section 3, it has been shown that before the transition to almost CS, there is in several oscillatory systems the regime of PS associated with the transition of a zero Lyapunov exponent to negative values. As discussed in Section 3, in time continuous autonomous chaotic systems $\dot{x} = f(x)$ ($f : R^n \to R^n$), there is a zero Lyapunov exponent λ_2 corresponding to perturbations to the motion along the trajectory, which in phase coherent chaotic systems, can be connected to the dynamics of phases. In such a system subjected to weak noise, $\dot{x} = f(x) + \xi$, most time it is $|f(x)| \gg |\xi|$ and one can also roughly speak of a motion along the trajectory and connect the original zero Lyapunov exponent to it and link it to the phase dynamics. Numerical results in the following show that λ_2 becomes negative for strong enough noise, and in parallel, the phases of the two slightly *nonidentical* systems coupled only by common noise become statistically correlated.

To study PS due to noise, Ref. [175] considers two systems with a small parameter mismatch; particularly, $\omega_1 = 0.97$ and $\omega_2 = 0.99$ in the Rössler system equation (5.3) and $\sigma_1 = 10$, $\rho_1 = 28$ and $\sigma_2 = 10.2$, $\rho_2 = 28.5$ in the Lorenz system equation (5.2). This slight parameter difference does not change considerably the Lyapunov exponent spectra of the systems.

In noisy chaotic systems, the phase of the dynamics is no longer coherent, i.e. a monotonically increasing function of time. Nevertheless, a phase variable can be defined as in the deterministic system (Section 3), e.g., $\phi = \arctan(v/u)$. Here $u = x - x_0$ and $v = y - y_0$ for the Rössler system, and $u = \sqrt{x^2 + y^2} - \sqrt{x_0^2 + y_0^2}$ and $v = z - z_0$ in the Lorenz system. (x_0, y_0, z_0) are the coordinates of the unstable focus point of the systems.

In such stochastic systems, it is impossible to observe perfect synchronization of the phases ϕ_1 and ϕ_2 of the two nonidentical systems, i.e., $|\phi_1 - \phi_2| < \text{const.}$, because the phases are locked only for some period of time, interrupted by noise-induced phase slips, even though the phases are locked perfectly in the absence of noise, see Section 3. An approach to study PS behavior in stochastic systems is to compute the distribution of cyclic phase difference on $[-\pi, \pi]$ [21,22]. A peak in the distribution exhibits that there is a preferred phase difference between the systems, which is an indication of PS between the noisy complex systems, i.e. PS is interpreted in a statistical sense [184].

Without noise the two nonidentical Rössler systems are not phase synchronized and the phase decreases almost monotonously (Fig. 5.5(a), $D = 0$). Hence, the distribution of the cyclic phase differences on $[-\pi, \pi]$ is very close to a uniform one (Fig. 5.5(b)). While for strong enough noise, where $\lambda_2 < 0$, one observes many plateaus in the phase difference, i.e. many phase-locking epochs (Fig. 5.5(a), $D = 3.0$), and this is reflected by a pronounced peak around $\Delta\phi = 0$ in the distribution of cyclic phase difference (Fig. 5.5(c)); this exhibits a noise-induced phase synchronization. For D

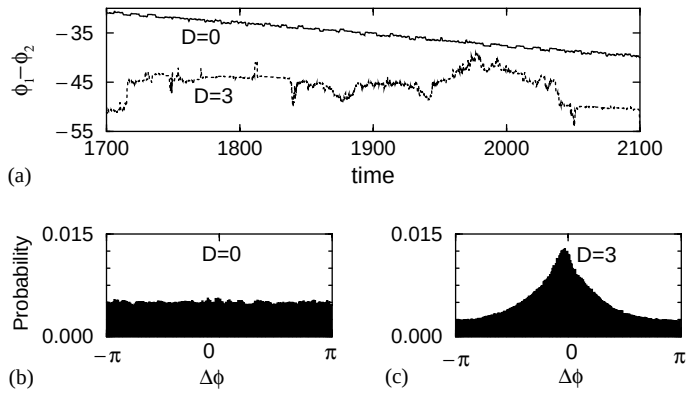

Fig. 5.5. (a) Time series of the phase difference of two nonidentical Rössler systems ($\omega_1 = 0.97$ and $\omega_2 = 0.99$), at noise intensity $D = 0$ and 3. In this presentation, the phases are lifted (plus 2π for each cycle). Distribution of the cyclic phase difference for $D = 0$ (b), and 3 (c).

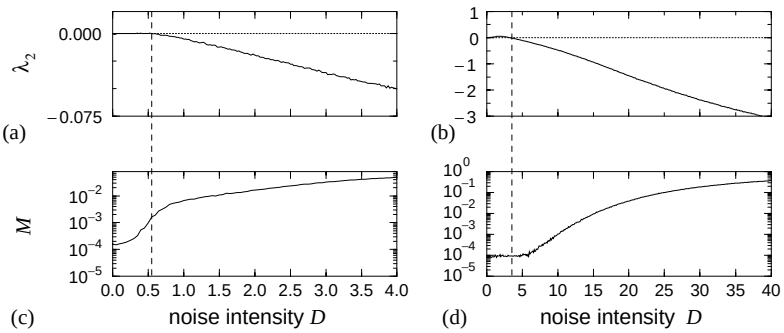

Fig. 5.6. The second Lyapunov exponent λ_2 of the Rössler system (a) and the Lorenz system (b) vs. the noise intensity D. Mutual information M the Rössler system (c) and the Lorenz system (d).

close to the transition of λ_2, the peak is not as pronounced and is not located around $\Delta\phi = 0$. Similar properties are observed in the Lorenz system.

To measure the degree of noise-induced phase synchronization, Ref. [175] calculates the mutual information between the cyclic phase dynamics (on $[-\pi, \pi]$) of the two systems,

$$M_1 = \sum_{i,j} p(i,j) \ln \frac{p(i,j)}{p_1(i)\,p_2(j)} \,, \tag{5.5}$$

where $p_1(i)$ and $p_2(j)$ are the probabilities when the phases ϕ_1 and ϕ_2 are in the ith and jth bins, respectively, and $p(i,j)$ is the joint probability that ϕ_1 is in the ith bin *and* ϕ_2 in the jth bin. The number of bins of $[-\pi, \pi]$ in the simulations is $N = 100$. To take into account the change of the individual distributions p_1 and p_2 with increasing noise intensity, the mutual information is normalized into $[0, 1]$ as $M = 2M_1/(S_1 + S_2)$, where $S_k = -\sum_i p_k(i) \ln p_k(i)$ is the Shannon entropy.

The results of mutual information M as a function of noise intensity are shown along with λ_2 in Fig. 5.6 for both the Rössler and the Lorenz system. Due to the incoherence of the phases, an exact

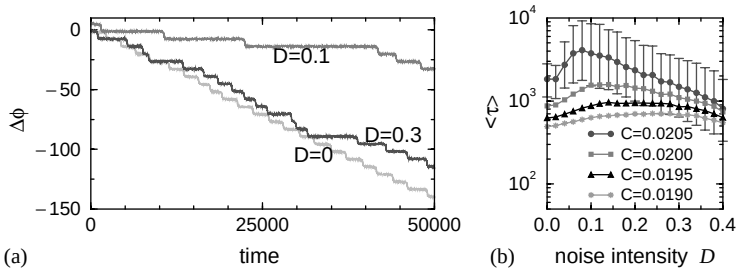

Fig. 5.7. Noise-enhanced PS in two weakly coupled chaotic Rössler oscillators ($C = 0.0205$). (a) Phase difference vs. time for different noise intensity D. (b) Average duration of PS epochs vs. noise intensity D for different coupling strength C. Error bars are only shown for $C = 0.0205$. Note that a log-scale is used in the y-axis in (b).

correspondence between the transition of λ_2 and PS would not be expected. Nevertheless, when λ_2 becomes appreciably negative, M increases rapidly, indicating an increasing degree of PS. Unlike PS in coupled deterministic chaotic systems or periodically driven chaotic systems shown in Section 3 (where the phase differences are bounded and no phase slips occur after the transition, while just before the transition phase-locking is interrupted by intermittent phase slips), in the noise-induced PS, phase-locking epochs show up only after the transition of λ_2 to appreciably negative values, but no pronounced phase-locking is seen shortly after the transition point. Phase-locking epochs occur more frequently, when λ_2 becomes more negative.

It is important to stress that noise-induced PS is observed in many perturbation configurations both in the Rössler and the Lorenz systems.

5.3. Noise-enhanced phase synchronization in weakly coupled chaotic oscillators

In the above sections, we have considered the case where the chaotic oscillators are not coupled but linked only by a common noise. In reality, such as in neuroscience or electrochemical oscillators, systems are often weakly coupled besides the common random forcing. It is interesting to study the interplay between weak coupling and common noise.

In this context Ref. [185] investigates two mutually coupled chaotic Rössler oscillators influenced by a common noise:

$$\dot{x}_{1,2} = -\omega_{1,2} y_{1,2} - z_{1,2} + C(x_{2,1} - x_{1,2}) \,, \tag{5.6}$$

$$\dot{y}_{1,2} = \omega_{1,2} x_{1,2} + 0.15 y_{1,2} + D\xi(t) \,, \tag{5.7}$$

$$\dot{z}_{1,2} = 0.4 + (x_{1,2} - 8.5) z_{1,2} \,. \tag{5.8}$$

Here $\omega_1 = 0.97$ and $\omega_2 = 0.99$. Without noise, the two oscillators achieve PS when the coupling strength $C > C_{\mathrm{PS}} = 0.0208$, where C_{PS} is the transition point to PS (Section 3). In the weak coupling region $C < C_{\mathrm{PS}}$, the phases are not yet synchronized. When C approaches C_{PS}, appreciable PS epochs can be observed between phase slips, and accordingly, there is a small peak in the distribution of the cyclic phase differences.

Ref. [185] analyzes first the dynamics shortly before the onset of PS, as shown in Fig. 5.7(a) for $C = 0.0205$. Without a common noise ($D = 0$), the phase difference $\Delta\phi = \phi_1 - \phi_2$ decreases

continuously. But there are many epochs of phase synchronization interrupted by phase slips; and typically the phase synchronization epochs last for about 300 cycles of oscillations. Adding a proper amount of common noise to the two oscillators (e.g. $D = 0.1$) can prolong remarkably the duration of the synchronization epochs: the two oscillators maintain phase synchronization for a period of about 3000 cycles of oscillations. However, for stronger noise (e.g. $D = 0.3$), phase slips occur more frequently again.

To characterize this phenomenon of noise-enhanced phase synchronization, Ref. [185] focuses on the duration τ of the phase synchronization epochs. τ can be estimated reliably for C close to C_{PS} using a threshold test of moving average of the frequency difference between the two oscillators. As indicated in Fig. 5.7(a), those very long epochs make the distribution of τ strongly asymmetrical around the mean value $\langle\tau\rangle$. To manifest those very long epochs which essentially dominate the synchronization behavior of the systems, the deviation $\sigma_\tau^2 = \langle(\tau - \langle\tau\rangle)^2\rangle$ is computed separately for $\tau < \langle\tau\rangle$ and $\tau > \langle\tau\rangle$, which is a good indication for an asymmetrical distribution, especially for large τ. It is found that the average duration $\langle\tau\rangle$ increases with the noise intensity D, reaches a maximal value and decreases for larger D for all coupling strengths analyzed (Fig. 5.7(b)). Thus there is an optimal amount of noise which enhances PS most significantly. Such a resonant-like behavior is typical in the interplay between noise and nonlinearity in dynamical systems [148–150,186,187]. In this case, the competition between noise-induced phase incoherence and common noise-enhanced phase synchronization underlies the reason for this resonant-like behavior. In the plot for $C = 0.0205$ (Fig. 5.7), the error bar corresponding to asymmetrical deviation σ_τ shows clearly that common noise induces very long synchronization epochs. This behavior is similar for other coupling strengths too.

It should be pointed out that common noise enhances PS even though the coupling is rather weak. In those cases, in the absence of noise, PS epochs last only for short time and may not be estimated reliably. But enhanced PS can be detected by a higher peak in the distribution of the cyclic phase difference [184]. A measure [21,22] of the sharpness of the peak shows a similar behavior: with increasing noise intensity D, the PS degree increases till too strong noise makes the oscillations rather incoherent. The optimal noise intensity moves to smaller values when C approaches the threshold C_{PS}. Beyond this threshold, in general, noise acts to degrade PS by introducing phase slips. In the limit of zero coupling $C = 0$, the common noise with an intensity considered here has no discernible effects on PS by itself (Fig. 5.6). On the other hand, noise may induce intermittent phase slips after the transition point.

Noise-induced PS has also been studied in bistable systems [188] and in excitable media [149,189]. A series of transitions from weak to strong degree of synchronization, similar to that in the coupled chaotic oscillators discussed in the Section 3, has been demonstrated in coupled noisy excitable systems [190].

6. Synchronization in extended systems

6.1. Cluster synchronization in ensembles of coupled identical systems

Synchronization effects in large populations of coupled chaotic dynamical units has also become a subject of active investigations [15,191,192].

When passing to space extended systems, a first approach consists in connecting a set of concentrated chaotic systems by means of a given coupling (local or global) between the individuals constituting the set. Space–time chaos synchronization for this kind of systems has been studied for populations of coupled dynamical systems [108], for systems formed by globally coupled Hamiltonian or bistable elements [15], for neural networks [193], for discrete-time maps with mean field global coupling [194,195], along with many other situations that will be summarized in the following.

Collective phenomena in networks of coupled periodic oscillators has been intensively studied in the past two decades [72] and still attract a strong interest of many investigators [90,196–202]. Such models have been used for the description of many physical [203–208], biological [209–211] and chemical [212] problems. Coupled oscillator models are also widely used as general models in studies of complex dynamics in nonequilibrium media [213,214].

6.2. Global and cluster synchronization in ensembles of coupled identical systems

In large ensembles of coupled identical chaotic as well as periodic elements the main types of synchronized behavior are global (full) and cluster (partial) synchronization. In this context, global synchronization can be considered as a generalization of CS. In global synchronization all elements of an ensemble display the same behavior for any initial conditions. The phenomenon of cluster synchronization is observed when the ensemble of oscillators splits into groups of mutually synchronized elements. These phenomena were studied in coupled map lattices [37,215–223], systems of globally coupled maps [216–219,224–226], locally and globally coupled continuous time chaotic oscillators [227–230]. In all mentioned cases the problem of cluster synchronization is related to the existence and stability of invariant manifolds corresponding to the synchronized behaviors in the considered systems.

Let us begin with an ensemble of N globally coupled chaotic maps [216,225,226,231]

$$x_i(n+1) = (1-\epsilon) f(x_i(n)) + \frac{\epsilon}{N} \sum_{j=1}^{N} f(x_j(n)) \ . \tag{6.1}$$

Here, $i = 1,\ldots,N$ is a space index, $x_i(n)$ the state variable in discrete time $n = 0,1,\ldots,\epsilon$ is the coupling parameter and $f(x) = ax(1-x)$ (the logistic map). This system was originally introduced by Kaneko [216] to study the collective dynamics in large populations of globally coupled identical chaotic oscillators. The simplest form of a cooperative behavior in such a population is global synchronization which takes place for relatively large coupling. This synchronous chaotic state resides on *a synchronization manifold* defined by $M = \{x_1 = x_2 = \cdots = x_{N-1} = x_N\}$. The dynamics in M is generated by the uncoupled map (in (6.1) $\epsilon = 0$). Full global synchronization occurs if M is globally asymptotically stable. As the coupling decreased the regime of global synchronization becomes unstable and breaks up into a number of clusters of mutually synchronized units. For a K-cluster structure, all x_i split in K groups such that in each group the variables are the same:

$$x_1 = x_2 = \cdots = x_{m_1} = X_1 \ , \tag{6.2}$$

$$x_{m_1+1} = x_{m_1+2} = \cdots = x_{m_1+m_2} = X_2 \ , \tag{6.3}$$

$$\ldots \tag{6.4}$$

$$x_{m_1+\cdots+m_{K-1}+1} = \cdots = x_N = X_K \ , \tag{6.5}$$

where $m_1, m_2, \ldots, m_k$ are the sizes of the clusters. Then the dynamics of the K-cluster structure can be described by the K-dimensional system for the cluster variables X_l:

$$X_l(n+1) = (1-\epsilon) f(X_l(n)) + \epsilon \sum_{k=1}^{K} p_k f(X_k(n)) \ , \tag{6.6}$$

where $p_l = m_l/N$ is the portion of the elements belonging to the lth cluster. With further increasing of coupling the regime of turbulent (fully desinchronized) state appears. In [225,226] a more detailed transition from global to cluster synchronization is presented.

A similar situation takes place in ensembles of coupled continuous time chaotic systems. Following [192,232,233] let us consider N identical diffusively coupled oscillators with periodic boundary conditions:

$$\dot{u}_j = f(u_j) + cE(u_{j+1} - 2u_j + u_{j-1}) \ , \tag{6.7}$$

where $j = 0, 1, \ldots, N-1$, $u_j \in R^n$, the function $f : R^n \to R^n$ is nonlinear, c is a scalar coupling parameter, and $E = \mathrm{diag}(e_1, \ldots, e_n)$ is a constant diagonal diffusion matrix with elements $0 \leqslant e_i \leqslant 1$. The regime of global synchronization corresponds to a spatial homogeneous state $u_0 = u_1 = \cdots = u_{N-1}$, which defines a n-dimensional invariant manifold M. In M the dynamics is governed by the equation of the uncoupled oscillator $\dot{s} = f(s)$. The stability of the synchronous state is determined by linearizing (6.7) about $s(t)$. This leads to

$$\dot{\xi}_j = Df(s)\xi_j + cE(\xi_{j+1} - 2\xi_j + \xi_{j-1}) \ , \tag{6.8}$$

where $\xi_j = u_j - s$, $Df(s)$ is the Jacobian of f on $s(t)$. The linear stability equations (6.8) can be diagonalized by expanding into spatial Fourier modes, $\xi_j = (1/\sqrt{(N)}) \sum_{k=0}^{N-1} \eta_k \exp(-2\pi \mathrm{i} jk/N)$. Carrying this out gives

$$\dot{\eta}_k = [Df(s) - 4c \sin^2(\pi k/N)E]\eta_k \ , \tag{6.9}$$

where $k = 0, 1, \ldots, N-1$. Solving Eq. (6.9) for a concrete function $f(s)$ and a concrete solution $s(t)$, one can obtain all Lyapunov exponents which determine the stability of the synchronization manifold M. In [192,232] it was found that for coupled Rössler systems increasing coupling can lead to destabilizing of the synchronous state. This phenomenon is called *a short-wavelength bifurcation*.

In addition to global and cluster synchronization in ensembles of identical systems, the phenomena of *antiphase* and *in-phase–antiphase* synchronization were observed [215,223,227,234,235]. These types of synchronization are defined by the existence of stable *linear* transversal invariant manifolds. Such *antiphase synchronization* is observed in a system of coupled oscillators where all corresponding variables of oscillators are equal with opposite sign. In *in-phase–antiphase synchronization*, one set of the corresponding variables is equal, whereas the other one is equal with opposite signs.

6.3. Synchronization phenomena in populations of coupled nonidentical chaotic units

Recently, the study of cooperative behavior in ensembles of chaotic oscillators has become very attractive. It has been demonstrated that typical phenomena in networks of coupled periodic and chaotic systems are quite similar [108,192,236–240]. This section is devoted to the description of the synchronization effects in arrays of coupled nonidentical chaotic oscillators.

As in the case of small (two-elements) ensembles of coupled chaotic elements, all types of synchronization can be considered in large (chains and lattices) ensembles. To demonstrate the typical phenomena in such ensembles, we will focus here on chains of nearest-neighbor diffusively coupled circle maps (CMs) and Rössler oscillators.

6.3.1. Synchronization in a chain of coupled circle maps

Phase synchronization in ensembles of locally coupled chaotic elements was firstly studied in chains of weakly diffusively coupled chaotic Rössler oscillators [107] (see next subsection). Many phenomena already observed in a population of periodic oscillators were found there too, especially to mention the formation of several clusters of mutually synchronized elements and global synchronization. In the latter case the main effects can be observed only by using of the phase equations. In this subsection we present results for chains of coupled circle maps which can be considered as the discrete in time analog of phase equations which appear in ensembles of coupled continuous in time limit-cycle oscillators.

As mentioned before, the study of PS effects requires the existence of equations for the evolution of phase variables or at least the existence of appropriate definitions of phases. There are so far no unambiguous methods to obtain such equations and definitions. But in some cases the topology of the chaotic attractors allows to define the phases of chaotic oscillators in a rather simple way. In several cases it is possible to obtain approximate equations which qualitatively describe the dynamics of the system of coupled elements. These equations are very similar to phase equations usually obtained for ensembles of coupled limit-cycle oscillators and can be written in the form [7]:

$$\dot{\phi}_n = \omega_n + F(\phi_n) + d(\sin(\phi_{n+1} - \phi_n) + \sin(\phi_{n-1} - \phi_n)), \quad n = 1, \ldots, N \ , \tag{6.10}$$

where ϕ_n is the phase variable, ω_n the natural frequency of a single element, N the number of elements, $F(\phi_n)$ some nonlinear function that is responsible to the non-uniformity of rotations in a single element. A good example, where such kind of equations can be used for a qualitative explanation of PS effects, is the Rössler oscillator in the regime of phase coherent chaotic attractor. For this attractor, if we choose the projection on the plane (x, y), the phase point rotates around the origin, and the projection looks like a smeared limit cycle.

Eqs. (6.10) do not account for the amplitude and other variables influence on the dynamics of phases. For uncoupled elements the corresponding equation (in (6.10) $d = 0$) does not possess a chaotic behavior. In order to partially avoid such disadvantages of Eq. (6.10) we consider a discrete analog of Eq. (6.10):

$$\phi_n^{k+1} = \omega_n + \phi_n^k - F(\phi_n^k) + d(\sin(\phi_{n+1}^k - \phi_n^k) + \sin(\phi_{n-1}^k - \phi_n^k)), \quad n = 1, \ldots, N \ . \tag{6.11}$$

Here ϕ_n^k is the phase variable at adjacent times $k = 1, 2, \ldots$. The parameter ω_n characterizes the partial frequency. The function $F(\phi_n)$ is taken in the following piece-wise linear form $F(\phi_n) = c\phi_n/\pi$. This function is defined in the interval $[-\pi, \pi]$ and c is the control parameter. In the presented

treatment the system is subjected to free-end boundary conditions, i.e. $\phi_0^k = \phi_1^k$ and $\phi_{N+1}^k = \phi_N^k$. By such an approach a single element in the chain is *a circle map* whose dynamics is described in Section 3.1.5. Because we are interested in the synchronization properties of chaotic elements, we analyze negative values of c only. So one has to investigate synchronization effects in a chain of coupled chaotic CMs [83].

Two criteria to test for $m_1 : m_2$ synchronization, where $m_{1,2}$ are integers, are usually used. $m_1 : m_2$ phase synchronization of chaotic rotations between two CMs can be defined as phase entrainment or locking

$$|m_1\phi_n^k - m_2\phi_{n+1}^k| < \text{Const} \tag{6.12}$$

for all $k = 1, 2, \ldots$. A weaker criterion for the analysis of phase synchronization in a chain of coupled CMs is based on their rotation numbers (3.19), i.e. we test for

$$m_1\rho_n = m_2\rho_{n+1} \ . \tag{6.13}$$

Here ρ_n is the rotation number defined as

$$\rho_n = \frac{1}{2\pi} \lim_{M\to\infty} \frac{\phi_n^M - \phi_n^1}{M} \ , \tag{6.14}$$

where M is the number of iterations. In the study of synchronization effects in a chain of coupled CMs, the fulfillment of the conditions (6.12) and (6.13) for all $n = 1, \ldots, N$ means the existence of global synchronization. If these conditions are satisfied only for several neighboring elements, a regime of cluster synchronization is formed.

We describe the results of numerical simulations with a chain of 50 elements with linear:

$$\omega_n = \omega_1 + \Delta(n-1), \quad n = 1, \ldots, N \tag{6.15}$$

and random distribution of the individual frequencies

$$\omega_n = \omega_1 + \Delta\xi_n, \quad n = 1, \ldots, N \ , \tag{6.16}$$

where $\Delta = \text{const}$ and ξ_n are uniformly distributed random numbers in the interval $[-0.5; 0.5]$. The rotation number ρ_n is calculated for each CM. We find that analogous to the self-synchronization in chains of periodic oscillators [201] and chains of chaotic phase coherent Rössler oscillators [107], mutual global synchronization in chains of coupled CMs can appear or vanish in two ways: soft and hard. The soft transition, i.e. transition without cluster formation, is characterized through a smooth locking of the rotation numbers and can be observed in chains with a very small frequency mismatch. But in the hard transition the appearance or disappearance of global synchronization is accompanied by the existence of cluster synchronization. This hard transition happens in rather long chains with a relatively large frequency mismatch. There the loss of global synchronization leads to the appearance of two clusters of elements which rotate at the same rotation number. With a further increase of the frequency mismatch, the formation of new clusters is typical. The values of the rotation number for each cluster (except the edge ones) are close to those obtained by averaging the individual rotation numbers over all the elements forming the cluster. In the soft transition after the loss of global synchronization most elements of the chain (except, perhaps, the edge ones) rotate with different rotation numbers. In the case of randomly distributed frequencies, only a hard transition is possible. For a linear distribution of the individual frequencies the rich spatio-temporal dynamics of the noncluster (smooth distribution of rotation numbers) (Fig. 6.1(a)) and cluster synchronization

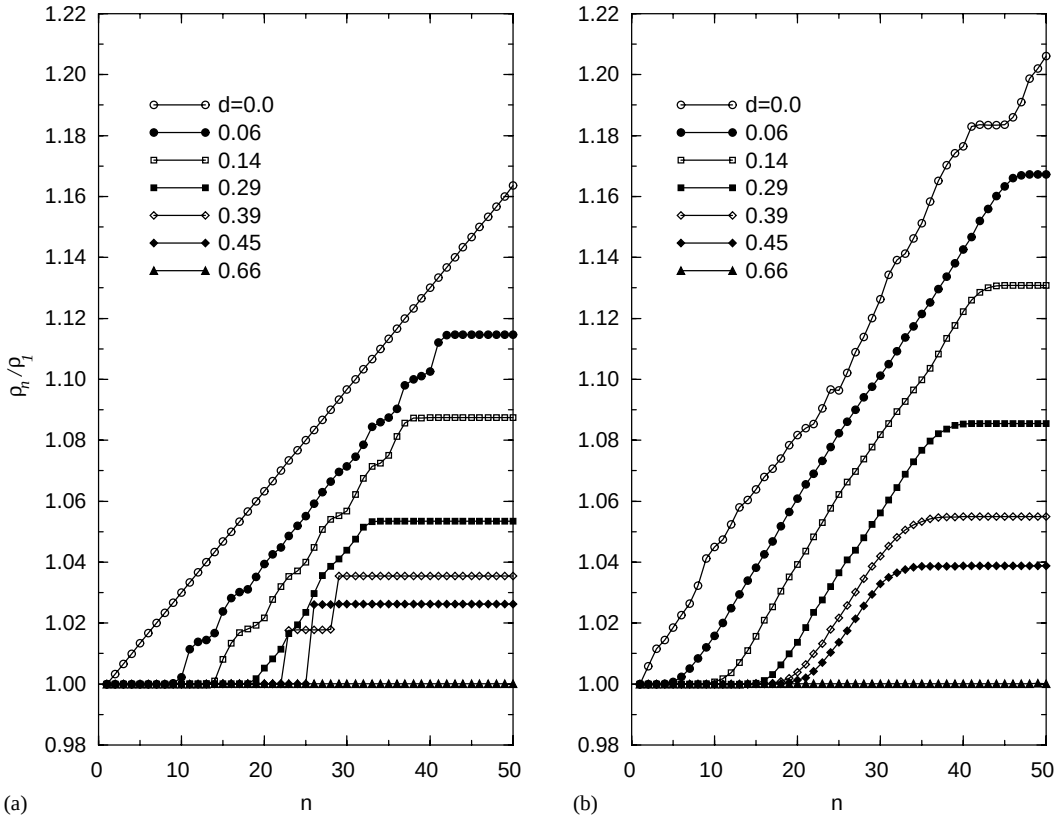

Fig. 6.1. Hard (a) and soft (b) transitions to global chaotic phase synchronization for a chain of coupled CMs (Eq. (6.11)) with $N = 50$. The relative rotation numbers ρ_n/ρ_1 for different coupling coefficients d for linear distribution of individual frequencies for $b_1 = 0.6$, frequency mismatch $\Delta b = 0.002$, $c = -0.002$ (a) and $c = -0.4$ (b).

structures (Fig. 6.1(b)) is illustrated in Fig. 6.2. In all plots the darker regions mark higher values of the presented variables. The two left panels show the quantity $\sin(\phi_n^k)$, so that the white stripes correspond to phases $\approx 3\pi/2$ and the black stripes to phases $\approx \pi/2$. The right panel shows the quantity

$$s_n = \sin^2\left(\frac{\phi_{n+1}^k - \phi_n^k}{2}\right) \tag{6.17}$$

which characterizes the instantaneous phase difference between neighboring oscillators. This yields that $s_n = 0$ if the phases are equal and $s_n = 1$ if they differ by π. The spatio-temporal behavior of the boundaries between clusters corresponds to the positions where phase slips or defects occur. These defects are clearly seen as maxima (black regions) of s_n. They can follow regularly in time at certain positions in the chain; this case corresponds to the existence of strong jumps between clusters (Fig. 6.2(c)). If the cluster structures do not exist or the borders between them are smooth, then defects appear irregularly in both space and time (Fig. 6.2(d)).

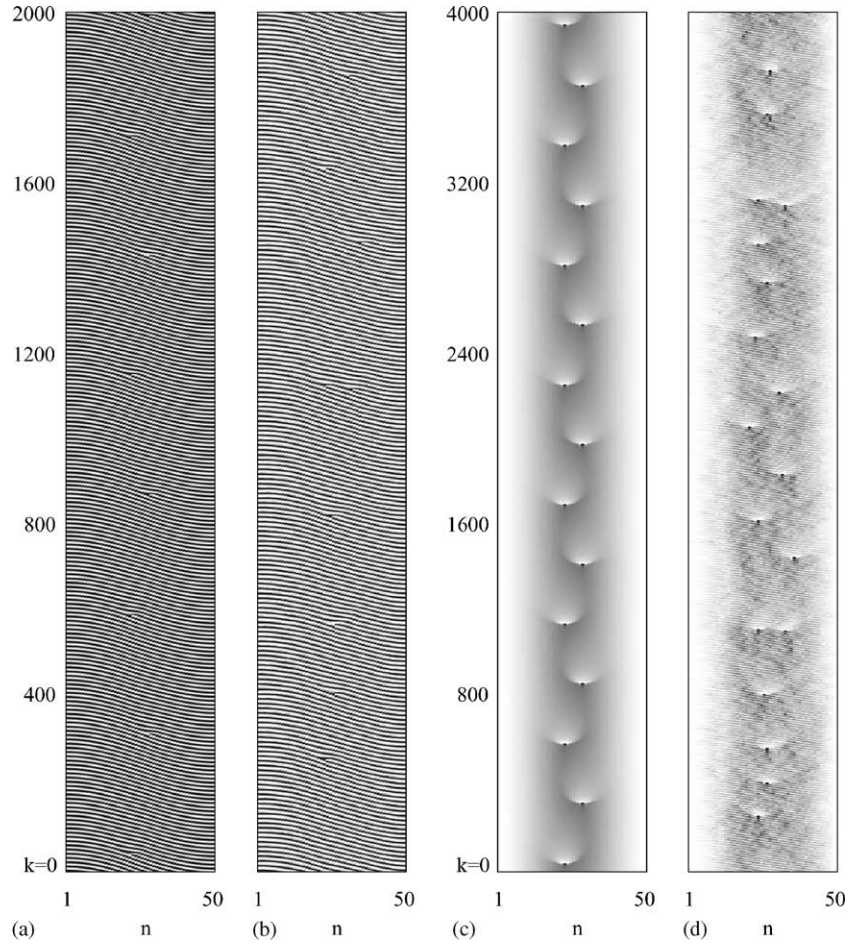

Fig. 6.2. Space–time plots of the evolution of (a, b) $\sin(x_\phi^k)$ and s_n (Eq. (6.17)) (c, d) by hard (a, c) and soft (b, d) transitions to global chaotic phase synchronization for a linear distribution of individual frequencies. Gray scale is used, with minimal values being represented by white and maximal by black. The parameters are $N = 50$, $b_1 = 0.6$, $\Delta b = 0.002$, $d = 0.39$ and $c = -0.002$ (a, c) resp. $c = -0.4$ (b, d).

Typical phenomena observed in numerical simulations for coupled chaotic CMs can be explained in the following way. As we have mentioned before, a chaotic behavior in a single CM takes place at any negative values of c. It is obvious that the phase evolution at very small c is very similar to the evolution of phases in the case of regular behavior at $c = 0$. Then we will consider the chain of coupled regular CMs and a linear distribution of the partial frequencies ω_n. In this case system (6.11) can be rewritten as

$$\phi_1^{k+1} = \omega_1 + \phi_1^k + d\sin(\theta_1^k)\,, \tag{6.18}$$

$$\theta_n^{k+1} = \Delta + \theta_n^k + d(\sin\theta_{n+1}^k - 2\sin\theta_n^k + \sin\theta_{n-1}^k), \quad n = 1,\ldots,N-1 \tag{6.19}$$

with $\Delta = \omega_{n+1} - \omega_n$, $\theta_n^k = \phi_{n+1}^k - \phi_n^k$ and the boundary conditions: $\theta_0^k = \theta_N^k = 0$. The stable fixed point $\theta_n^{k+1} = \theta_n^k = \bar{\theta}_n$ for each $n = 1, \ldots, N-1$ in system (6.19) corresponds to a regime of global synchronization in the chain. Then the equations for the stationary phase differences $\bar{\theta}_n$ can be written as

$$\Delta + d(\sin\bar{\theta}_2 - 2\sin\bar{\theta}_1) = 0 \ ,$$

$$\Delta + d(\sin\bar{\theta}_{n+1} - 2\sin\bar{\theta}_n + \sin\bar{\theta}_{n-1}) = 0, \quad n = 2, \ldots, N-2 \ ,$$

$$\Delta + d(\sin\bar{\theta}_N - 2\sin\bar{\theta}_{N-1}) = 0 \ . \tag{6.20}$$

As follows from [198], the distribution of $\bar{\theta}_n$ obtained as a solution of the system (6.20) is

$$\sin\bar{\theta}_n = \frac{\Delta}{2d}(Nn - n^2) \ . \tag{6.21}$$

It follows from (6.21) that the system (6.19) has 2^{N-1} fixed points. As the frequency mismatch Δ is increased, the condition for the existence of fixed points:

$$\left|\frac{\Delta}{2d}(Nn - n^2)\right| < 1 \tag{6.22}$$

is violated first for $n = N/2$ at even N, i.e. for the middle element in the chain. Thus, the condition for the existence of a fixed point in the N-element chain is given by the inequality

$$\left|\frac{\Delta N^2}{2d}\right| < 1 \ . \tag{6.23}$$

As one can easily obtain from Eq. (6.18) by global synchronization, the rotation numbers for all elements are equal to the rotation number of the middle element $\rho_{N/2}$. For $\Delta = 8d/N^2$, we have the following value $\bar{\theta}_N/2 = \pi/2$. In this case, the stable and unstable fixed points merge and a rotatory behavior is born in the phase space of Eq. (6.19). All the elements of the chain are coupled. Consequently, as the phase difference between the middle element and its neighbor increases, the stationary regimes of global synchronization changes to the regime of oscillations θ_n^k (except the middle element) near a certain constant value $\bar{\theta}_n$, where the oscillation amplitude depends on n in all elements of the chain. The closer the elements are to the ends of the chain, the smaller the amplitude of the oscillations is. In the case of a long chain, the current values of θ_n^k are nearly constant (or constant) for the edge elements, i.e. the regime of synchronization occurs. Thus the array is divided into two clusters of equal sizes ($N/2$) that of mutually synchronized with different rotation numbers. The rotation number value by global synchronization and condition of existence of global synchronization in system (6.11) at $c = 0$ are in a good agreement with the results of the numerical experiments for small negative values c.

6.3.2. Phase synchronization phenomena in a chain of nonidentical Rössler oscillators

Now, the case of a chain of continuous in time oscillators is treated. To get a deeper insight in the formation of chaotic PS of coupled elements and underline the similarity of synchronization phenomena in networks of periodic and chaotic systems, we present results on a chain of nonidentical Rössler oscillators with a nearest-neighbors diffusive coupling [107].

The model of this chain can be written as a set of ordinary differential equations:

$$\dot{x}_n = -\omega_n y_n - z_n \ ,$$

$$\dot{y}_n = \omega_n x_n + a y_n + \epsilon(y_{n+1} - 2y_n + y_{n-1}) \ ,$$

$$\dot{z}_n = 0.4 + (x_n - 8.5) z_n \ . \tag{6.24}$$

Here $n = 1, \ldots, N$ are the numbers the oscillators in the chain and ϵ is the coupling coefficient. The parameter ω_n corresponds to the natural frequency of the individual oscillator. Like in the previous section, we introduce the gradient distribution of natural frequencies $\omega_n = \omega_1 + \delta(n-1)$, where δ is the frequency mismatch between neighboring systems. Another variant considered below is a random distribution of natural frequencies in the range $[\omega_1, \omega_1 + \delta(N-1)]$. We again assume free-end boundary conditions:

$$y_0(t) = y_1(t), \quad y_{N+1}(t) = y_N(t) \ . \tag{6.25}$$

Because the Rössler system typically has windows of periodic behavior as the parameter ω is changed, we choose ω_1 and δ in such a way that at least large periodic windows are avoided.

As already discussed, for the Rössler system the definition of phase for phase coherent attractor can be introduced in a simple way:

$$\phi_n = \arctan(y_n / x_n) \ . \tag{6.26}$$

The amplitude correspondingly can be defined as

$$A_n = \sqrt{x_n^2 + y_n^2} \ . \tag{6.27}$$

As the phase of this highly phase-coherent chaotic system is well-defined, one can straightforwardly calculate the phase difference between neighboring oscillators $\phi_n - \phi_{n+1}$. If the phase difference does not grow with time, but remains bounded, we have a $1:1$ phase locking. A weaker condition of synchronization is the coincidence of the averaged partial frequencies defined as

$$\Omega_n = \langle \dot{\phi}_n \rangle = \lim_{T \to \infty} \frac{\phi_n(T) - \phi_n(0)}{T} \ . \tag{6.28}$$

We emphasize that the mean frequency of chaotic oscillations Ω_n can be also calculated as

$$\Omega_n = \lim_{T \to \infty} 2\pi \frac{M_T^n}{T} \ , \tag{6.29}$$

where M_T^n is the number of rotations of the phase point around the origin during time T. This method can be directly applied to observed time series, when one e.g. takes for M_T^n the number of maxima of $x_n(t)$. For the Rössler attractor, estimates (6.28) and (6.29) practically coincide.

The result of numerical simulations performed with chains of 20–50 oscillators is presented for different values of the parameters $\delta, \omega_1, \epsilon$. The main calculated quantities are the observed frequencies Ω_n. Generally, by increasing coupling all the frequencies Ω_n become equal; that means global PS sets in. As in the case of coupled periodic oscillators and coupled chaotic circle maps, the regime of global synchronization in the chain (Eq. (6.24)) can again appear in two ways, depending on the relatively frequency mismatch δ/ω_1. Below these two scenarios, referred to as the soft and the hard

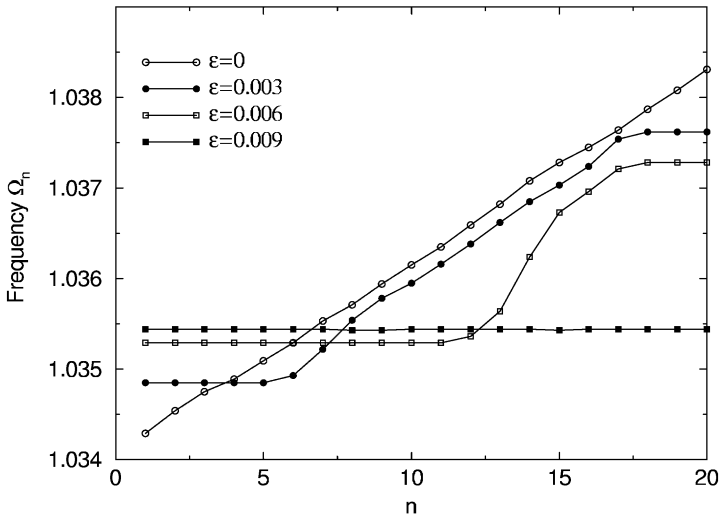

Fig. 6.3. Soft transition to global synchronization in a chain of Rössler oscillators (6.24). Mean frequencies Ω_n for different values of coupling ϵ. The parameters are: $N = 20$, the frequency mismatch $\delta = 2 \times 10^{-4}$ and $\omega_1 = 1$.

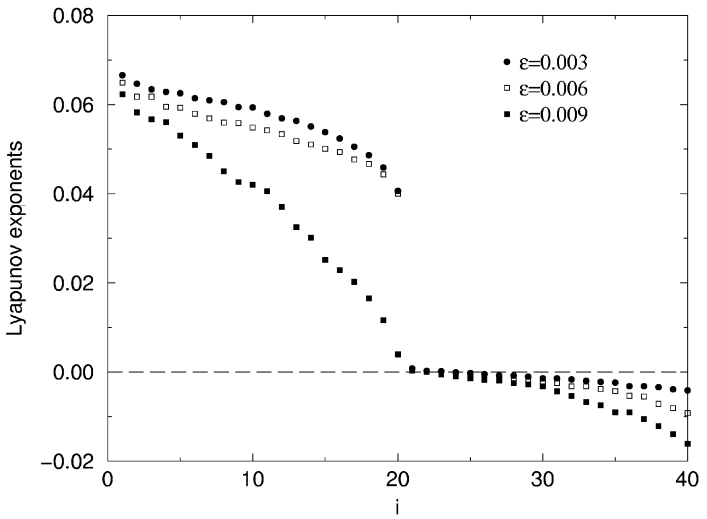

Fig. 6.4. 40 largest Lyapunov exponents λ_i for the regimes reported in Fig. 6.3.

transitions, are described:

(i) We first consider the case of a relatively small frequency mismatch $\delta/\omega_1 \ll 1$. Then a soft transition to global synchronization is observed (Fig. 6.3). In this transition the amplitudes of the oscillators remain chaotic, which is clearly marked by the spectrum of Lyapunov exponents (Fig. 6.4). As has been shown in [7], the appearance of PS in a system of two coupled oscillators manifests itself in the Lyapunov spectrum, namely, one of the zero exponents becomes negative, while the two largest ones remain positive. For the chain, the N largest Lyapunov exponents remain positive, while

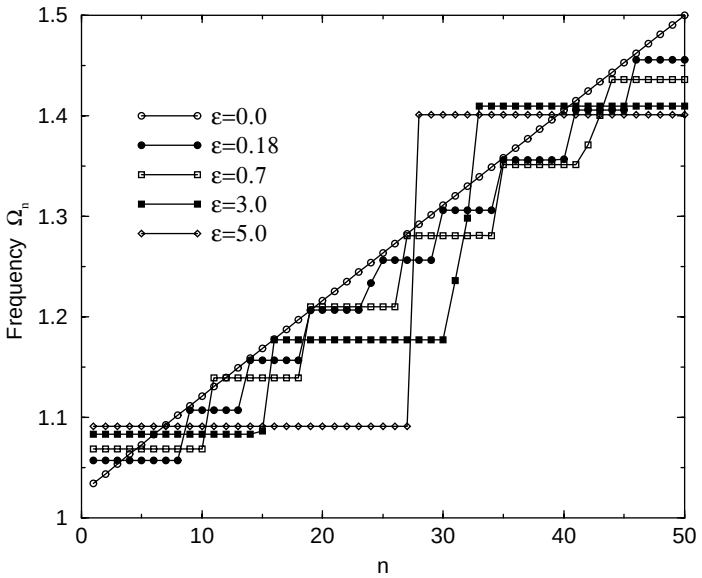

Fig. 6.5. Hard transition to global synchronization in a chain of Rössler oscillators (Eq. (6.24)). Mean frequencies Ω_n for different values of coupling ϵ. The parameters are: $N = 50$, the frequency mismatch $\delta = 9 \times 10^{-3}$ and $\omega_1 = 1$.

only one zero exponent survives, and $N - 1$ become negative. Then, a high-dimensional (number of positive Lyapunov exponents is equal to the number of coupled elements) synchronized chaos is observed.

(ii) For a relatively large frequency mismatch δ/ω_1 the transition to global synchronization via clustered states occurs, i.e. a hard transition takes place (Fig. 6.5). As a rule, with an increase of ϵ, the clusters of mutually synchronized oscillators appear rather abruptly. With a further increase of coupling the width of the clusters grows in parallel, the number of clusters decreases, and, finally, only one cluster remains, i.e. global synchronization appears. The behavior of the Lyapunov spectrum is quite different to the case of soft transition. As the coupling ϵ grows, the number of positive Lyapunov exponents decreases. Before any synchronization effects are seen, only a few Lyapunov exponents are positive (see Fig. 6.6). The cluster formation is clearly visible in a space–time diagram (Fig. 6.7). In all panels a gray scale is used with minimal values being represented by white and maximal by black. The left panel shows the quantity $\sin(\phi_n) = y_n/A_n$ (see Eqs. (6.26) and (6.27)). The right panel shows the amplitudes of the oscillators. To characterize the instantaneous phase difference between neighboring oscillators, the quantity

$$s_n = \sin^2\left(\frac{\phi_{n+1}(t) - \phi_n(t)}{2}\right) \tag{6.30}$$

is plotted in the center panel. The defects, which are clearly seen as maxima (black regions) of s_n and minima (white regions) of the local amplitude, appear regularly at certain positions on the chain. In this case the border between the clusters is sharp (see Fig. 6.7). Obviously, the frequency difference between the clusters (beat frequency) is equal to the frequency of the defects appearance.

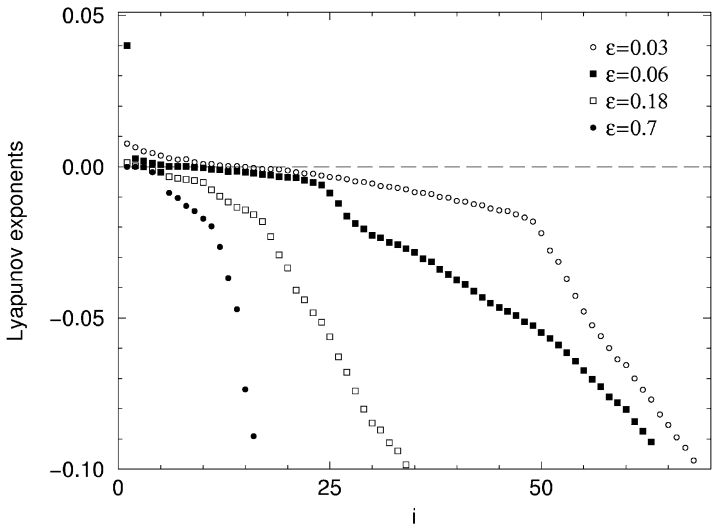

Fig. 6.6. 70 largest Lyapunov exponents λ_i for the regimes reported in Fig. 6.5.

Let us briefly describe PS effects occurring in a chain with randomly distributed natural frequencies. As in the case of linear increasing of frequencies, the regime of global synchronization arises via the formation of clusters (hard transition) (Fig. 6.8). The essential difference is that for the same mismatch between the largest and the smallest partial frequencies ω_n, global synchronization appears for considerably lower values of coupling than in the case of a linear distribution. Qualitatively, this can be explained as follows. For the case of linearly distributed frequencies, the left neighbor of some element is in average behind in phase, and the right neighbor is respectively ahead. Hence they "pull" the oscillator in different directions, and in this sense their actions are compensated. For the random case it is possible that both neighbors are behind (or ahead) in phase, and respectively both speed the element down (or up). As a result, their frequencies tend to each other, and these elements form a synchronous cluster. Such clusters can arise in arbitrary places in the chain and coexist with the oscillators that belong to no cluster. With the increase of coupling the clusters are firstly formed at the location of elements with a smaller frequency mismatch. The effect of nonlocal synchronization [241,242], where an oscillator or a cluster of oscillators is synchronized not to a nearest oscillator or clusters of oscillators, but to a next-to-the-nearest-neighbor oscillator or cluster.

The presented PS effects in chains of coupled chaotic elements support the idea that PS is a universal phenomenon of coupled chaotic systems and is similar to synchronization in networks of periodic oscillators. Recently, the limits for the appearance of collective phase-locked states in a chain of unidirectionally coupled chaotic Rössler oscillator has been investigated [243] and it has been pointed out that not always phase synchronized states can be produced without at least partial correlation in the chaotic amplitudes of the oscillators.

6.4. Synchronization in continuous extended systems

In this section we will go further in the analysis of continuous space–time systems, i.e. systems modeled by partial differential equations. This problem has been addressed only recently, and

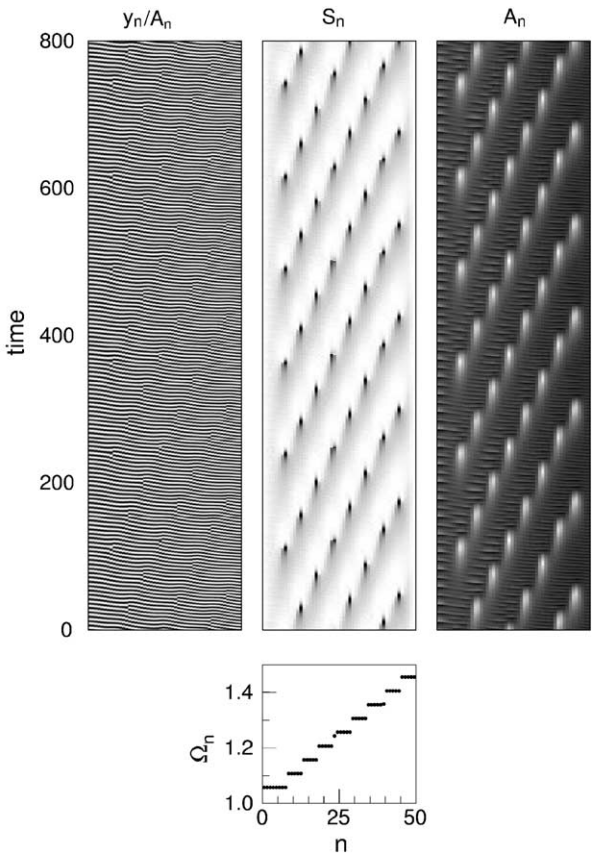

Fig. 6.7. Mean frequencies Ω_n and space–time plots in a chain of 50 coupled Rössler oscillators with a frequency mismatch $\delta = 9 \times 10^{-3}$ and coupling $\epsilon = 0.18$. All plots show a gray-scale representation of corresponding quantities. Minimal values are represented by white and maximal by black.

therefore only few works are available on this topic. Synchronization of continuous extended fields has been studied in several different situations [16,238,244–247]. Here, we will focus on the case of two fields obeying one-dimensional complex Ginzburg–Landau equations (CGL), both for identical CGL [17,248] and for nonidentical CGL. In this latter case a comparison is possible between bidirectional coupling [18,249], unidirectional coupling [250] and external forcing [19]. The relevance of CGL depends on the fact that such an equation is known to model the universal pattern forming features close to the emergence of an Hopf bifurcation [251], and it has been used to describe many different situations in laser physics [252], fluid dynamics [253], chemical turbulence [254], bluff body wakes [255], etc.

Let us describe the case of a bidirectional symmetric coupling between two nonidentical one-dimensional fields, ruled by CGL

$$\dot{A}_{1,2} = A_{1,2} + (1 + \mathrm{i}\alpha_{1,2})\partial_x^2 A_{1,2} - (1 + \mathrm{i}\beta_{1,2})|A_{1,2}|^2 A_{1,2} + \epsilon(x)(A_{2,1} - A_{1,2}) \ . \tag{6.31}$$

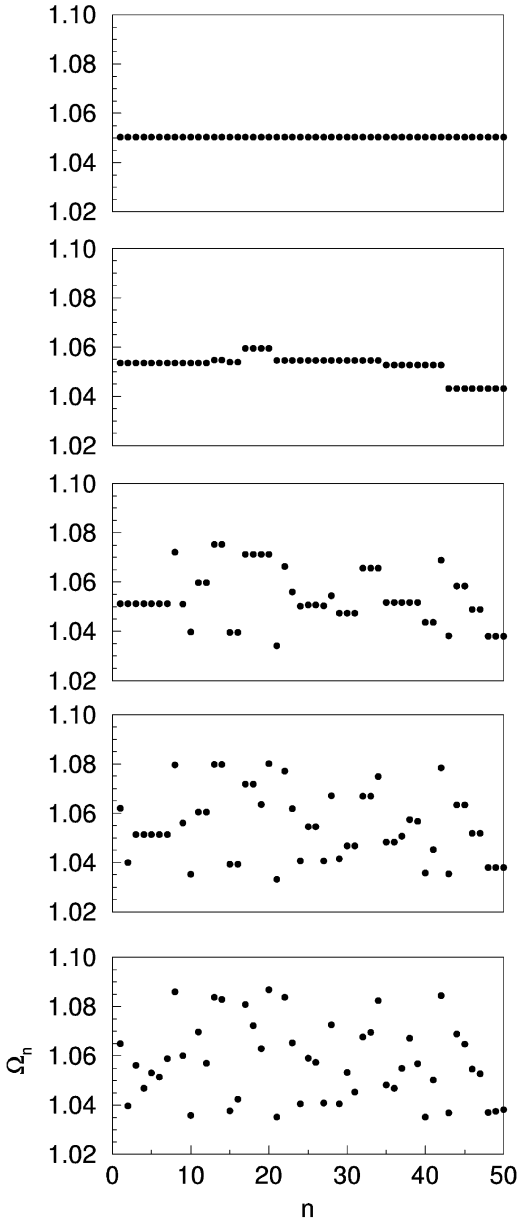

Fig. 6.8. Mean frequencies Ω_n in a chain of Rössler oscillators with randomly distributed natural frequencies ω_n in the interval $[1, 1.05]$. The number of elements $N = 50$, $\omega_1 = 1$. From bottom to top different coupling strengths $\epsilon = 0, 0.01, 0.02, 0.05, 0.2$.

Here $A_{1,2}(x,t) \equiv \rho_{1,2}(x,t)e^{(i\psi_{1,2}(x,t))}$ are two complex fields of amplitudes $\rho_{1,2}$ and phases $\psi_{1,2}$, $\partial_x^2 A_{1,2}$ is the second derivative of $A_{1,2}$ with respect to the space variable $0 \leqslant x \leqslant L$, L is the system extension, $\alpha_{1,2}, \beta_{1,2}$ are suitable real control parameters, $\epsilon(x)$ is a space distributed coupling factor, and for the time being we will explicitly consider periodic boundary conditions.

The synchronization of space–time chaotic states generated by CGL has been the subject of three recent papers [18,248,249]. Namely, in Ref. [248], it is reported the synchronization of two identical CGL ($\alpha_1 = \alpha_2,\ \beta_1 = \beta_2$) as a result of a coupling in a finite number N_c of controllers, i.e. with a coupling function given by

$$\epsilon(x) = \sum_{i=1}^{N_c} \epsilon\delta(x - x_i)\ , \tag{6.32}$$

where x_i indicated the position where the ith coupling acts. In the following we will refer to it as the position of the ith *controller*. Ref. [248] made use of an adaptive recognition [256] and control [257–260] method, that was successfully applied also to several other situations, such as discrimination of deterministic dynamics in biophysical signals [261], control of infinite dimensional chaotic dynamics [134,262], targeting of chaos [263], secure communication processes [264], and filtering of noise using wavelet techniques [265].

Eq. (6.32) indicates that the coupling acts only in discrete points of the mesh, which were selected to be equally separated in space ($x_i - x_{i-1} = \xi$). In fact, perturbing Eq. (6.31) with a coupling of the kind of (6.32) would not give any effect: δ perturbations in space are not able to modify a fully developed partial differential equation. This is the reason why in Eq. (6.32) δ *is not* a δ-Dirac function, but it will indicate that the coupling at position x_i is extended over all the space extension of the ith controller, which usually corresponds to a single mesh point. It is important to highlight that this is the case in practical applications, where the controllers have in general a spatial size, and never act on the system in a point-like region. One possibility is considering locally space extended controllers, and studying how the extension of the controllers influences synchronization [266,267]. Another possibility is fixing once forever the mesh precision, thus selecting the space extension of the controllers [18,248,249]. In the following we will pursuit this latter strategy.

Ref. [248] highlights that already a finite number of controllers is sufficient to warrant CS of two identical systems, in a robust way as far as a controller is placed approximately each two correlation lengths ($\xi \leqslant 2\xi_c$).

Ref. [18] extended the study to synchronization of two fields coming from different dynamics ($\alpha_1 \neq \alpha_2,\ \beta_1 \neq \beta_2$), in the case in which the coupling function was extended over all the N mesh points ($\epsilon(x) \equiv \epsilon$). In this latter case a transition is found for large parameter mismatches from no synchronization to CS mediated by a state where a kind of PS was observed. The intermediate PS state has been better characterized in a more recent work [250] in the case of a unidirectional coupling. Space–time Fourier analysis of this state indicated that the synchronization phenomenon has rather a temporal behavior than a spatial one and the intermediate stage is the one with larger variations in the mean temporal frequencies of the two systems [249].

A relevant question is whether synchronization between nonidentical systems can be achieved with a *discrete* coupling, i.e. a coupling extended only on some of the mesh points. In the following we will show that this is in fact possible in the limit $\xi \leqslant \xi_c$ provided that the coupling strength ϵ increases *integrally* when the number of controllers decreases.

Let us first discuss the properties of CGL in the absence of the coupling. Different chaotic regimes can be identified in Eqs. (6.31) in different regions of the parameter space (α, β) [269,270], depending on the stability properties of the plane wave solutions $A_q = \sqrt{1 - q^2}\,e^{i(qx+\omega t)}$ ($-1 \leqslant q \leqslant 1$, where

q is the wavenumber in the Fourier space, and $\omega = -\beta - (\alpha - \beta)q^2$). In particular, for $\alpha\beta > -1$ there exists a critical value $q_c = \sqrt{(1+\alpha\beta)/(2(1+\beta^2)+1+\alpha\beta)}$, such that all plane waves in the range $-q_c \leqslant q \leqslant q_c$ are linearly stable. Such plane waves become unstable outside this range through the so-called Eckhaus instability [268]. Now, q_c vanishes as the product $\alpha\beta$ approaches -1. Therefore, all plane waves become unstable when crossing from below the so-called Benjamin–Feir line $\alpha\beta = -1$ in the parameter space. Three different turbulent states may be identified above the Benjamin–Feir line [269,270], namely phase turbulence (PT), amplitude turbulence (AT) or defect turbulence, and bichaos. In particular PT and AT have received a special attention in the scientific community [271–275].

PT is a state characterized by a chaotic evolution of the phase, whereas the amplitude changes smoothly, and it is always bounded away from zero. On the contrary, in AT the amplitude dynamics becomes chaotic, leading to large amplitude oscillations which can occasionally cause the occurrence of a space–time defect in the point where the amplitude is locally vanishing.

This implies that choosing in (6.31) a sufficiently large parameter mismatch between the equations governing the fields $A_{1,2}$ is tantamount to selecting the uncoupled evolutions of the two fields to be in AT and PT respectively (for the time being $\alpha_1 = \alpha_2 = 2.1$, $\beta_1 = -1.2$ and $\beta_2 = -0.83$). The correlation length in the AT case (and for a spatial extension $L = 256$) is $\xi_c = 5.38$ [276]. Let us now switch on the coupling term on a set of equispaced controllers, and study the synchronization features emerging in the evolution of the two fields, as a function of both the coupling coefficient ϵ and the controllers number N_c.

To fix a reference, we first will describe the case of a coupling coefficient that is active for all mesh points ($N_c = N$). All details about the numerical method can be found in Ref. [276]. The spatial extension is $L = 256$ and the number of mesh points is $N = 2048$. The two systems $A_{1,2}$ are left uncoupled for a time sufficient to wash out the initial transient and to be in a chaotic AT (for A_1) and PT state (for A_2). After this initial step, the coupling is switched on.

Fig. 6.9 shows the patterns arising from the space–time representations of ρ_1 (a, c, e, g) and ρ_2 (b, d, f, h) for $\epsilon = 0.05$ (a, b), $\epsilon = 0.14$ (c, d), $\epsilon = 0.2$ (e, f), $\epsilon = 2$ (g, h). At small coupling strengths, the two systems do not synchronize (a, b). At intermediate coupling (Fig. 6.9 (c, d)), the two systems enter both in a AT state and space–time defects ($\rho_2 = 0$) are created in the system A_2. For even larger coupling (Fig. 6.9(e, f)), the two system return both in a synchronized PT state, and defects no longer appear in both systems. If one further increases the coupling (Fig. 6.9(g, h)), the two states hold in a completely synchronized configuration, but creation–annihilation of defects in both systems takes place. A possible explanation is that the two dynamics for A_1 and A_2 are not compatible and the combined dynamics of the synchronized state must deal with this incompatibility by having an "intermittency" type dynamics.

In order to describe the above scenario, we need to introduce some quantitative indicator, such as the number of defects N_{def} that are present in the system. In Fig. 6.10(a), a statistics is made of N_{def} as a function of ϵ. The inset reports the situation for small coupling strength and corresponds to the first three cases of Fig. 6.9. The number of defects of A_1 is decreasing to zero when the coupling ϵ is increased. As for A_2, its defect number vs. ϵ is not evolving monotonically, but it increases to a maximum value (for $\epsilon \simeq 0.12$ where the number of defects is equal to the number of defects for A_1) and then decreases to reach zero for $\epsilon \simeq 0.16$. However, a further increase of the coupling generates an increasing of the defect number (e.g. for $\epsilon = 2$, $N_{\mathrm{def}} = 79$).

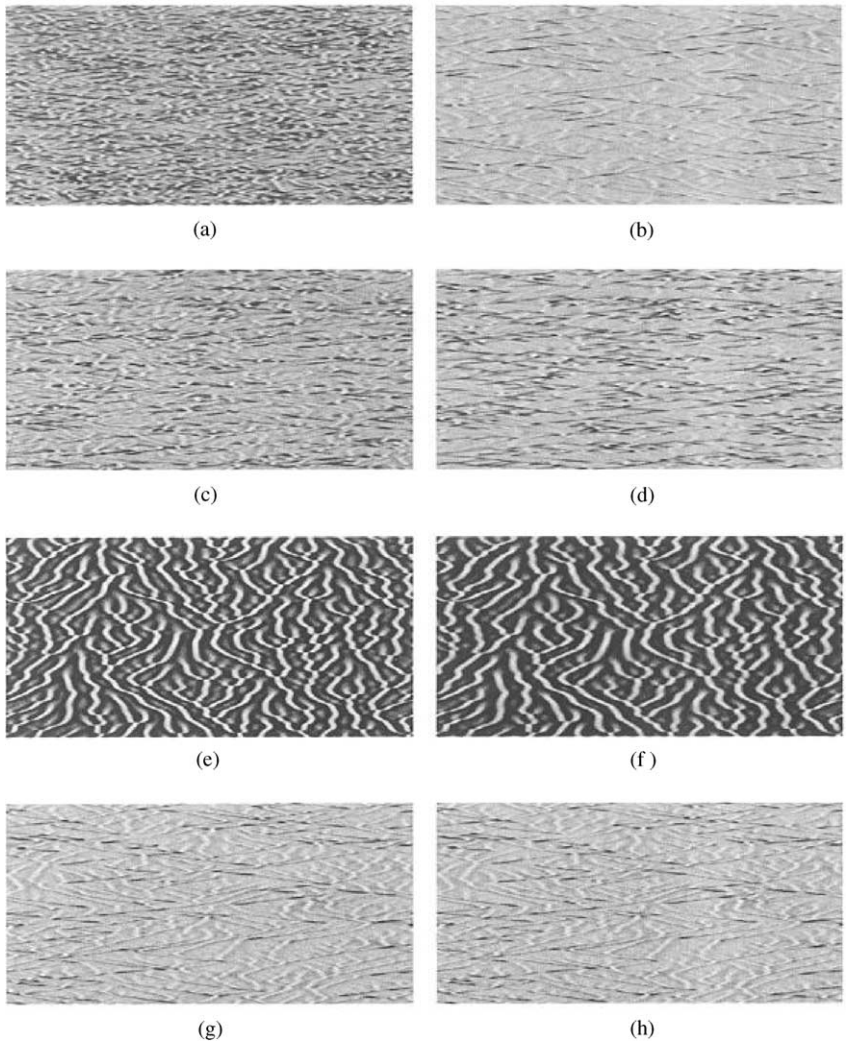

Fig. 6.9. From Ref. [276]. *Case*: $N_c = N$ in Eq. (6.31): Space (horizontal)–time (vertical) plots of the moduli ρ_1 (a, c, e, g) and ρ_2 (b, d, f, h). Parameters in Eq. (6.31) are: $\alpha_1 = \alpha_2 = 2.1$, $\beta_1 = -1.2$, $\beta_2 = -0.83$. Time increases downwards from 500 to 1500 (u.t.). The first 500 time units (not plotted) after coupling has been started are not represented. Note that the two systems were prepared in two independent chaotic states (AT for A_1 and PT for A_2). (a) and (b) correspond to $\epsilon = 0.05$, (c) and (d) to $\epsilon = 0.14$, (e) and (f) to $\epsilon = 0.2$, (g) and (h) to $\epsilon = 2$.

Two other indicators for the synchronization are reported in Fig. 6.10b, namely the average (in space and time) of the modulus difference (solid line)

$$\langle \Delta\rho \rangle = \left\langle \frac{|\rho_1 - \rho_2|}{\rho_1 + \rho_2} \right\rangle_{x,t} \tag{6.33}$$

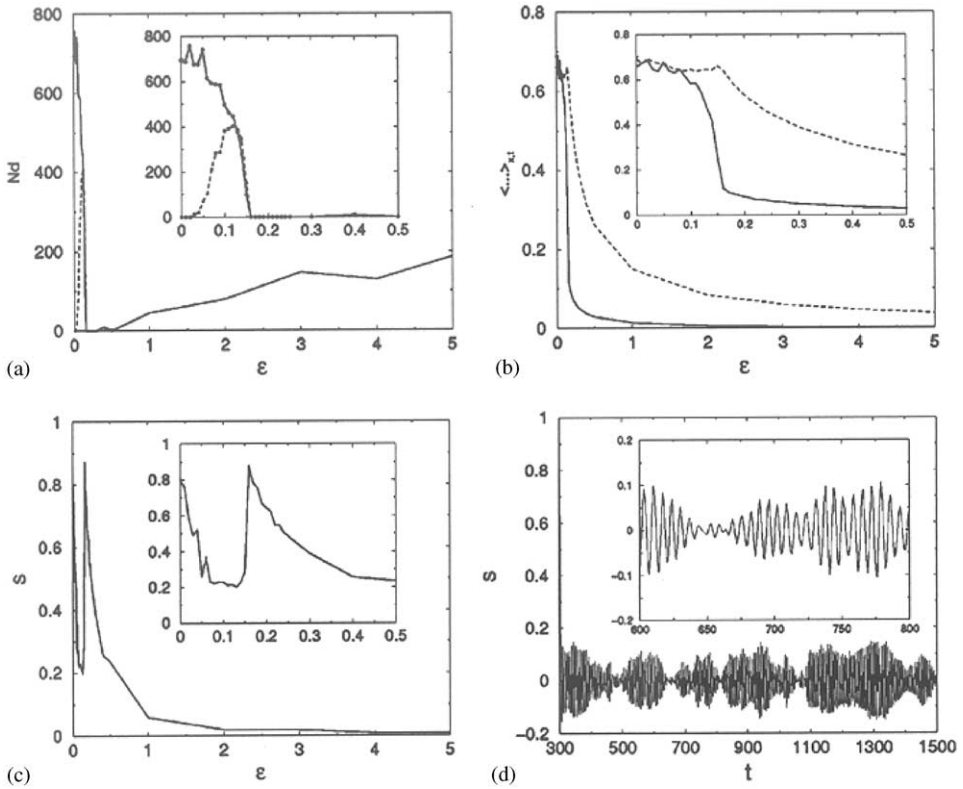

Fig. 6.10. From Ref. [276]. *Case*: $N_c = N$ in Eq. (6.31): Indicators of synchronization. (a) Total number of defects versus the coupling strength ϵ for A_1 (solid line) and A_2 (dashed line). The inset reports the zoom at small ϵ values. (b) The modulus (solid line) and phase (dashed line) indicators vs. ϵ (see text for definition). The modulus indicator has been multiplied by a factor 7 in order to get the same vertical scale for the two indicators. The inset reports the zoom at small ϵ values. (c) SYG indicator (see text for definition) vs. ϵ (Eq. (6.36)). The inset reports the zoom at small ϵ values. (d) SYG indicator vs. time (in arbitrary units) for a fixed coupling strength $\epsilon = 2$. The inset is a zoom from $t = 600$ to 800. Parameters are the same as in the caption of Fig. 6.9.

and the same average for the phase difference (dashed line)

$$\langle \Delta\psi \rangle = \left\langle \frac{|\psi_1 - \psi_2|}{|\psi_1| + |\psi_2|} \right\rangle_{x,t} . \tag{6.34}$$

The inset again reports the situation at small coupling values. The modulus difference decreases much faster than the phase difference, as the coupling increases, and therefore one can infer that the defects first synchronize before having a CS [18].

In Fig. 6.10(c, d) two other indicators are shown, namely

$$\mathrm{SYG}(t, \epsilon) = \langle \mathrm{Re}(A_1 - A_2) + \mathrm{Im}(A_1 - A_2) \rangle_x \tag{6.35}$$

and

$$\mathrm{SYG}(\epsilon) = \langle \mathrm{SYG}(t, \epsilon) \rangle_t , \tag{6.36}$$

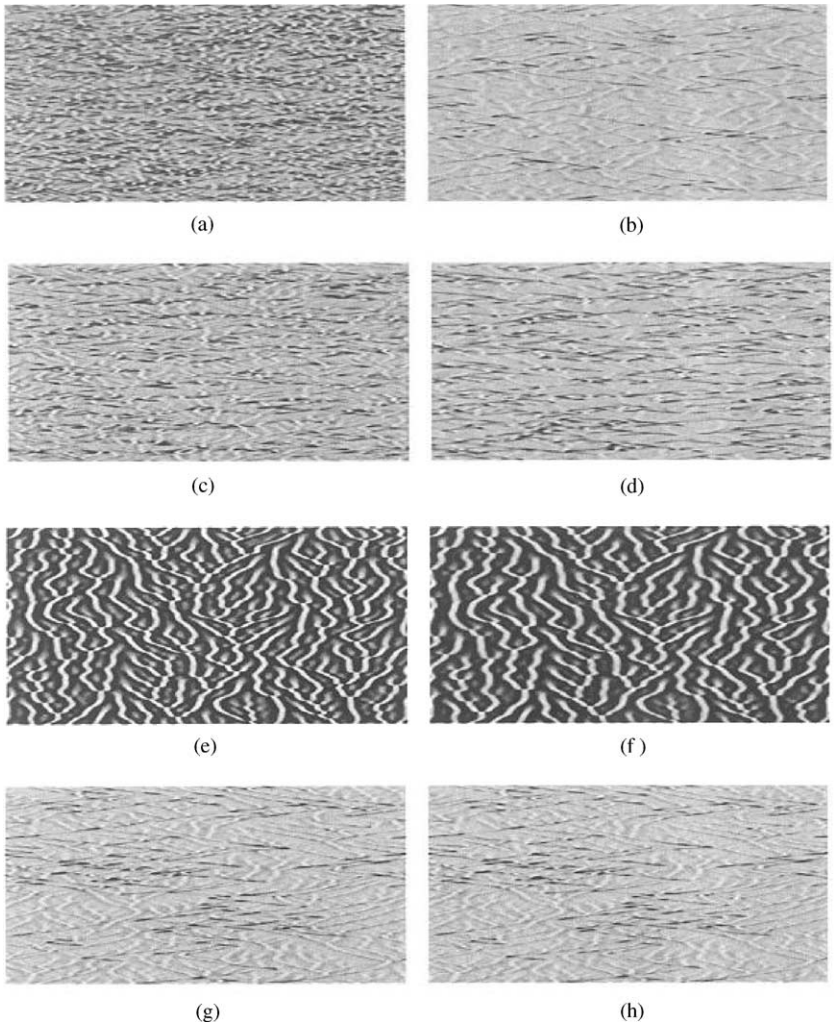

Fig. 6.11. From Ref. [276]. *Case*: $N_c = N/5$ in Eq. (6.31): Space (horizontal)–time (vertical) plots of the moduli ρ_1 (a, c, e, g) and ρ_2 (b, d, f, h). $\alpha_1 = \alpha_2 = 2.1$, $\beta_1 = -1.2$, $\beta_2 = -0.83$. Time increases downwards from 500 to 1500 (u.t.). Same general stipulations as in the caption of Fig. 6.9. (a) and (b) correspond to $\epsilon = 0.25$, (c) and (d) to $\epsilon = 0.70$, (e) and (f) to $\epsilon = 1$, (g) and (h) to $\epsilon = 10$.

which are an hybrid between the phase and modulus difference indicators. Fig. 6.10(c) shows SYG(ϵ). This indicator has the property of being not a monotonous function of ϵ. In particular, when the number of defect vanishes, a sudden increase in the corresponding value of the SYG indicator is observed. Fig. 6.10(d) reports the temporal evolution of SYG(t, ϵ) at large coupling ($\epsilon = 2$), indicating that the synchronization is not a stable process, and that some kind of intermittency phenomena occur.

Let us now move to describe the case of a *discrete* coupling. Fig. 6.11 shows the space–time plots of ρ_1 (a, c, e, g) and ρ_2 (b, d, f, h) for $N_c = N/5$. Notice that in Fig. 6.11 $\epsilon = 0.25$ (a, b), $\epsilon =$

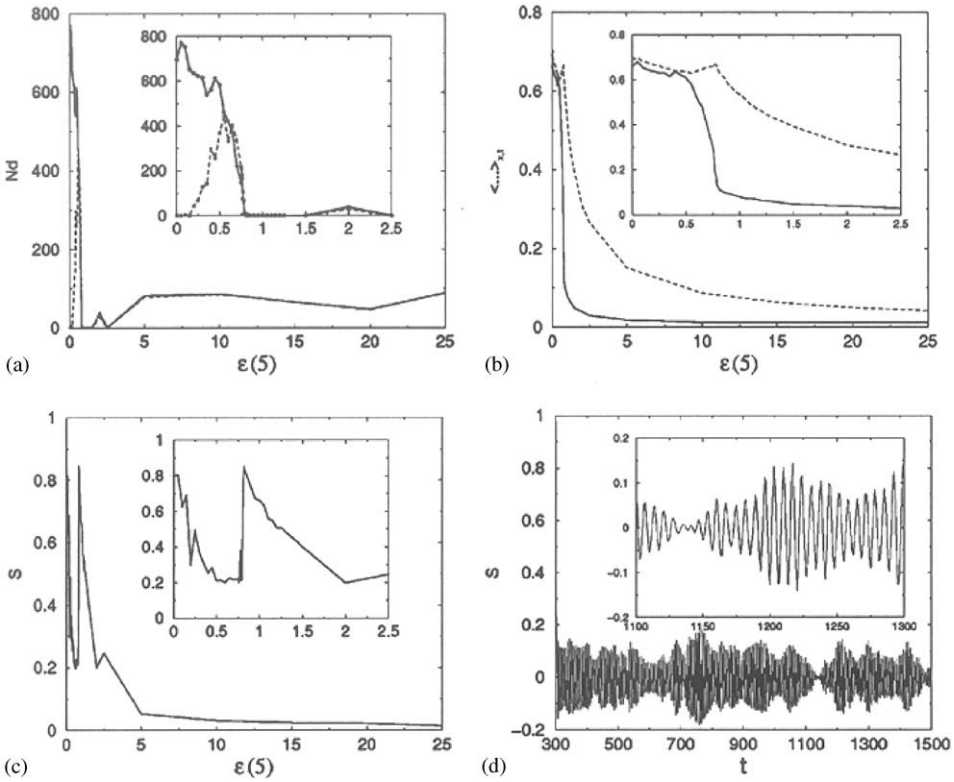

Fig. 6.12. From Ref. [276]. *Case*: $N_c = N/5$ in Eq. (6.31): Same indicators of synchronization as in Fig. 6.10. (a) Total number of defects vs. the coupling strength ϵ for A_1 (solid line) and A_2 (dashed line). The inset reports the zoom at small ϵ values. (b) The modulus (solid line) and phase (dashed line) indicators vs. ϵ. The modulus indicator has been multiplied by a factor 7 in order to get the same vertical scale. The inset reports the zoom at small ϵ values. (c) SYG indicator vs. ϵ. The inset reports the zoom at small ϵ values. (d) SYG indicator vs. time (in arbitrary units) for a fixed coupling strength $\epsilon = 2$. The inset is a zoom from $t = 1100$ to 1300. In (a, b, c) $\epsilon(5)$ means that we take one controller each five mesh points. Notice that the corresponding transitions occur for coupling strengths five times larger than in Fig. 6.10.

0.70 (c, d), $\epsilon = 1$ (e, f), and $\epsilon = 10$ (g, h) which are exactly five times the coupling strengths used in Fig. 6.9 for $N_c = N$. By comparing with Fig. 6.9, it is nearly impossible to distinguish between the two scenarios of synchronization stages. Fig. 6.12 reports the behavior of the above indicators in the case $N_c = N/5$, showing the same succession of events as for discrete synchronization, except that the coupling strength has to be multiplied by the factor N_c/N.

An ultimate test to show up the limitation of this integral behavior, may be done by defining ϵ^* as the minimum coupling strength for which the number of defects in A_1 and A_2 vanishes, and by reporting ϵ^* vs. ξ/ξ_c. The outcome of this test is shown in Fig. 6.13, where the integral behavior is witnessed by the fact that the results align quasi perfectly on a straight line for $\xi/\xi_c < 1/3$.

Similar approaches, based on local coupling schemes, have been successfully applied for control and synchronization purposes in coupled Ginzburg–Landau [267] and Kuramoto–Sivashinsky [266,277] equations.

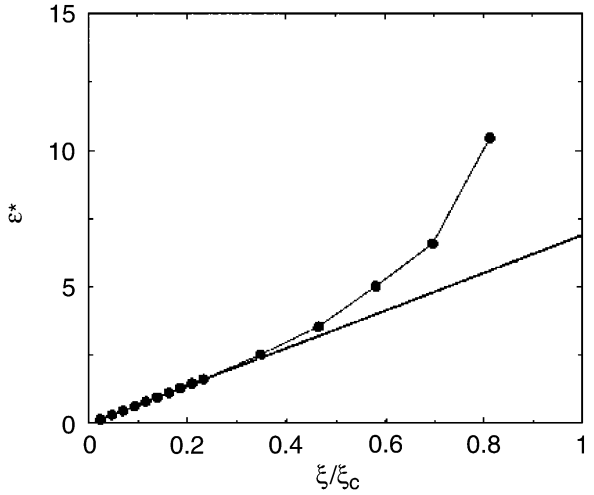

Fig. 6.13. From Ref. [276]. ϵ^* (see text for definition) as a function of the ratio ξ/ξ_c. The straight line aligning the results witnesses the existence of an integral behavior for the discrete synchronization in the limit of at least three controllers per spatial correlation length.

7. Experimental synchronization of chaos

In the last sections, we have shown that when nonlinear dynamical systems are coupled or influenced by a common driving signal, synchronization can be established among the systems. The type and the degree of synchronization depend on the coupling strength as well as on the structures of the systems. When the subsystems are nearly identical and the coupling is strong enough, complete synchronization may be observed between the states $x(t)$ and $y(t)$ of two coupled system, or with an appreciable time lag τ, as is called lag synchronization. When two different systems are coupled with sufficiently strong coupling strength, generalized synchronization may occur and two systems establish a functional relationship $y(t) = \psi(x(t))$ between their states. Rather weak coupling may already affect the time scales of the systems, and two chaotic oscillators may achieve phase locking, while the amplitude can remain only weakly correlated.

Many laboratory or natural systems are essentially composed of subsystems coupled some times in a sophisticated manner. Due to the coupling, interdependence between the subsystems is established and synchronization may set in and play an important functional role in the system behavior. However, laboratory or natural systems often have the following features:

(i) They are hardly found fully identical and in many cases, considerable drifting of system parameters makes the systems rather nonstationary.
(ii) Noise is always present in experimental systems.
(iii) Accurate descriptions of such systems are often very complicated, and simple and tractable models are often not available, and most likely the only accessible information are a few recorded time series from different subsystems.

(iv) While in some experimental systems the coupling can be adjusted to examine how the synchronization behavior changes, in most natural systems there is often no access or it is very difficult to perform such a control of system parameters.

These features call for special data analysis tools for detecting synchronization behavior in experimental data. In this chapter, we first review several tools for the detection of synchronization or more generally interdependence of two nonlinear time series. After the summary of the tools, we discuss synchronization found in experimental and natural systems.

7.1. Data analysis tools for detecting synchronized regimes

While CS can be easily detected by visualizing the difference between the two time series, the identification of other types of synchronization or even weaker interdependence is not straightforward and requires more sophisticated approaches.

The most well-known method to search interdependence between two time series $\{x_i\}$ and $\{y_i\}$ sampled with a time step Δt is to calculate the cross correlation function (more generally, considering a time lag $\tau = l\Delta t$)

$$C(X, Y, \tau) = \langle [(x_i - \langle x \rangle)(y_{i-l} - \langle y \rangle)] \rangle \,, \tag{7.1}$$

where $\langle \cdot \rangle$ stands for average over time. It is important to emphasize that $C(X, Y, \tau)$ measures only the linear interdependence between the time series. To measure nonlinear interaction, concepts from information theory, such as mutual information

$$I(X, Y) = H(X) + H(Y) - H(X, Y) \tag{7.2}$$

which is based on the Shannon entropies $H(X)$ and $H(Y)$ of both time series and the entropy $H(X, Y)$ of the joint probability function, are often applied [129]. In Section 5.3, mutual information is used to measure the dependence between noisy phases due to a common random forcing. One should note that such statistical measures basing on the stationary probability distributions $p(X)$, $p(Y)$ and $p(X, Y)$ are hard to estimate reliably due to nonstationary and limited length of real data.

Many modern methods for the nonlinear analysis of multivariate time series are based on the assumption that deterministic dynamics are responsible for the recorded complex time series [139,278]. The phase space structure of the dynamics then should be able to be unfolded and reconstructed equivalently in a high enough dimensional embedding space with only a scalar time series according to Taken's embedding theorem. Often the vectors in the m dimensional embedding space can be constructed by the time-delay (e.g. $\tau = l\Delta t$) coordinates of the time series as

$$\mathbf{x}_i = (x_i, x_{i-l}, \ldots, x_{i-(m-1)l}).$$

For multivariate time series, the embedding parameters m and l can be different and often should be chosen individually for X and Y. Readers are referred to Refs. [139,278] for detailed discussion on optimizing these parameters. In a proper embedding space, many methods then have been proposed to reduce the measurement noise and to compute invariant quantities, such as Lyapunov exponents λ_i or dimensions D_i. Prediction of the time series can be performed, and local or global models may be constructed.

Despite those rather general methods of nonlinear data analysis, special techniques for synchronization analysis have been recently developed. In the following we review such methods for generalized and phase synchronization.

7.1.1. Generalized synchronization

According to Section 3.6, where the occurrence of generalized synchronization has been discussed, the two (sub)systems are connected by a functional relationship $Y = \psi(X)$, i.e. whenever two states $\mathbf{x}_i$ and $\mathbf{x}_j$ are close to each other, the contemporary states $\mathbf{y}_i$ and $\mathbf{y}_j$ are also close to each other. Based on this idea, Ref. [10] proposed the method of *mutual false nearest neighbor* to detect GS, which has been mentioned briefly in Section 4.1.

Actually, the mutual false nearest neighbor method belongs to a variation of a somewhat more general method proposed in Ref. [123], which considers closeness not only by the nearest neighbor point, but an ε region in the neighborhood. Ref. [123] introduces the *mean conditional dispersion*

$$\sigma_{XY}(\varepsilon) = \left[\sum_{i \neq j} \|\mathbf{y}_i - \mathbf{y}_j\|^2 \Theta(\varepsilon - \|\mathbf{x}_i - \mathbf{x}_j\|) \Big/ \sum_{i \neq j} \Theta(\varepsilon - \|\mathbf{x}_i - \mathbf{x}_j\|) \right]^{1/2} , \tag{7.3}$$

where Θ it the Heaviside function with $\Theta(z > 0) = 1$ and $\Theta(z \leqslant 0) = 0$. When X and Y are in generalized synchronization, $\sigma_{XY}(\varepsilon)$ should decrease with decreasing ε, while if they are not related, $\sigma_{XY}(\varepsilon)$ is independent of ε. With this measure, interdependence may be detected, while linear correlation indicates no significant interrelation. With a similar idea, Ref. [110] developed a set of statistics for mathematical properties, such as continuity and differentiability, of maps between time series in terms of probabilities or confidence levels.

In a similar spirit, other variations of the method have been proposed in Ref. [125] and investigated further in Refs. [126,279]. They included the k nearest neighbors $r_i(j)$, $(j = 1, \ldots, k)$ of a state $\mathbf{x}_i$ and the k nearest neighbors $s_i(j)$, $(j = 1, \ldots, k)$ of the state $\mathbf{y}_i$. The squared mean distance and the conditional distance then are given by

$$R_i^{(k)}(X) = \frac{1}{k} \sum_{j=1}^{k} (\mathbf{x}_i - \mathbf{x}_{r_i(j)})^2, \quad R_i^{(k)}(X|Y) = \frac{1}{k} \sum_{j=1}^{k} (\mathbf{x}_i - \mathbf{x}_{s_i(j)})^2 ,$$

respectively. With these quantities, a measure for interdependence can be defined as

$$S^{(k)}(X|Y) = \frac{1}{N} \sum_{i=1}^{N} \frac{R_i^{(k)}(X)}{R_i^{(k)}(X|Y)} , \tag{7.4}$$

which vanishes when X and Y are independent and takes a value close to 1 when generalized synchronization occurs. Based on the conditional distance, another measure was also proposed similar to Eq. (7.4), but using the distance of random points, $R_i = (N-1)^{-1} \sum_{j \neq i} (\mathbf{x}_i - \mathbf{x}_j)$ instead of that from the k nearest neighbors for comparison, which reads

$$H^{(k)}(X|Y) = \frac{1}{N} \sum_{i=1}^{N} \frac{R_i(X)}{R_i^{(k)}(X|Y)} . \tag{7.5}$$

Both measures have proven to be quite useful in real data applications [125] and simple toy models [126,279].

There are a few other methods based on predictability of time series. Ref. [113] used mutual prediction for detecting dynamical interdependence. With the k nearest neighbors $r_i(j)$, $(j=1,\ldots,k)$ of a state $\mathbf{x}_i$, the average value after L steps translation can be taken as the prediction of the state L steps ahead, e.g.

$$\hat{\mathbf{x}}_{i+L}(X) = \frac{1}{k}\sum_{j=1}^{k} \mathbf{x}_{r_i(j)+L} \tag{7.6}$$

and the average prediction error is

$$e(X) = \frac{1}{N}\sum_{i=1}^{N} |\mathbf{x}_{i+L} - \hat{\mathbf{x}}_{i+L}(X)| \ ,$$

which then is further normalized by the prediction error when taking the mean value of the time series as the predicted value, i.e.

$$e_{\text{mean}}(X) = \frac{1}{N}\sum_{i=1}^{N} |\mathbf{x}_{i+L} - \langle \mathbf{x} \rangle| \ ,$$

giving

$$\Delta(X) = \frac{e(X)}{e_{\text{mean}}(X)} \ . \tag{7.7}$$

$\Delta(X) = 1$ indicates that there is no predictability in the time series. Similarly, prediction can be performed with mutual nearest neighbors $s_i(j)$, so that

$$\hat{\mathbf{x}}_{i+L}(X|Y) = \frac{1}{k}\sum_{j=1}^{k} \mathbf{x}_{s_i(j)+L}$$

and

$$e(X|Y) = \frac{1}{N}\sum_{i=1}^{N} |\mathbf{x}_{i+L} - \hat{\mathbf{x}}_{i+L}(X|Y)| \ .$$

Likewise, the normalized mutual prediction error can be calculated,

$$\Delta(X|Y) = \frac{e(X|Y)}{e_{\text{mean}}(X)} \ . \tag{7.8}$$

When X and Y are in GS, bidirectional mutual prediction can be observed, i.e. $\Delta(X|Y) < 1$ and $\Delta(Y|X) < 1$.

Following the spirit in Ref. [110], Ref. [280] presented a statistics for predictability and functionality in terms of significance level and applied it to detect functional relationships between experimental time series.

Recently another prediction approach for multivariate time series has been proposed in Ref. [121], based on the idea of *mixed state embedding*. It goes as follows: when two nonlinear systems are coupled, the dynamics of the whole system can be unfolded and reconstructed in a higher

dimensional embedding space and predictability of subsystems can be obtained consequently with nearest neighbors in the mixed state space

$$\mathbf{p}_i(m,n) = (x_i, x_{i-l}, \ldots, x_{i-(m-1)l};\ y_i, y_{i-l}, \ldots, y_{i-(n-1)l}) \ .$$

With k nearest neighbors $r_i(j)$, $j = 1, \ldots, k$ *in the mixed state space*, the prediction value $\hat{\mathbf{x}}_{i+L}(X)$ of L ($L = 1$ and $k = 1$ are considered in Ref. [121]) steps ahead can be computed as in Eq. (7.6), and the prediction error is given by

$$e(X,m,n) = \frac{1}{N}\sum_{i=1}^{N} |\mathbf{x}_{i+L} - \hat{\mathbf{x}}_{i+L}(X)| \ . \tag{7.9}$$

Since the nearest neighbors in subspace X or Y may turn out to be false nearest neighbors in the mixed embedding, the prediction may be improved by a mixed state embedding. Then by examining the pattern of $e(X,m,n)$ in the (m,n) space, interdependence between X and Y can be detected.

When a functional relationship is identified with the above measures, one may go further to numerically approximate the function ψ. A method based on empirical global modeling of time series [139] was suggested in Ref. [112]. But also other modeling techniques basing e.g. on the maximal correlation function can be applied [281,282].

Furthermore, the problem of testing whether two chaotic one-dimensional processes reconstructed from different measured variables can be considered as dynamically equivalent, has been the object of a recent study, that used experimental data from electronic circuits to illustrate a general technique [283].

7.1.2. Coupling direction

The next problem in the synchronization analysis is determination of the coupling direction. Due to different coupling configurations, interdependence between X and Y may be asymmetrical. For example in unidirectional coupling from X to Y, Y is affected by X, however, X is free and is not influenced by Y. On the contrary, in bidirectional coupling, both are influenced by each other. The correlation function in Eq. (7.1) and mutual information in Eq. (7.2) is symmetric when exchanging X and Y. Thus both cannot provide information on the coupling direction. All other measures mentioned above are in general asymmetrical when exchanging X and Y, and could be useful for detecting coupling asymmetry. Besides the measure in Eq. (7.9) based on the mixed state embedding with only the assumption that the underlying dynamics are coupled deterministic nonlinear (chaotic) dynamics, the other measures are based on the further assumption that X and Y are in GS, so that closeness in the phase space is mapped to each other. Interestingly, in the presence of GS, this mapping of closeness is mutual, and the degree of asymmetry of these measures often become lower compared to that in weaker coupling region where synchronization has not been established [113,125,279]. To make this statement more concrete, let us discuss the measure of mutual prediction of Eq. (7.8). For unidirectional coupling from X to Y, when the coupling is weak, there is a predictability of Y from X, but not for the inverse, i.e. $\Delta(Y|X) < 1$ but $\Delta(X|Y) \approx 1$, and the driver–response relationship can be detected. When GS sets in, bidirectional mutual prediction is observed, and unidirectional coupling may not be distinguished from a bidirectional one by this measure. However, if it is known a priori that the coupling is unidirectional, then bidirectional mutual predictability implies GS. Note that the measures of the asymmetry degree have a nontrivial

dependence on other parameters of the data, such as the number N of data points and the number k of nearest neighbors, and in some cases, the interpretation of this information is difficult [125,279].

A method to detect chaotic drive–response geometry in GS, which is able to display when GS manifolds exist, and to characterize its nature has also been introduced [284].

An information-theoretic measure, the coarse-grained information rates, has been recently introduced [122] so that interdependence as well as the direction of information flow can be detected in coupled systems. Detecting direction of coupling in interacting oscillators has also been studied using the phase dynamics [285], which would provide a more promising detection when the interdependence between amplitudes is weaker than that of phases due to weak interaction.

It should be pointed out that the above described methods are subjected to the same restrictions as other time series analysis approaches [278], and application to real data is nontrivial due to noise, nonstationary and limited length of data, especially from biological systems.

7.1.3. Phase synchronization

In the following we turn to discuss detecting interdependence between time series from the viewpoint of PS. As shown in Section 3.1, PS sets in at much weaker coupling regime where a strong connection between the amplitudes has usually not been established and a functional relationship is usually not expected. In this case, measures based on the assumption of existence of a mapping between the time series very likely are not able to detect this weak interdependence with confidence.

To detect PS, one looks for correlation between phases of the time series rather than the states themselves. The first step is then to compute phases from the time series. Section 3.1 has presented a discussion on this problem. Here we would like to discuss the calculation of the phase from the viewpoint of filtering. For narrow-band signals $x(t)$, e.g. a signal from a system with a proper rotation around a reference point, the phase can be obtained by means of the analytic signal $V(t)$ using the Hilbert transform Eq. (3.5), which is equivalent to filtering the signal with a filter $F(t) = \delta(t) + (\mathrm{j}/\pi)P(1/t)$ ($P(1/t)$ means the principal part of $1/t$) whose amplitude response is unity, and whose phase response is a constant $\pi/2$ lag at all frequencies. Writing

$$V(t) = A(t)\mathrm{e}^{\mathrm{j}\phi(t)} = x(t) \odot F(t) \,, \tag{7.10}$$

where $\odot$ denotes convolution, the computing of the phase then becomes a problem of filtering the signal. More importantly, one can consider other choices of the filter $F(t)$. Note that PS is in fact a phenomenon of adjusting time scales by weak interaction, and many systems have a broad distribution of time scales and very possibly not all time scales are synchronized. It is thus interesting and important to detect synchronization between some particular time scales and the definition of phase with filtering becomes very natural. One useful choice can be a Gaussian type of filter around a characteristic frequency ν_0 with a width σ, e.g. $F(t) = (\sigma/\sqrt{2\pi})\exp[-\mathrm{j}\nu_0 t + \sigma^2 t^2/2]$. This definition of phase was discussed in Refs. [32,286].

When phases (lifted to the whole real line, i.e. not modulated to $[0, 2\pi]$) are defined and computed for individual time series, instantaneous frequencies may also be estimated by the derivative of the polynomial function fitted to the phases on an interval essentially larger than the characteristic period of oscillations. With the phase and frequency information, one is ready to detect synchronization. Due to several effects, such as borderline of phase synchronization, imperfect synchronization, noise

and nonstationarity, phases are most likely not locked perfectly, but often interrupted by phase slips. Ref. [103] presents a few methods to detect phase synchronization of noisy data:

(a) *Analysis of phase difference.* Phase locking epochs may be manifested by horizontal plateaus in the plot of difference $\Delta\phi_{n,m} = n\phi_x - m\phi_y$ of lifted phases ϕ_x and ϕ_y. However, due to strong noisy or chaotic fluctuations in the signal, clear plateaus may not be easily detectable, and one should analyze the distribution of the cyclic phase difference $\Delta\Phi_{n,m} = \Delta\phi_{n,m} \bmod 2\pi$ over a moving window, where peaks indicate preferred phase differences between the two systems. The degree of phase synchronization can be measure more quantitatively. Ref. [22] proposes two measures of the $n : m$ synchronization index. The first one based on the Shannon entropy is defined as

$$\rho_{nm} = (S_{\max} - S)/S_{\max} ,$$

where $S = -\sum_{k=1}^{N} p_k \ln p_k$ is the entropy of the distribution of $\Delta\Phi_{n,m}$ and $S_{\max} = \ln N$ (N is the number of bins) is the entropy of the uniform distribution. Normalized in this way, $0 \leqslant \rho_{nm} \leqslant 1$, and larger ρ_{nm} corresponds to a higher degree of phase synchronization. The second index is based on conditional probability. The intervals of two phases ϕ_x and ϕ_y, $[0, n2\pi]$ and $[0, m2\pi]$, are divided into N bins. Then for each bin l, one calculates

$$\gamma_l(t_j) = \frac{1}{M_l} \sum \mathrm{e}^{\mathrm{i}\phi_y(t_j)}$$

for all j such that $\phi_x(t_j)$ belongs to bin l and M_l is the number of points in this bin. Averaging $\gamma_l(t_j)$ over all the N bins gives the synchronization index

$$\lambda_{nm} = \frac{1}{N} \sum_{l=1}^{N} |\gamma_l(t_j)| ,$$

which assumes a value between 0 and 1. A similar quantity can also be defined based on the phase difference $\Delta\Phi_{n,m}$, as

$$\tilde{\lambda}_{nm} = \langle \sin^2 \Delta\Phi_{n,m} \rangle + \langle \cos^2 \Delta\Phi_{n,m} \rangle .$$

Similar to the conditional probability, mutual information between the distributions of the phases ϕ_x and ϕ_y can be calculated as a quantitative measure of the degree of phase synchronization, as demonstrated in Section 5. Mutual information combined with a test of its statistical significance has been used to detect PS in noisy systems [287].

(b) *Instantaneous frequency ratio.* For synchronized systems, this ratio should fluctuate around a rational number. Its advantage is that there is no need to search for appropriate values of n and m. However, due to noise, nonstationarity and short interval of synchronization epochs, this one may not be able to distinguish synchronization from occasional coincidence of frequencies, and this method can be used only in addition to the analysis of phase differences.

(c) *Constructing a synchrogram.* This method employs the idea of a phase stroboscope: when the cyclic phase of one system attains a certain fixed value θ at a moment t_k, e.g. $\phi_x(t_k) = \theta$, the cyclic phase of the other system is plotted vs. t_k to construct a m order synchrogram, i.e.

$$\psi_m(t_k) = \phi_y(t_k) \bmod 2\pi m . \tag{7.11}$$

In this graphic presentation, $n : m$ synchronization can be visualized by n distinct horizontal lines and transitions between different ratios of phase locking can be traced, which is extremely useful

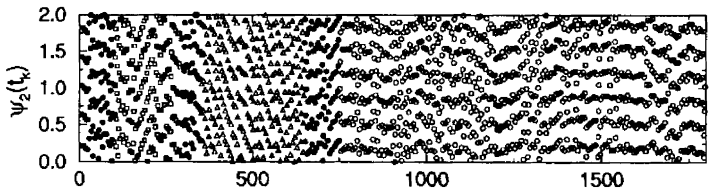

Fig. 7.1. A synchrogram ($m = 2$) for the cardiorespiratory system of a human subject which shows the transition from a 5-band structure (5 : 2 locking) to a 6-band structure (3 : 1 locking). (From Ref. [103].)

for application to biological data where nonstationarity is often strong [21]. A typical synchrogram ($m = 2$) is shown in Fig. 7.1 for the cardiorespiratory system of a human subject which shows the transition from a 5-band structure (5 : 2 locking) to a 6-band structure (3 : 1 locking).

It has been recently shown that it is also possible to recover a complete synchronization diagram of the form in Fig. 3.9 from only a very few sets of bivariate data [288]. This technique allows to estimate the relative strength of the coupling and the parameter mismatch of both subsystems. The method is most efficient if only points from the nonsynchronized regime are taken for learning the model.

7.2. Synchronization phenomena in laboratory experiments

CS and GS phenomena in controlled laboratory experiments were demonstrated for electronic circuits [6,36,48,289], as well as for laser systems [23,290–293]. In driven chaotic systems, different stages of chaotic synchrony, such as GS, PS and LS have been observed [294,295]. Furthermore, both CS and GS have been largely demonstrated in experiments that tried to validate secure communication schemes. These experimental setups include digital phase-locked loops [296], modified Chua's oscillators [297,298], semiconductor lasers exhibiting chaotic emission on subnanosecond time scales [299], experimental systems operating at radio frequency [300], and chaotic diode lasers [301,302].

PS of a chaotic oscillator by an external periodic driving signal has been demonstrated in a plasma discharge tube paced with a low amplitude wave generator [29,303]. Real-time observation of synchronization and unsynchronization states is made by taking a stroboscopic sampling at each period of the pacing signal. In Ref. [30], PS of homoclinic chaos in a CO_2 laser with feedback is achieved by a tiny periodic modulation of a control parameter. Different ratios of phase locking can be realized in this system. Chaotic oscillation of an electrochemical oscillator can be phase-locked or even suppressed by external periodic forcing [304].

PS of coupled chaotic oscillators has been demonstrated in electronic circuits, lasers, convective flow and others systems. Ref. [305] shows PS in electronic circuits of two unidirectionally chaotic Rössler systems. Ref. [95] observes noise-induced intermittent phase slips and demonstrates that the scaling of the average duration between successive phase slips obeys that of superpersistent chaotic transients. Ref. [306] and Ref. [307] have shown frequency-locking and PS between two mutually coupled chaotic modes of an optically pumped NH_3 ring laser, and between the chaotic oscillation of a single mode ring laser and a chaotic driving signal, respectively. Ref. [308] presents experimental evidence that the outputs in two unidirectionally coupled semiconductor lasers with an external cavity, when operating in the regime of low-frequency fluctuations, are synchronized in their

dropout events but remain uncorrelated in the process of power recovery. In this case, PS is not complete, but is achieved between some slow-time scale motions. Similarly, PS between different frequency components of the oscillator dynamics that are not otherwise apparent are detected in a linear laser array [32], with phase variables computed by applying a Gaussian filter as discussed in the Section 7.1. Different types of synchronization, including complete, lag and phase synchronization has been observed in master and slave channels in a dual-wavelength class-B laser with modulated losses [309]. In Ref. [310], it is shown that due to the effect of PS, in a rather counterintuitive way, the repulsive Coulomb interaction can hold a large number of ions into a packet and make them oscillate synchronously in an electrostatic trap. This absence of dispersion due to PS has application for mass spectrometry with extremely high resolution.

Evidence of PS in a laboratory experiment was offered in a thermocapillary driven convective cell in a time-dependent chaotic regime [25]. The relevance of this experiment relies in the fact that convective systems have been studied along the last two centuries as paradigmatic examples of systems yielding a very rich scenario of dynamical phenomena (from strongly ordered states to strongly disordered states, to turbulence). In particular, the time-dependent regimes of fluid layers submitted to a temperature gradient is a subject of current interest. An example is the convection with free surface (so called Bénard–Marangoni convection). Its relevance is related to the fact that, at a planetary scale, it plays an important role in geophysical [311,312] or atmospheric [313] energetic transport. Indeed, the quasi-periodic oceanic circulation patterns, like El Niño current [314,315], are intimately correlated with the variation of the global pattern of rainfall, and their phases are considered a good quantitative measure for predicting the future rainfall [316].

Lag synchronization has been observed in electric circuits [104] and lasers [309,317]. In the presence of large parameter mismatches, lag synchronization characterized by an approximate functional relation between time-lagged dynamical variables of coupled oscillators, has been experimentally observed in coupled circuits [318].

7.3. Synchronization phenomena in natural systems

Synchronization phenomena has been largely studied also in nature. The dynamics e.g. of the human cardiorespiratory system [21], of an extended ecological system [31], of the magnetoencephalographic activity of Parkinsonian patients [22], and of electrosensitive cells of the paddlefish [24], have been shown to display synchronization features.

As pointed out in the beginning of this section, CS of natural systems may be exceptional because the systems are generically heterogeneous and coupling is often complicated and weak. Nonlinear time series analysis tools have been applied to detect synchronization and coupling (direction) in natural systems.

One approach is based on the assumption that a rather strong, although may be complicated, relation may be established between the systems, thus revealing the settings of GS. A possible method has been discussed already in Section 4. Recently, GS has been studied in the context of a pair of quasi-two-dimensional channel models, describing the Atlantic and Pacific sectors of the Earth's climate system [319].

Another approach directed to PS of oscillators has been demonstrated to be very successful in the detection of synchronization and coupling in natural systems. Due to heterogeneity and relatively complicated and weak coupling, a relation may only be established between phases but

not in amplitudes of the systems. The phase analysis is completely insensitive to amplitude and may considerably reduce the error from uncorrelated amplitudes, thus detects successfully a hidden synchronization. The advantages of phase analysis also come from the fact that these methods are applicable independent of whether the systems are chaotic or noisy, or even nonstationary.

The methods of PS analysis have been successfully applied to the cardiorespiratory system. Apart from respiratory modulation of heart rate known as 'respiratory sinus arrhythmia' (RSA), previously, it was believed that there is comparatively weak coupling between respiration and the cardiac rhythm, and the resulting rhythms are generally not phase locked. However, when applying the phase analysis techniques, Refs. [21,103] reveal long period of hidden cardiorespiratory synchronization during spontaneous breathing. Different locking ratios have been detected even for noisy and nonstationary data.

Many further studies have been carried out on the coupling of cardiac rhythm with other systems. Ref. [320] compares the cardioventilatory coupling (CVC) under the condition of spontaneous ventilation and conditions where the ventilatory period is fixed, and demonstrates that CVC does not exist in the latter case. Comparison of CVC in different anaesthetized animals and human subjects has been carried out in Ref. [321]. Ref. [322] analyzes RSA with respect to respiratory phase and observes PS between heartbeat and paced breathing with breath hold periods, showing that phase analysis techniques might be useful for elucidating detailed mechanisms for RSA. It is also revealed that the strength of PS is inversely related to the extent of RSA [323]. A quantitative analysis of cardiorespiratory synchronization in healthy infants has found that the average degree of synchronization varies with the age of the newborns [324]. During anaesthesia in rats, it is found that the system passes reversibly through a sequence of different cardiorespiratory phase-synchronized states as the anaesthesia level changes, and the synchronization state may be used to characterize the depth of anaesthesia [325]. The phase analysis techniques have also been used to study spatial synchronization of oscillations in blood distribution systems [326]. The cardiac and respiratory oscillation at different sites of the system are strongly phase and frequency synchronized, while the spatial synchronization of oscillations that originate locally is weaker, showing that the entire cardiovascular system is characterized by the same dynamics.

Besides CVC, the cardiac rhythm may be affected by other factors. Using phase analysis, a possible link between the cardiac cycle and the timing of recurrent hiccups has been explored in Ref. [327]. Ref. [328] has demonstrated that the cardiorhythm can be synchronized by a weak external forcing, such as periodic sequences of light and sound pulses, or aperiodic sequences of the variation of RR intervals of another subject. An entrainment of cardiac and locomotor rhythms in humans has been demonstrated in Ref. [329].

The phase analysis techniques have also been applied successfully to study synchronization of biological neuron activities. Ref. [22] applies these methods to magnetoencephalography (MEG) signals and records of muscle activity of a Parkinsonian patient. The analysis detects $1:1$ PS between the activity of certain brain areas, and $1:2$ PS between the activity of these areas and the muscle activity recorded by electromyography (EMG). These results reveal that the temporal evolution of the peripheral tremor rhythms directly reflects the time course of the synchronization of abnormal activity between cortical motor areas and addresses a fundamental problem in neuroscience that cortico-cortical synchronization is necessary for establishing coordinated muscle activity. A similar analysis with MEG has later demonstrated interhemispheric PS and amplitude correlation of beta oscillations in human subjects [330]. Ref. [331] has found that propofol anaesthesia induces phase

synchronization changes in electroencephalography (EEG). The changes are different in the alpha, theta and beta frequency bands. The passband and location-specific behavior of these changes reveal effects of the anaesthesia to different neural mechanisms. Phase analysis on the gamma-band of EEG has shown that the degree of PS between frontal cortex and right parietal cortex is significantly increased during mental rotation with respect to rest [332], whereby musicians show significant higher degrees of synchronization than nonmusicians. Enhanced PS in EEG gamma band has also been found for musicians while listening to music [333,334], and left-hemispheric dominance in the degree of PS is observed in musicians, while right-hemispheric dominance is generally observed in nonmusicians [332–334]. A quantification of synchronization processes by coherence and phase and its application to higher-level cognitive processes have been carried out [335] with EEG recorded during word processing. The information transfer through the propagation of oscillations could be verified by phase analysis.

Application of the phase analysis to the optical topography obtained by using multi-channel near-infrared spectroscopy has revealed spatially synchronized oscillations of changes in the concentration of oxy- and deoxy-hemoglobin throughout the occipital cortex of newborn infants [336]. Optical topography of oxy- and deoxy-hemoglobin concentration also reveals PS between the motor cortex hemodynamics and periodic motor stimulation conditions [337]. Application of phase analysis to the EEG of epilepsy patients has shown distinct differences in the degree of synchronization between recordings from seizure-free intervals and those before an impending seizure, indicating an altered state of brain dynamics prior to seizure activity [338]. Although other nonlinear analysis methods [339] or information-theoretic methods [340] have also been applied to characterize and detect neurodynamics changes leading to seizures, the analysis of PS is proved to be the most robust one [341]. The success of phase analysis may be due to its complete insensitivity to amplitude, which may provide a significant source of error when there is no established relation between amplitudes due to weak coupling or when the data is very noisy or nonstationary.

Readers interested in more details on the neurodynamics can refer to a few recent review articles in different subjects. Ref. [342] presents a review on synchronized oscillations of the human sensorimotor cortex. There it is pointed out that the development of refined signal analysis methods are important factors that lead to an increasing interest in studies of sensorimotor oscillations. The investigation proceeds from phenomenology to function and provides an interesting approach to address questions in human motor physiology and pathophysiology. A review of the corticomuscular coherence measured between EEG or MEG and EMG is presented in Ref. [343]. Ref. [344] reviews the mechanisms of large-scale integration in brainweb that counterbalance the distributed anatomical and functional organization of brain activity to enable the emergence of coherent behavior and cognition. Although the mechanisms involved in large-scale integration are still largely unknown, it is argued that the most plausible candidate is the formation of dynamics links mediated by PS over multiple frequency bands. Nonlinear time series analysis of epilepsy is summarized in Refs. [339,341]. A review of the synchronization and rhythmic processes in physiology is presented in Ref. [345]. Mathematical and physical techniques combined with physiology and medical studies are addressing questions concerning the dynamics of the rhythmic processes, their interaction with each other and with the external environment and controlling pathological rhythms, etc., and are transforming our understanding of the rhythms.

In Ref. [24], it is shown that the noise-mediated oscillator in the electrosensitive cells in the paddlefish can be synchronized by a weak electric and/or magnetic field. Different types of noisy

phase-locked regimes are observed. Synchronization behavior at different time-scales can be observed in coupled biological neurons possessing slow oscillation of membrane potential and fast spikes [346].

PS of chaotic oscillation has also been observed in other biological systems. Ref. [347] observes synchronization phenomena in nephron–nephron interaction in rat kidneys. PS has been demonstrated [31,348] in extended ecological systems—Canadian hare-lynx cycle—over large geographical regions. Spatial PS leads to the emergence of complex chaotic traveling-wave structures which may be crucial for species persistence.

Phase analysis methods have also been applied to solar activity. In Ref. [349], phase synchronization of the sunspot cycle and a fast component of the solar inertial motion has been found and confirmed with statistical significance in different epochs. The result can be considered as a quantitative support for the hypothesis that there is a weak interaction of gravity and solar activity. A nonlinear interaction between the intensity oscillations of chromospheric bright points has been identified with phase analysis [350].

Acknowledgements

The authors are grateful to V. Anishchenko, F.T. Arecchi, E. Barreto, V. Belykh, J. Bragard, S. Bressler, R. Brown, M.J. Bünner, T. Carroll, H. Chaté, A. Farini, A. Giaquinta, B. Gluckman, C. Grebogi, H. Kantz, L. Kocarev, K. Josić, Y.-C. Lai, A. Lemaitre, I. Leyva, R. Livi, H. Mancini, D. Maza, A.S. Mikhailov, E. Ott, U. Parlitz, L.M. Pecora, A. Pikovsky, A. Politi, I. Procaccia, M. Rabinovich, M.G. Rosenblum, R. Roy, N. Rulkov, S. de San Roman, T. Sauer, S. Schiff, V. Shalfeev, K. Showalter, P. So, M. Spano, A. Vallone, J. Yorke, M. Zaks, D.H. Zanette for the many past and present fruitful discussions on the subjects covered by this report. We acknowledge the Max Planck Institut für Physik komplexer Systeme for having hosted us during the final preparation of the present paper, in connection with the Seminar on Control, Communication and Synchronization in Chaotic Dynamical Systems (October 14–November 23, 2001). Work partly supported by EEC Network n. HPRN-CT-2000-00158. J. Kurths acknowledges the SFB 555 and DFG Research Group "Conflicting Rules in Cognitive Systems". G. Osipov acknowledges the INTAS Project 01-867. C.S. Zhou was supported by the Humboldt Foundation (Germany).

References

[1] A.S. Hornby, Oxford Advanced Dictionary, Oxford University Press, Oxford, 1974.
[2] C. Hugenii, Horoloquium Oscilatorium, Apud F. Muguet, Parisiis, 1673. **
[3] I.I. Blekman, Synchronization in Science and Technology, Nauka, Moscow, 1981 (in Russian); ASME Press, New York, 1988 (in English). **
[4] H. Fujisaka, T. Yamada, Prog. Theor. Phys. 69 (1983) 32. *
[5] V.S. Afraimovich, N.N. Verichev, M.I. Rabinovich, Izvestiya Vysshikh Uchebnykh Zavedenii Radiofizika 29 (9) (1986) 1050. *
[6] L.M. Pecora, T.L. Carroll, Phys. Rev. Lett. 64 (1990) 821. **
[7] M.G. Rosenblum, A.S. Pikovsky, J. Kurths, Phys. Rev. Lett. 76 (1996) 1804. **
[8] E.R. Rosa, E. Ott, M.H. Hess, Phys. Rev. Lett. 80 (1998) 1642.
[9] M.G. Rosenblum, A.S. Pikovsky, J. Kurths, Phys. Rev. Lett. 78 (1997) 4193. *
[10] N.F. Rulkov, M.M. Sushchik, L.S. Tsimring, H.D.I. Abarbanel, Phys. Rev. E 51 (1995) 980. **

[11] L. Kocarev, U. Parlitz, Phys. Rev. Lett. 76 (1996) 1816. *
[12] S. Boccaletti, D.L. Valladares, Phys. Rev. E 62 (2000) 7497.
[13] M.A. Zaks, E.-H. Park, M.G. Rosenblum, J. Kurths, Phys. Rev. Lett. 82 (1999) 4228.
[14] R. Femat, G. Solis-Perales, Phys. Lett. A 262 (1999) 50.
[15] D.H. Zanette, Phys. Rev. E 55 (1997) 5315.
[16] P. Parmananda, Phys. Rev. E 56 (1997) 1595.
[17] A. Amengual, E. Hernández-García, R. Montagne, M. San Miguel, Phys. Rev. Lett. 78 (1997) 4379.
[18] S. Boccaletti, J. Bragard, F.T. Arecchi, H.L. Mancini, Phys. Rev. Lett. 83 (1999) 536.
[19] H. Chaté, A. Pikovsky, O. Rudzick, Physica D 131 (1999) 17.
[20] S. Boccaletti, D.L. Valladares, J. Kurths, D. Maza, H. Mancini, Phys. Rev. E 61 (2000) 3712.
[21] C. Schafer, M.G. Rosenblum, J. Kurths, H.H. Abel, Nature 392 (1998) 239. *
[22] P. Tass, M.G. Rosenblum, M.G. Weule, J. Kurths, A. Pikovsky, J. Volkmann, A. Schnitzler, H.J. Freund, Phys. Rev. Lett. 81 (1998) 3291.
[23] G.D. Van Wiggeren, R. Roy, Science 279 (1998) 1198. *
[24] A. Neiman, X. Pei, D. Russell, W. Wojtenek, L. Wilkens, F. Moss, H.A. Braun, M.T. Huber, K. Voigt, Phys. Rev. Lett. 82 (1999) 660.
[25] D. Maza, A. Vallone, H. Mancini, S. Boccaletti, Phys. Rev. Lett. 85 (2000) 5567.
[26] G.M. Hall, S. Bahar, D.J. Gauthier, Phys. Rev. Lett. 82 (1999) 2995.
[27] A.R. Yehia, D. Jeandupreux, F. Alonso, M.R. Guevara, Chaos 9 (1999) 916.
[28] J.-W. Shuai, D.M. Durand, Phys. Lett. A 264 (1999) 289.
[29] C.M. Ticos, E. Rosa Jr., W.B. Pardo, J.A. Walkenstein, M. Monti, Phys. Rev. Lett. 85 (2000) 2929.
[30] E. Allaria, F.T. Arecchi, A. Di Garbo, R. Meucci, Phys. Rev. Lett. 86 (2001) 791.
[31] B. Blasius, A. Huppert, L. Stone, Nature 399 (1999) 354.
[32] D.J. DeShazer, R. Breban, E. Ott, R. Roy, Phys. Rev. Lett. 87 (2001) 044101.
[33] E. Barreto, P. So, B.J. Gluckmann, S.J. Schiff, Phys. Rev. Lett. 84 (2000) 1689.
[34] E. Barreto, P. So, Phys. Rev. Lett. 85 (2000) 2490.
[35] A.S. Pikovsky, Z. Phys. B 55 (1984) 149. *
[36] L.M. Pecora, T.L. Carroll, Phys. Rev. A 44 (1991) 2374.
[37] K. Pyragas, Phys. Rev. E 54 (1996) R4508.
[38] R. He, P.V. Vaidya, Phys. Rev. A 46 (1992) 7387.
[39] T. Kapitaniak, Phys. Rev. E 50 (1994) 1642.
[40] R.E. Amritkar, N. Gupte, Phys. Rev. E 47 (1993) 3889.
[41] L. Kocarev, U. Parlitz, Phys. Rev. Lett. 74 (1995) 5028.
[42] U. Parlitz, L. Kocarev, T. Stojanovski, H. Preckel, Phys. Rev. E 53 (1996) 4351.
[43] J. Güemez, M.A. Matías, Phys. Rev. E 52 (1995) R2145.
[44] C.W. Wu, L.O. Chua, Int. J. Bifurc. Chaos 4 (1994) 979.
[45] C. Sparrow, The Lorenz Equations, Bifurcations, Chaos, and Strange Attractors, Springer, New York, 1982.
[46] N. Balmforth, Ch. Tresser, P. Worfolk, C.W. Wu, Chaos 7 (1997) 392.
[47] J.M. Kowalski, G.L. Albert, G.W. Gross, Phys. Rev. A 42 (1990) 6260.
[48] K.M. Cuomo, A.V. Oppenheim, Phys. Rev. Lett. 71 (1993) 65. *
[49] T.L. Carroll, L.M. Pecora, Physica D 67 (1993) 126.
[50] T.L. Carroll, Phys. Rev. E 50 (1994) 2580.
[51] F. Verhulst, Nonlinear Differential Equations and Dynamical Systems, Springer, Berlin, Heidelberg, 1990.
[52] L. Yu, E. Ott, Q. Chen, Phys. Rev. Lett. 65 (1990) 2935.
[53] D.J. Gauthier, J.C. Bienfang, Phys. Rev. Lett. 77 (1996) 1751.
[54] G. Benettin, C. Froeschlé, H.P. Scheidecker, Phys. Rev. A 19 (1976) 454.
[55] I. Shimada, T. Nagashima, Prog. Theor. Phys. 61 (1979) 1605.
[56] A. Wolf, J.B. Swift, H.L. Swinney, J.A. Vastano, Physica D 16 (1985) 285.
[57] J.L. Willems, Stability Theory of Dynamical Systems, Wiley, New York, 1970.
[58] K. Murali, M. Lakshmanan, Phys. Rev. E 49 (1994) 4882.
[59] R. Brown, N.F. Rulkov, Phys. Rev. Lett. 78 (1997) 4189.
[60] R. Brown, N.F. Rulkov, Chaos 7 (1997) 395.

[61] P. Ashwin, J. Buescu, I. Stewart, Phys. Lett. A 193 (1994) 126. *
[62] P. Ashwin, J. Buescu, I.N. Stewart, Nonlinearity 9 (1996) 703.
[63] E. Ott, J.C. Sommerer, J.C. Alexander, I. Kan, J.A. Yorke, Phys. Rev. Lett. 71 (1993) 4143. *
[64] J. C. Sommerer, E. Ott, Nature (London) 365 (1993) 136.
[65] Y.C. Lai, C. Grebogi, J.A. Yorke, S.C. Venkataramani, Phys. Rev. Lett. 77 (1996) 55.
[66] E. Ott, J.C. Sommerer, Phys. Lett. A 188 (1994) 39.
[67] V. Astakhov, A. Shabunin, T. Kapitaniak, V. Anishchenko, Phys. Rev. Lett. 79 (1997) 1014.
[68] S.C. Venkataramani, B.R. Hunt, E. Ott, Phys. Rev. E 54 (1996) 1346.
[69] S.C. Venkataramani, B.R. Hunt, E. Ott, Phys. Rev. Lett. 77 (1996) 5361.
[70] H.U. Voss, Phys. Rev. E 61 (2000) 5115.
[71] H.U. Voss, Phys. Rev. Lett. 87 (2001) 014102.
[72] Y. Kuramoto, Chemical Oscillations, Waves and Turbulence, Springer, Berlin, 1984. **
[73] H.Z. Risken, The Fokker–Planck Equation, Springer, Berlin, 1989.
[74] A.S. Pikovsky, M. Rosenblum, G.V. Osipov, M. Zaks, J. Kurths, Physica D 104 (1997) 219.
[75] O.E. Roessler, Phys. Lett. A 57 (1976) 397.
[76] D. Gabor, J. IEE London 93 (1946) 429.
[77] A. Pikovsky, M. Rosenblum, J. Kurths, Synchronization—A Unified Approach to Nonlinear Science, Cambridge University Press, Cambridge, 2001. *
[78] K. Josić, D.J. Mar, Phys. Rev. E 64 (2001) 066234.
[79] E.F. Stone, Phys. Lett. A 163 (1992) 367. *
[80] A. Pikovsky, G. Osipov, M. Rosenblum, M. Zaks, J. Kurths, Phys. Rev. Lett. 79 (1997) 47.
[81] A.S. Pikovsky, M. Zaks, M. Rosenblum, G. Osipov, J. Kurths, Chaos 7 (1997) 680.
[82] V.S. Anishchenko, T.E. Vadivasova, D.E. Postnoy, M.A. Safonova, Int. J. Bifurc. Chaos 2 (1992) 633.
[83] G.V. Osipov, J. Kurths, Phys. Rev. E 65 (2002) 016216.
[84] A. Katok, B. Hasselblatt, Introduction to the Modern Theory of Dynamical Systems, Cambridge University Press, Cambridge, 1995.
[85] H.G. Schuster, Deterministic Chaos, An Introduction, VCH-Verlag, Weinheim, 1988. *
[86] G. Goldztein, S.H. Strogatz, Int. J. Bifurc. Chaos 5 (1995) 983.
[87] W.C. Lindsey, Synchronization Systems in Communication and Control, Prentice-Hall, Englewood Cliffs, NJ, 1972.
[88] I.P. Keener, Trans. AMS 26 (2) (1980) 589.
[89] V.S. Afraimovich, V.I. Nekorkin, G.V. Osipov, V.D. Shalfeev, Stability, Structures Chaos in Nonlinear Synchronization Networks, World Scientific, Singapore, 1995.
[90] S.H. Strogatz, R.E. Mirollo, Physica D 31 (1988) 143. *
[91] P. Manneville, Y. Pomeau, Physica D 1 (1980) 219.
[92] K.J. Lee, Y. Kwsk, T.K. Lim, Phys. Rev. Lett. 81 (1998) 321.
[93] W.H. Kye, C.M. Kim, Phys. Rev. E 62 (2000) 6304.
[94] V. Andrade, R.L. Davidchack, Y.C. Lai, Phys. Rev. E 61 (2000) 3230.
[95] L.Q. Zhu, A. Raghu, Y.C. Lai, Phys. Rev. Lett. 86 (2001) 4017.
[96] A.S. Pikovsky, P. Grassberger, J. Phys. A 24 (1991) 4587.
[97] H.L. Yang, Phys. Rev. E 63 (2001) 026213.
[98] S.P. Kuznetsov, I.R. Sataev, Phys. Rev. E 64 (2001) 046214.
[99] S.P. Kuznetsov, I.R. Sataev, Phys. Lett. A 162 (1992) 236.
[100] M.J. Feigenbaum, J. Stat. Phys. 19 (1978) 25.
[101] E.H. Park, M. Zaks, J. Kurths, Phys. Rev. E 60 (1999) 6627.
[102] M.A. Zaks, E.-H. Park, J. Kurths, Int. J. Bifurc. Chaos 10 (2000) 2649.
[103] C. Schäfer, M.G. Rosenblum, H.H. Abel, J. Kurths, Phys. Rev. E 60 (1999) 857.
[104] S. Taherion, Y.C. Lai, Phys. Rev. E 59 (1999) R6247.
[105] J.F. Heagy, T.L. Carroll, L.M. Pecora, Phys. Rev. E 52 (1995) R1253.
[106] C.S. Zhou, C.H. Lai, Phys. Rev. E 59 (1999) R6243.
[107] G. Osipov, A. Pikovsky, M. Rosenblum, J. Kurths, Phys. Rev. E 55 (1997) 2353.
[108] A. Pikovsky, M. Rosenblum, J. Kurths, Europhys. Lett. 34 (1996) 165.
[109] H.D.I. Abarbanel, N.F. Rulkov, M.M. Sushchik, Phys. Rev. E 53 (1996) 4528.

[110] L.M. Pecora, T.L. Carroll, J.F. Heagy, Phys. Rev. E 52 (1995) 3420.
[111] B.R. Hunt, E. Ott, J.A. Yorke, Phys. Rev. E 55 (1997) 4029.
[112] R. Brown, Phys. Rev. Lett. 81 (1998) 4835.
[113] S.J. Schiff, P. So, T. Chang, R.E. Burke, T. Sauer, Phys. Rev. E 54 (1996) 6708.
[114] P. Grassberger, I. Procaccia, Phys. Rev. Lett. 50 (1983) 346.
[115] J.L. Kaplan, J.A. Yorke, Functional differential equations and approximation of fixed points, in: H.-O. Peitgen, H.-O. Walther (Eds.), Springer Lecture Notes in Mathematics, Vol. 730, Springer, Berlin, 1979, p. 204. *
[116] J. Guckenheimer, P. Holmes, Nonlinear Oscillations, Dynamical Systems, and Bifurcations of Vector Fields, Springer, Berlin, New York, 1983. *
[117] I.I. Blekhman, A.L. Fradkov, H. Nijmeijer, A.Yu. Pogromsky, Systems Control Lett. 31 (1997) 299. *
[118] R. Brown, L. Kocarev, Chaos 10 (2000) 344.
[119] S. Boccaletti, L.M. Pecora, A. Pelaez, Phys. Rev. E 63 (2001) 066219. *
[120] S. Boccaletti, D.L. Valladares, L.M. Pecora, H.P. Geffert, T. Carroll, Reconstructing embedding spaces of coupled dynamical systems from multivariate data, Phys. Rev. E 65 (2002) 035204 (R).
[121] M. Wiesenfeldt, U. Parlitz, W. Lauterborn, Int. J. Bifurc. Chaos 11 (2001) 2217.
[122] M. Palus, V. Komarek, Z. Hrncir, K. Sterbova, Phys. Rev. E 63 (2001) 046211.
[123] A. Cenys, G. Lasiene, K. Pyragas, Physica D 52 (1991) 332. *
[124] M. Le Van Quyen, J. Martinerie, C. Adam, F.J. Varela, Physica D 127 (1999) 250.
[125] J. Arnhold, P. Grassberger, K. Lehnertz, C.E. Elger, Physica D 134 (1999) 419.
[126] R.Q. Quiroga, J. Arnhold, P. Grassberger, Phys. Rev. E 61 (2000) 5142.
[127] C. Merkwirth, U. Parlitz, W. Lauterborn, Phys. Rev. E 62 (2000) 2089.
[128] N. Tanaka, H. Okamoto, M. Saito, Physica D 147 (2000) 1.
[129] B. Pompe, J. Stat. Phys. 73 (1993) 587.
[130] G.A. Johnson, D.J. Mar, T.L. Carroll, L.M. Pecora, Phys. Rev. Lett. 80 (3956) 1998.
[131] F.T. Arecchi, et al., Phys. Rev. A 45 (1992) R4225.
[132] G. Giacomelli, et al., Phys. Rev. Lett. 73 (1994) 1099.
[133] G. Giacomelli, A. Politi, Phys. Rev. Lett. 76 (1996) 2686.
[134] S. Boccaletti, D. Maza, H. Mancini, R. Genesio, F.T. Arecchi, Phys. Rev. Lett. 79 (1997) 5246.
[135] K. Pyragas, Phys. Rev. E 58 (1998) 3067.
[136] M.J. Bünner, W. Just, Phys. Rev. E 58 (1998) R4072.
[137] J.D. Farmer, Physica D 4 (1982) 366.
[138] K. Ikeda, M. Matsumoto, J. Stat. Phys. 44 (1986) 955.
[139] H.D.I. Abarbanel, Analysis of Observed Chaotic Data, Springer, Berlin, New York, 1996. *
[140] E. Ott, C. Grebogi, J.A. Yorke, Phys. Rev. Lett. 64 (1990) 1196. *
[141] For a review of control techniques and algorithms see S. Boccaletti, C. Grebogi, Y.-C. Lai, H. Mancini, D. Maza, Phys. Rep. 329 (2000) 103. **
[142] R. Benzi, A. Sutera, A. Vulpiani, J. Phys. A 14 (1981) L453.
[143] K. Wiesenfeld, F. Moss, Nature 373 (1995) 33.
[144] L. Gammaitoni, P. Hänggi, P. Jung, F. Marchesoni, Rev. Mod. Phys. 70 (1998) 223.
[145] A.A. Zaikin, J. Kurths, L. Schimansky-Geier, Phys. Rev. Lett. 85 (2000) 227.
[146] A.A. Zaikin, J. Garcia-Ojalvo, L. Schimansky-Geier, J. Kurths, Phys. Rev. Lett. 88 (2002) 010601.
[147] G. Hu, T. Ditzinger, C.Z. Ning, H. Haken, Phys. Rev. Lett. 71 (1993) 807.
[148] A.S. Pikovsky, J. Kurths, Phys. Rev. Lett. 78 (1997) 775.
[149] B. Hu, C. Zhou, Phys. Rev. E 61 (2000) R1001.
[150] C. Zhou, J. Kurths, B. Hu, Phys. Rev. Lett. 87 (2001) 98101.
[151] Z.F. Mainen, T.J. Sejnowski, Science 268 (1995) 1503.
[152] O.N. Bjornstad, R.A. Ims, X. Lambin, Trends Ecol. Evol. 14 (1999) 427.
[153] P.J. Hudson, I.M. Cattadori, Trends Ecol. Evol. 14 (1999) 1.
[154] F. Jeltsch, C. Wissel, Ecol. Modelling 75/76 (1994) 111.
[155] A.S. Pikovsky, in: R.Z. Sagdeev (Ed.), Nonlinear and Turbulent Processes in Physics, Harwood Academic Publisher, New York, 1984, pp. 1601–1604.
[156] A.S. Pikovsky, Radiophys. Quantum Electron. 27 (1984) 576.

[157] R.V. Jensen, Phys. Rev. E 58 (1998) R6907.
[158] K. Matsumoto, I. Tsuda, J. Stat. Phys. 31 (1983) 87.
[159] H.P. Herzel, W. Ebeling, Phys. Lett. A 111 (1985) 1.
[160] H.P. Herzel, B. Pompe, Phys. Lett. A 122 (1987) 121.
[161] A.S. Pikovsky, Phys. Lett. A 165 (1992) 33.
[162] J.F. Heagy, N. Platt, S.M. Hammel, Phys. Rev. E 49 (1994) 1140.
[163] C.S. Zhou, C.-H. Lai, Physica D 135 (2000) 1.
[164] N. Platt, E.A. Spiegel, C. Tresser, Phys. Rev. Lett. 70 (1993) 279.
[165] A. Mritan, J.R. Banavar, Phys. Rev. Lett. 72 (1994) 1451;
A. Mritan, J.R. Banavar, Phys. Rev. Lett. 73 (1994) 2932.
[166] A.S. Pikovsky, Phys. Rev. Lett. 73 (1994) 2931.
[167] L. Longa, E.M.F. Curado, A.A. Oliveira, Phys. Rev. E 54 (1996) R2201.
[168] H. Herzel, J. Freund, Phys. Rev. E 52 (1995) 3238.
[169] G. Malescio, Phys. Rev. E 53 (1996) 6551.
[170] P.M. Gade, C. Basu, Phys. Lett. A 217 (1996) 21.
[171] E. Sanchez, M.A. Matias, V. Perez-Munuzuri, Phys. Rev. E 56 (1997) 4068.
[172] C.-H. Lai, C.S. Zhou, Europhys. Lett. 43 (1998) 376.
[173] C.S. Zhou, T.L. Chen, Neurocomputing 30 (2000) 293.
[174] R. Toral, C.R. Mirasso, E. Hernandez-Garcia, O. Piro, Chaos 11 (2001) 665.
[175] C.S. Zhou, J. Kurths, Noise-induced phase synchronization and synchronization transitions in chaotic oscillators, Phys. Rev. Lett., submitted for publication.
[176] L. Arnold, Random Dynamical Systems, Springer, Berlin, Heidelberg, 1998.
[177] G. Paladin, M. Serva, A. Vulpiani, Phys. Rev. Lett. 74 (1995) 66.
[178] A. Witt, A. Neiman, J. Kurths, Phys. Rev. E 55 (1997) 5050.
[179] A.L. Hodgkin, A.F. Huxley, J. Physiol. 117 (1952) 500.
[180] H.A. Braun, M.T. Huber, M. Dewald, K. Schäfer, K. Voigt, Int. J. Bifurc. Chaos 8 (1998) 881.
[181] See, for example, B. Hille, Ionic Channels of Excitable Membranes, 2nd Edition, Sinauer, Sunderland, MA, 1992.
[182] H.A. Braun, H. Bade, H. Hensel, Pflugers Arch, Ges. Physiol. Menschen Tiere 386 (1980) 1.
[183] U. Feudel, A. Neiman, X. Pei, W. Wojtenek, H.A. Braun, M. Huber, F. Moss, Chaos 10 (2000) 231.
[184] R.L. Stratonovich, Topics in the Theory of Random Noise, Gordon and Breach, New York, 1963. **
[185] C.S. Zhou, J. Kurths, I.Z. Kiss, J.L. Hudson, Noise enhanced phase synchronization of chaotic oscillators, Phys. Rev. Lett., submitted for publication.
[186] R. Benzi, A. Sutera, A. Vulpiani, J. Phys. A 14 (1981) L453.
[187] C.S. Zhou, C.H. Lai, Phys. Rev. E 60 (1999) 3928.
[188] A. Neiman, A. Silchenko, V. Anishchenko, L. Schimansky-Geier, Phys. Rev. E 58 (1998) 7118.
[189] A. Neiman, L. Schimansky-Geier, A. Cornell-Bell, F. Moss, Phys. Rev. Lett. 83 (1999) 4896.
[190] B. Hu, C.S. Zhou, Phys. Rev. E 63 (2001) 026201.
[191] S.H. Strogatz, S.E. Mirollo, P.C. Matthews, Phys. Rev. Lett. 68 (1992) 2730.
[192] J.F. Heagy, L.M. Pecora, T.L. Carroll, Phys. Rev. Lett. 74 (1994) 4185.
[193] D.H. Zanette, A.S. Mikhailov, Phys. Rev. E58 (1998) 872.
[194] F.S. de San Roman, S. Boccaletti, D. Maza, H.L. Mancini, Phys. Rev. Lett. 81 (1998) 3639;
see also the Erratum, Phys. Rev. Lett. 82 (1998) 674.
[195] D. Maza, S. Boccaletti, H. Mancini, Int. J. Bifurc. Chaos 10 (2000) 829.
[196] Y. Kuramoto, Physica D 50 (1991) 15.
[197] H. Sakaguchi, S. Shinomoto, Y. Kuramoto, Prog. Theor. Phys. 77 (1987) 1005.
[198] G.B. Ermentrout, N. Kopell, SIAM (Soc. Ind. Appl. Math.) J. Math. Anal. 15 (1984) 215. *
[199] L. Ren, G.B. Ermentrout, SIAM J. Math. Anal. 29 (1998) 208.
[200] M. Zhan, Z.G. Zheng, G. Hu, X.H. Peng, Phys. Rev. E 62 (2000) 3552.
[201] G.V. Osipov, M.M. Sushchik, Phys. Rev. E 58 (1998) 7198.
[202] T.E. Vadivasova, G.I. Strelkova, V.S. Anishchenko, Phys. Rev. E 63 (2001) 036225.
[203] P. Hadley, M.R. Beasley, K. Wiesenfeld, Phys. Rev. B 38 (1988) 8712.
[204] K. Wiesenfeld, P. Colet, S.H. Strogatz, Phys. Rev. Lett. 76 (1996) 404.
[205] K. Wiesenfeld, P. Colet, S.H. Strogatz, Phys. Rev. E 57 (1998) 1563.
[206] J. Benford, et al., Phys. Rev. Lett. 62 (1989) 969.

[207] S.K. Han, C. Kurrer, Y. Kuramoto, Phys. Rev. Lett. 75 (1995) 3190.
[208] Y. Braiman, J.F. Lindner, W.L. Ditto, Nature (London) 378 (1995) 465.
[209] L. Glass, M.C. Mackey, From Clocks to Chaos, Princeton University Press, Princeton, 1988. **
[210] A.T. Winfree, The Geometry of Biological Time, Springer, New York, 1980. **
[211] J.D. Murray, Mathematical Biology, Springer, Berlin, 1989.
[212] Y. Kuramoto, Prog. Theor. Phys. 79 (1974) 212.
[213] H.D.I. Abarbanel, et al., Usp. Fiz. Nauk 166 (1996) 3;
H.D.I. Abarbanel, et al., Phys. Usp. 39 (1996) 337.
[214] M.I. Rabinovich, M.M. Sushchik, Usp. Fiz. Nauk 160 (1990) 3;
M.I. Rabinovich, M.M. Sushchik, Phys. Usp. 33 (1990) 1.
[215] V.N. Belykh, E. Mosekilde, Phys. Rev. E 54 (1996) 3196.
[216] K. Kaneko, Physica D 41 (1990) 137. *
[217] K. Kaneko, Physica D 54 (1991) 5.
[218] K. Kaneko, Physica D 55 (1992) 368.
[219] K. Kaneko, Physica D 75 (1994) 55.
[220] A. Crisanti, M. Falcioni, A. Vulpiani, Phys. Rev. Lett. 76 (1996) 612.
[221] M.S. Vieira, A.J. Lichtenberg, Phys. Rev. E 56 (1997) R3741.
[222] D.H. Zanette, A.S. Mikhailov, Phys. Rev. E 57 (1998) 276.
[223] M. Hasler, Yu. Maistrenko, O. Popovich, Phys. Rev. E 58 (1998) 6843.
[224] S.C. Manrubia, A.S. Mikhailov, Phys. Rev. E 60 (1999) 1579.
[225] O. Popovich, Yu. Maistrenko, E. Mosekilde, Phys. Rev. E 64 (2001) 026205.
[226] A. Pikovsky, O. Popovich, Yu. Maistrenko, Phys. Rev. Lett. 87 (2001) 044102.
[227] V. Belykh, I. Belykh, M. Hasler, Phys. Rev. E 62 (6332) 2000.
[228] Y. Zhang, G. Hu, H. Cerdeira, S. Chen, T. Braun, Y. Yao, Phys. Rev. E 63 (2001) 026211.
[229] V. Belykh, I. Belykh, M. Hasler, Phys. Rev. E 63 (2001) 036216.
[230] W. Wang, I.Z. Kiss, J.l. Hudson, Chaos 10 (2000) 248.
[231] K. Kaneko, Phys. Rev. Lett. 63 (1989) 219.
[232] L.M. Pecora, Phys. Rev. E 58 (1998) 347.
[233] L. Pecora, T. Carroll, G. Johnson, D. Mar, K.S. Fink, Int. J. Bifurc. Chaos 10 (2000) 273.
[234] H.L. Yang, Phys. Rev. E 64 (2001) 026206.
[235] G. Hu, Y. Zhang, H.A. Cerdeira, S. Chen, Phys. Rev. Lett. 85 (2000) 3377.
[236] J.F. Heagy, T.L. Carroll, L.M. Pecora, Phys. Rev. E 50 (1994) 1874.
[237] L. Brunnet, H. Chate, P. Mannevile, Physica D 78 (1994) 141.
[238] L. Kocarev, U. Parlitz, Phys. Rev. Lett. 77 (1996) 2206.
[239] L.M. Pecora, et al., Chaos 7 (1997) 520.
[240] M. Zhan, G. Hu, Y. Zhang, D. He, Phys. Rev. Lett. 86 (2001) 1510.
[241] G.V. Osipov, M.M. Sushchik, Phys. Lett. A 201 (1995) 205.
[242] Z. Zheng, G. Hu, B. Hu, Phys. Rev. Lett. 81 (1998) 5318.
[243] D.L. Valladares, S. Boccaletti, F. Feudel, J. Kurths, Collective phase locked states in a chain of coupled chaotic oscillators, Phys. Rev. E Rapid Communications, submitted for publication.
[244] L. Kocarev, Z. Tasev, U. Parlitz, Phys. Rev. Lett. 79 (1997) 52.
[245] N. Parekh, S. Parthasarathy, S. Sinha, Phys. Rev. Lett. 81 (1998) 1401.
[246] G. Hu, Z. Qu, Phys. Rev. Lett. 72 (1994) 68.
[247] R.O. Grigoriev, M.C. Cross, H.G. Schuster, Phys. Rev. Lett. 79 (1997) 2795.
[248] S. Boccaletti, J. Bragard, F.T. Arecchi, Phys. Rev. E 59 (1999) 6574.
[249] J. Bragard, F.T. Arecchi, S. Boccaletti, Int. J. Bifurc. Chaos 10 (2000) 2381.
[250] L. Junge, U. Parlitz, Phys. Rev. E 62 (2000) 438.
[251] see M. Cross, P. Hohenberg, Rev. Mod. Phys. 65 (1993) 851 and reference therein. *
[252] P. Coullet, L. Gil, F. Roca, Opt. Commun. 73 (1989) 403.
[253] P. Kolodner, S. Slimani, N. Aubry, R. Lima, Physica D 85 (1995) 165.
[254] Y. Kuramoto, S. Koga, Prog. Theor. Phys. Suppl. 66 (1981) 1081.
[255] T. Leweke, M. Provansal, Phys. Rev. Lett. 72 (1994) 3174.

[256] F.T. Arecchi, G. Basti, S. Boccaletti, A.L. Perrone, Europhys. Lett. 26 (1994) 327.
[257] S. Boccaletti, F.T. Arecchi, Europhys. Lett. 31 (1995) 127.
[258] S. Boccaletti, F.T. Arecchi, J. Tech. Phys. 37 (1996) 285.
[259] S. Boccaletti, F.T. Arecchi, Physica D 96 (1996) 9.
[260] S. Boccaletti, A. Farini, F.T. Arecchi, Chaos Solitons Fractals 8 (1997) 1431.
[261] L. Narici, S. Boccaletti, A. Giaquinta, F.T. Arecchi, Europhys. Lett. 42 (1998) 247.
[262] D. Maza, H. Mancini, S. Boccaletti, R. Genesio, F.T. Arecchi, Int. J. Bifurc. Chaos 8 (1998) 1843.
[263] S. Boccaletti, A. Farini, E.J. Kostelich, F.T. Arecchi, Phys. Rev. E 55 (1997) R4845.
[264] S. Boccaletti, A. Farini, F.T. Arecchi, Phys. Rev. E 55 (1997) 4979.
[265] S. Boccaletti, A. Giaquinta, F.T. Arecchi, Phys. Rev. E 55 (1997) 5393.
[266] L. Junge, U. Parlitz, Z. Tasev, L. Kocarev, Int. J. Bifurc. Chaos 9 (2000) 2265.
[267] L. Junge, U. Parlitz, Phys. Rev. E 61 (2000) 3736.
[268] B. Janiaud, et al., Physica D 55 (1992) 269.
[269] B. Shraiman, et al., Physica D 57 (1992) 241.
[270] H. Chaté, Nonlinearity 7 (1994) 185.
[271] H. Sakaguchi, Prog. Theor. Phys. 84 (1990) 792.
[272] D. Egolf, H. Greenside, Nature (London) 369 (1994) 129.
[273] R. Montagne, E. Hernández-García, M. San Miguel, Phys. Rev. Lett. 77 (1996) 267.
[274] A. Torcini, Phys. Rev. Lett. 77 (1996) 1047.
[275] M. van Hecke, Phys. Rev. Lett. 80 (1998) 1896.
[276] J. Bragard, S. Boccaletti, Phys. Rev. E 62 (2000) 6346.
[277] Z. Tasev, L. Kocarev, L. Junge, U. Parlitz, Int. J. Bifurc. Chaos 10 (2000) 869.
[278] H. Kantz, T. Schreiber, Nonlinear Time Series Analysis, Cambridge University Press, Cambridge, England, 1997. *
[279] A. Schmitz, Phys. Rev. E 62 (2000) 7508.
[280] C.L. Goodridge, L.M. Pecora, T.L. Carroll, F.J. Rachford, Phys. Rev. E 64 (2001) 026221.
[281] H. Voss, J. Kurths, Phys. Lett. A 234 (1997) 336.
[282] H. Voss, P. Kolodner, M. Abel, J. Kurths, Phys. Rev. Lett. 83 (1999) 3422.
[283] G.-C. Yuan, J.A. Yorke, T.L. Carroll, E. Ott, L.M. Pecora, Phys. Rev. Lett. 85 (2000) 4265.
[284] L.M. Pecora, T.L. Carroll, Int. J. Bifurc. Chaos 10 (2000) 875.
[285] M.G. Rosenblum, A.S. Pikovsky, Phys. Rev. E 64 (2001) 045202.
[286] J.P. Lachaux, E. Rodriguez, M. Le Van Quen, A. Lutz, J. Martinerie, F.J. Varela, Int. J. Bifurc. Chaos 10 (2000) 2429.
[287] M. Palus, Phys. Lett. A 235 (1997) 341.
[288] M.I. Tokuda, J. Kurths, E. Rosa, Phys. Rev. Lett. 88 (2002) 014101.
[289] A. Kittel, J. Parisi, K. Pyragas, Physica D 112 (1998) 459.
[290] R. Roy, K.S. Thornburg Jr., Phys. Rev. Lett. 72 (1994) 2009.
[291] T. Sugawara, M. Tachikawa, T. Tsukamoto, T. Shimizu, Phys. Rev. Lett. 72 (1994) 3502.
[292] A. Uchida, M. Shinozuka, T. Ogawa, F. Kannari, Opt. Lett. 24 (1999) 890.
[293] K. Otsuka, R. Kawai, S.-L. Hwong, J.-Y. Ko, J.-L. Chern, Phys. Rev. Lett. 84 (2000) 3049.
[294] D.Y. Tang, R. Dykstra, M.W. Hamilton, N.R. Heckenberg, Chaos 8 (1998) 697.
[295] D.Y. Tang, R. Dykstra, M.W. Hamilton, N.R. Heckenberg, Phys. Rev. E 57 (1998) 5247.
[296] M. de Sousa Vieira, P. Khoury, A.J. Lichtenberg, M.A. Lieberman, W. Wonchoba, J. Gullicksen, Y.J. Huang, R. Sherman, M. Steinberg, Int. J. Bifurc. Chaos 2 (1992) 645.
[297] Y. Yuan Zhao, Int. J. Bifurc. Chaos 7 (1997) 1401.
[298] M. Itoh, T. Yang, L.O. Chua, Int. J. Bifurc. Chaos 9 (1999) 1393.
[299] I. Fisher, L. Yun, P. Davis, Phys. Rev. A 62 (2000) 011801.
[300] W. Chak-Nam, T. Kim-Fung, N. Ming-Kai, S. Xiang-Quan, Microwave Opt. Tech. Lett. 26 (2000) 407.
[301] S. Sivaprakasam, I. Pierce, P. Rees, P.S. Spencer, K.A. Shore, A. Valle, Phys. Rev. A 64 (2001) 013805.
[302] F. Rogister, A. Locquet, D. Pieroux, M. Sciamanna, O. Deparis, P. Megret, M. Blondel, Opt. Lett. 26 (2001) 1486.
[303] E. Rosa, W.B. Pardo, C.M. Ticos, J. Walkenstein, M. Monti, Int. J. Bifurc. Chaos 10 (2000) 2551.
[304] I.Z. Kiss, J.L. Hudson, Phys. Rev. E 64 (2001) 046215.

[305] U. Parlitz, L. Junge, W. Lauterborn, L. Kocarev, Phys. Rev. E 54 (1996) 2115.
[306] D.Y. Tang, N.R. Heckenberg, Phys. Rev. E 55 (1997) 6618.
[307] D.Y. Tang, R. Dykstra, M.W. Hamilton, N.R. Heckenberg, Phys. Rev. E 57 (1998) 3649.
[308] L. Wallace, D.J. Yu, W.P. Lu, R.G. Harrison, Phys. Rev. A 63 (2001) 013809.
[309] B.F. Kuntsevich, A.N. Pisarchik, Phys. Rev. E 64 (2001) 046221.
[310] H.B. Pedersen, D. Strasser, S. Ring, O. Heber, M.L. Rappaport, Y. Rudich, I. Sagi, D. Zajfman, Phys. Rev. Lett. 87 (2001) 055001.
[311] J.G. Williams, R.P. Von Herzen, Geology 2 (1986) 327.
[312] C.A. Stein, S. Stein, J. Geophys. Res. 99 (1994) 3081.
[313] A.K. Blackadar, Turbulence and Diffusion in the Atmosphere, Springer, Berlin, Heidelberg, 1997.
[314] T.P. Guilderson, D.P. Schrag, Science 281 (1998) 240.
[315] R.-H. Zhang, L.M. Rothstein, A.J. Busalacchi, Nature 391 (1998) 879.
[316] R.C. Stone, G.L. Hammer, T. Marcussen, Nature 384 (1996) 252.
[317] T. Heil, I. Fischer, W. Elsässer, J. Mulet, C.R. Mirasso, Phys. Rev. Lett. 86 (2001) 795.
[318] L.Q. Zhu, Y.C. Lai, Phys. Rev. E 64 (2001) 045205.
[319] G.S. Duane, J.J. Tribbia, Phys. Rev. Lett. 86 (2001) 4298.
[320] P.D. Larsen, E.L. Trent, D.C. Galletly, Brit. J. Anaesth. 82 (1999) 546.
[321] P.D. Larsen, D.C. Galletly, Pflug. Arch. Eur. J. Physiol. 437 (1999) 910.
[322] K. Kotani, I. Hidaka, Y. Yamamoto, S. Ozono, Method Inform. Med. 39 (2000) 153.
[323] M.B. Lotric, A. Stefanovska, Physica A 283 (2000) 451.
[324] R. Mrowka, A. Patzak, M.G. Rosenblum, Int. J. Bifurc. Chaos 10 (2000) 2479.
[325] A. Stefanovska, H. Haken, P.V.E. McClintock, M. Hozic, F. Bajrovic, S. Ribaric, Phys. Rev. Lett. 85 (2000) 4831.
[326] A. Stefanovska, M. Hozic, Prog. Theor. Phys. Suppl. 139 (2000) 270.
[327] B.Y. Chen, K. Vasilakos, D. Boisteanu, L. Garma, J.P.H. Derenne, W.A. Whitelaw, J. Appl. Physiol. 88 (2000) 2159.
[328] V.S. Anishchenko, A.G. Balanov, N.B. Janson, N.B. Igosheva, G.V. Bordyugov, Int. J. Bifurc. Chaos 10 (2000) 2339.
[329] K. Nomura, Y. Takei, Y. Yanagida, Eur. J. Appl. Physiol. 84 (2001) 373.
[330] V.V. Nikouline, K. Linkenkaer-Hansen, J. Huttunen, R.J. Ilmoniemi, Neuroreport 12 (2001) 2487.
[331] M. Koskinen, T. Seppanen, J. Tuukkanen, A. Yli-Hankala, V. Jantti, Clin. Neurophysiol. 112 (2001) 386.
[332] J. Bhattacharya, H. Petsche, U. Feldmann, B. Rescher, Neurosci. Lett. 311 (2001) 29.
[333] J. Bhattacharya, H. Petsche, Neuroreport 12 (2001) 371.
[334] J. Bhattacharya, H. Petsche, Phys. Rev. E 64 (2001) 012902.
[335] B. Schack, P. Rappelsberger, C. Anders, S. Weiss, E. Moller, Int. J. Bifurc. Chaos 10 (2000) 2565.
[336] G. Taga, Y. Konishi, A. Maki, T. Tachibana, M. Fujiwara, H. Koizumi, Neurosci. Lett. 282 (2000) 101.
[337] V. Toronov, M.A. Franceschini, M. Filiaci, S. Fantini, M. Wolf, A. Michalos, E. Gratton, Med. Phys. 27 (2000) 801.
[338] F. Mormann, K. Lehnertz, P. David, C.E. Elger, Physica D 144 (2000) 358.
[339] M. Le Van Quyen, J. Martinerie, V. Navarro, M. Baulac, F.J. Varela, J. Clin. Neurophysiol. 18 (2001) 191.
[340] M. Palus, V. Komarek, T. Prochazka, Z. Hrncir, K. Sterbova, IEEE Eng. Med. Biol. 20 (2001) 65.
[341] K.K. Jerger, T.I. Netoff, J.T. Francis, T. Sauer, L. Pecora, S.L. Weinstein, S.J. Schiff, J. Clin. Neurophysiol. 18 (2001) 259.
[342] A. Schnitzler, J. Gross, L. Timmermann, Acta Neurobiol. Exp. 60 (2000) 271.
[343] T. Mima, M. Hallett, J. Clin. Neurophysiol. 16 (1999) 501.
[344] F. Varela, J.P. Lachaux, E. Rodriguez, J. Martinerie, Nat. Rev. Neurosci. 2 (2001) 229. *
[345] L. Glass, Nature 410 (2001) 277.
[346] R.C. Elson, A.I. Selverston, R. Huerta, N.F. Rulkov, M.I. Rabinovich, H.I. Abarbanel, Phys. Rev. Lett. 81 (1998) 5692.
[347] N.H. Holstein-Rathlou, K.P. Yip, O.V. Sosnovtseva, E. Mosekilde, Chaos 11 (2001) 417.
[348] B. Blasius, L. Stone, Int. J. Bifurc. Chaos 10 (2000) 2361.
[349] M. Palus, J. Kurths, U. Schwarz, D. Novotna, I. Charvatova, Int. J. Bifurc. Chaos 10 (2000) 2519.
[350] J. Bhattacharya, E. Pereda, R. Kariyappa, P.P. Kanjilal, Sol. Phys. 199 (2001) 267.